JAEA-Review
2005-004

JP0650009

JAEA-Review

JAERI TANDEM Annual Report 2004
April 1, 2004 - March 31, 2005

Department of Research Reactor and Tandem Accelerator

Nuclear Science Research Institute
Tokai Research and Development Center

January 2006

Japan Atomic Energy Agency

日本原子力研究開発機構

JAEA-Review 2005-004

JAERI TANDEM Annual Report 2004
April 1, 2004 – March 31, 2005

Department of Research Reactor and Tandem Accelerator

Nuclear Science Research Institute
Tokai Research and Development Center
Japan Atomic Energy Agency
Tokai-mura, Naka-gun, Ibaraki-ken

(Received November 9, 2005)

This annual report describes research activities, which have been performed with the JAERI tandem accelerator and its energy booster from April 1, 2004 to March 31, 2005. Summary reports of 48 papers, and lists of publication, personnel and cooperative research with universities are contained.

The JAERI (Japan Atomic Energy Research Institute) have been unified with JNC (Japan Nuclear Fuel Cycle Development Institute) and became JAEA (Japan Atomic Energy Agency) on October 1st, 2005.

Keywords: JAERI Tandem, Nuclear Structure, Nuclear Reactions, Nuclear Chemistry, Nuclear Theory, Atomic Physics, Solid State Physics, Radiation Effects in Materials, Progress Report.

Editors : Tetsuro ISHII, Suehiro TAKEUCHI, Masumi OSHIMA, Yuichiro NAGAME, Satoshi CHIBA and Masao SATAKA

原研タンデム加速器2004年度年次報告

日本原子力研究開発機構東海研究開発センター原子力科学研究所
研究炉加速器管理部

(2005年11月9日受理)

本年次報告書は、東海研究所の原研タンデム加速器及びブースターを利用し、2004年4月1日から2005年3月31日までの間に行われた研究活動をとりまとめたものである。
(1)加速器の運転状況及び開発　(2)原子核構造　(3)原子核反応　(4)核化学　(5)原子核理論　(6)原子分子物理及び固体物理　(7)材料の照射効果の7部門にまたがる42編の研究報告、公表された文献、関与した職員及び大学等との協力研究のリストを収録している。

日本原子力研究所は１０月１日から独立行政法人日本原子力研究開発機構となり、タンデム加速器施設は、東海研究開発センター　原子力科学研究所　研究炉加速器管理部の所属となりました。
本報告書の研究は旧名称時の研究であるため従来の所属表示としてあります。

原子力科学研究所：〒319-1195　茨城県那珂郡東海村白方白根2-4
（編集者）石井哲朗、竹内末広、大島真澄、永目諭一郎、千葉　敏、左高正雄

Foreword

This report covers research and development activities with the tandem accelerator and its superconducting booster at JAERI, Tokai, for the period of FY 2004 (April 1, 2004 to March 31, 2005). During this period, the accelerator was operated over a total of 216 days and delivered 19 different ions over 123 beam times to experiments in the field of nuclear structure, nuclear reactions, nuclear chemistry, atomic physics, solid state physics and radiation effects in materials. Sixty-nine research programs were carried out in collaboration with about 180 researchers from universities and research institutes. The following are some of the highlights in FY 2004.

In the JAERI-KEK joint RNB (Radioactive Nuclear Beam) project, construction of the RNB facility, TRIAC (Tokai Radioactive Ion Accelerator Complex), was completed in the end of July, 2004. The JAERI-ISOL (Isotope-Separator On-Line) was connected to the CB-ECRIS (Charge Breeder –ECR ion source) through a low-energy beam transport line. The TRIAC machine tuning started in August 2004, together with RNB production using a uranium-target and a 30 MeV proton beam. With an ion-source attached to the JAERI-ISOL, so far, 98 radioactive isotopes in 16 elements were ionized and mass-separated. The linacs accelerated $^{14}N^{2+}$ and $^{16}O^{2+}$ ions with output energy of 1.1 MeV/u. In March 2005, ^{138}Xe ($T_{1/2}$=14.08 m) produced in the proton-induced fission of uranium was successfully accelerated through the CB-ECRIS to the end of the linacs. The charge state of ^{138}Xe was bred to 20^{+} by the CB-ECRIS and acceleration energy of 1.1 MeV/u was achieved. The TRIAC will be available for users from October, 2005. Four experimental proposals were approved by the TRIAC program advisory committee held in January 2005.

In the development of the tandem accelerator, the maximum terminal voltage was getting higher after the original acceleration tube was replaced with NEC compressed tube in FY2003. The voltage during a high-voltage conditioning in 2004 was very stable at 18.7 MV without beams and at 18.0 MV with beams. These were the highest records in the history of the JAERI tandem accelerator

In research of nuclear structure, the electromagnetic properties of low-lying states in ^{82}Kr and $^{92,94,96}Zr$ have been studied by multiple Coulomb excitation. A prolate deformation of ^{82}Kr and a strong octupole correlation in $^{92,94,96}Zr$ have been found. In-beam γ-rays in a neutron-rich nucleus of ^{240}U, which was produced in the two neutron transfer reaction $^{238}U(^{18}O,^{16}O)^{240}U$, were measured by a particle-γ coincidence method. The ground-state and octupole bands of ^{240}U were established up to medium spin states.

In research of nuclear reactions, fusion barrier distributions were experimentally extracted by taking the first derivative of the measured excitation functions of backward quasi-elastic scattering in the reactions of $^{48}Ti+^{208}Pb$, $^{56}Fe+^{208}Pb$ and $^{64}Ni+^{208}Pb$, relating to the cold fusion for production of elements 104, 108 and 110, respectively. Astrophysical nuclear reaction rates of $^{8}Li(\alpha,n)$ and $^{12}B(\alpha,n)$ were exclusively measured by using low-energy radioactive nuclear beams separated with the JAERI-RMS (Recoil Mass Separator).

In research of nuclear chemistry, fluoride complexation of element 104, rutherfordium (Rf), produced in the $^{248}Cm(^{18}O,5n)^{261}Rf$ reaction was studied by anion-exchange chromatography on an atom-at-a-time scale. The result clearly demonstrated that the formation of the fluoride complexes of Rf is much weaker than those of the homologues Zr and Hf.

In research of nuclear theory, it was concluded that the intruder state is dominant at N=19 isotope of Na, and shell evolution occurs in neutron-rich nuclei due to the spin-isospin dependence of the effective interaction. Effects of charge polarization on the barrier-height of fusion reactions and structure of high-density matter are investigated.

In research of radiation damage of materials, a high-temperature up to 1200℃ irradiation apparatus were developed in order to simulate the radiation damage of oxide nuclear fuel. It has been found that typical high-energy fission product such as Xe ion has sufficient energy to create highly damaged columnar defects in CeO_2, which has a same crystallographic structure as UO_2.

Hiroshi Ikezoe
Director
Department of Materials Science

Contents

目次

1. Accelerator Operation and Development

This is a blank page.

JP0650010

1.1 OPERATION AND USAGE OF TANDEM ACCELERATOR AND BOOSTER

S. TAKEUCHI, Y. TSUKIHASHI, T. YOSHIDA, S. KANDA, K. HORIE, I. OUCHI,
S. HANASHIMA, S. ABE, N. ISHIZAKI, H. TAYAMA, M. MATSUDA,
T. NAKANOYA, H. KABUMOTO, T. SATO and M. NAKAMURA

The operations of the tandem accelerator and booster were given to conducting experiments over two machine time periods, May 20 to September 30 and November 25 to March 30. The total operation time of the tandem accelerator was 5,034 hours (216 days), and 123 different beam deliveries were performed for experiments during the operation time. The experiment proposals and the usage of beam times from May 20, 2004 to March 30, 2005 are summarized in table 1 and table 2, respectively.

Table 1. Experiment Proposals.

Research Proposals Accepted by the Program Committee:		
In-house Staff Proposals		7
Collaboration Proposals		33
Number of Experiments Proposed		69
Number of Scientists Participating in Research	from out side	176
	in-house	193
Number of Institutions Represented		39

Table 2. Usage of Beam-times in Different Research Fields.

Research fields	Beam Time		Beam delivery	
Nuclear physics	86 days	39.8 %	34	times
Nuclear chemistry	38	17.6	14	
Atomic and solid state physics	70	32.4	60	
Material research	3	1.4	3	
Detector	2	0.9	2	
Accelerator development (TRIAC)	17	7.9	10	
Total	216 days		123	times

The distributions of the terminal voltages and ion species are listed in table 3 and table 4, respectively. The stable high voltage limit of the tandem accelerator was gradually increasing without very aggressive conditioning, after the whole acceleration tubes were replaced in the beginning of the last fiscal year to the new compressed geometry tube which were cleaned by a high-pressure water jet [1,2,3]. The voltmeter recorded a very stable high voltage of 18.7MV during a high voltage test done in October, 2004 and it was confirmed that the terminal voltage was stable with beams at 18.0MV. These voltages were the highest since the tandem accelerator was constructed.

Table 3. Distribution of Terminal Voltages.

>17	MV	2	days	0.9	%
16-17		14		6.5	
15-16		70		32.4	
14-15		53		24.5	
13-14		16		7.4	
12-13		14		6.5	
11-12		4		1.9	
10-11		10		4.6	
9-10		4		1.9	
8-9		5		2.3	
7-8		5		2.3	
6-7		3		1.4	
5-6		16		7.4	

Compared with the last fiscal year, there were operations above 16MV. We have yet to operate above 18MV for user's experiments, because we have not confirmed if the electronics in the accelerator are safe from full sparks above 18MV. The operation voltages spread widely down to 5-6 MV level. At the very low terminal voltages, a beam of ^{7}Li was accelerated to produce ^{8}Li secondary beams for experiments of nuclear astrophysics and Li diffusion in solid materials. With respect to the ion beams, the accelerator provided a total of 19 different ion species (30 different nucleides) for research.

Table 4. Distribution of Ion Species Accelerated for Experiments.

^{1}H	27	days	^{48}Ti	3	days
^{6,7}Li	16		^{56}Fe	7	
^{11}B	6		^{58,60,64}Ni	22	
^{12,13}C	3		^{70,74,76}Ge	10	
^{16,18}O	50		^{70}Zn	3	
^{19}F	4		^{82}Se	3	
^{28,30}Si	3		^{90,92}Zr	6	
^{32,33}S	8		^{132,136}Xe	28	
^{35}Cl	6		^{197}Au	6	
^{40}Ar	5				

Among the ions in table 4, inert gas ions Ar and Xe were accelerated from the in-terminal ECR ion source. The ^{16,18}O beams stood out most in popularity commanding over 23% of all beam time. They were mostly used for nuclear chemistry on actinides. The ^{1}H and ^{136}Xe beams also had a high popularity of about 13%. The ^{1}H beams contributed to generating radioactive ion beams from the proton induced fission products of uranium in the R&D of the Tokai Radioactive Ion Accelerator Complex(TRIAC).

The super-conducting booster was operated a total of 37 days for boosting 11 different beams from the tandem accelerator to conduct 12 experiments. The booster also played a role of the beam transport line to the booster experimental hall for a total of 38 days. There were no big troubles in FY2004 as before. We were, however, beginning to have helium leaks from indium gaskets, which were attributed to frequent thermal cycles since 1993 and needed re-tightening of the loosened bolts. Forty super-conducting resonators were all in good condition to run and the average acceleration field gradient was 4.1 MV/m at an RF input of 4 watts. The ion species boosted for experiments, their boosted energies and beam times are shown in table 5. All the boosted beams were used for nuclear physics and it means that 35% of the beam time for nuclear physics needed an energy boost.

Table 5. Boosted Ion Beams for Experiments:

^{16}O	200	MeV	3	days
^{18}O	200		3	
^{48}Ti	270		3	
^{56}Fe	300		3	
^{58}Ni	286		3	
^{60}Ni	256-363		4	
^{64}Ni	263-310		7	
^{76}Ge	741		2	
^{82}Se	630		3	
^{92}Zr	390		3	
^{132}Xe	410		3	

With TRIAC, which was installed in the tandem facility in collaboration with KEK [4,5], the first beam acceleration test was carried out using the beam time of 17 days. The R&D team succeeded in accelerating $^{138}Xe(T_{1/2}$ = 14min) and the TRIAC was established as a licensed accelerator facility in March, 2005. The system and the test result are to be reported elsewhere in this annual report. The safety interlock system was reconstructed to cope with the addition of TRIAC.

References

[1] S. Takeuchi, et al, Nucl. Instrum, and Meth., **A 513**,(2003) 429.

[2] S. Takeuchi, et al, JAERI Tandem Annual Report **2002**(2003) pp6-7.

[3] S. Takeuchi, et al, JAERI Tandem Annual Report **2003**(2004) p6.

[4] H. Miyatake, et al, Nucl. Instrum. and Meth., **B204**(2003) 746.

[5] S. Takeuchi, *Application of Accelerators in Research and Industry:17th Int'l Conf.*; AIP 0-7354-0149-7/03, (2003) pp229-236.

1.2 TRIAC PROJECT

S.ICHIKAWA, H.MIYATAKE[1)]
on behalf of JAERI-KEK TRIAC COLLABORATORS

Construction of the radioactive nuclear beam (RNB) facility, TRIAC[2)], consisting of the Charge-Breeding Electron Cyclotron Resonance Ion-Source (CB-ECRIS), the Split-Coaxial Radio-Frequency Quadrupole (SCRFQ) and Interdigital-H (IH) linacs was completed in the end of July, 2004 [1]. An Isotope-Separator On-Line (JAERI-ISOL) was connected to the CB-ECRIS through a low-energy beam transport line. The TRIAC machine tuning started in August 2004, together with RNB production using a uranium-target and a 30 MeV proton beam.

In February 2005, the linacs accelerated $^{14}N^{2+}$ and $^{16}O^{2+}$ ions with output energy of 1.1 MeV/u. On of related data is shown in fig. 1. The measured transmission efficiency was 70%. The efficiency and energy spread of the output beam are expected to improve further in the future to the design values of 91% for the transmission and 0.6% for the spread, respectively.

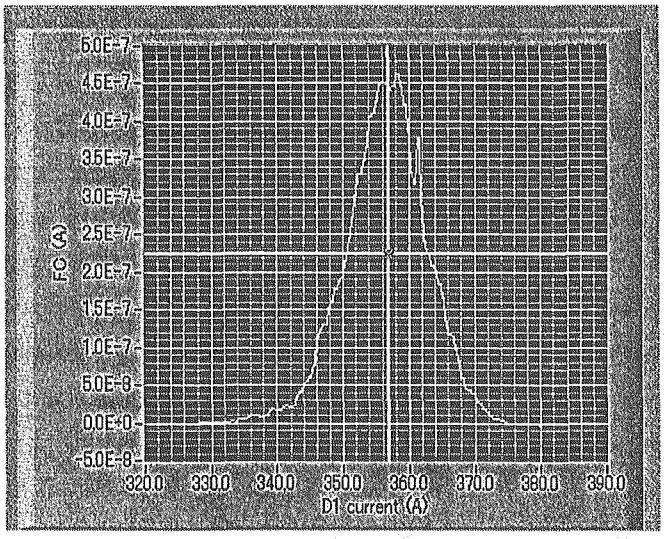

Fig. 1 Intensity profile of the accelerated $^{14}N^{2+}$-beam as a function of the electric current of the analyzing magnet set at the exit of the IH linac.

In the development of RNB, neutron-rich isotopes produced in the proton-induced fission of uranium have been ionized with a surface ionization type and/or a FEBIAD type ion-sources attached to the JAERI-ISOL. A uranium-carbide target with a thickness of 300-mg/cm^2 and a 30-MeV proton beam delivered from the tandem accelerator with intensity of about 100 nA were used in this development. So far, 98 radioactive isotopes in 16 elements were ionized and mass-separated. The mass-separated yields of ^{138}Xe and ^{132}Sn, for example, were 2.5 x 10^5 atoms/s, 9.7 x 10^3 atoms/s, respectively [2]. For the thickness of 2.6 g/cm^2 uranium-target and proton beam intensity of 3 μA, the mass-separated yields of ^{138}Xe and ^{132}Sn are estimated to be 6.5 x 10^7 atoms/s, and 2.5 x 10^6 atoms/s, respectively . In addition, we have already developed short-lived light RNBs, ^8Li , ^{18}F and ^{20}F with the mass-separated intensity of 1 x 10^7 atoms/s, 1 x 10^6 atoms/s and 2.5 x 10^5 atoms/s, respectively.

---

1) Institute of Particle and Nuclear Studies, High Energy Accelerator Research Organization (KEK)

2) TRIAC (Tokai Radioactive Ion Accelerator Complex) has been operated as a joint research project of the JAERI-Tokai and KEK-IPNS (Institute of Particle and Nuclear Studies) at the JAERI Tandem accelerator facility, since FY2001.

In March 2005, ^{138}Xe ($T_{1/2}$=14.08 min.) was successfully accelerated through the CB-ECRIS to the end of the linacs. The charge state of ^{138}Xe was bred to 20^{+} by the CB-ECRIS and acceleration energy of 1.1 MeV/u was achieved. Figure 2 shows the decay curve of the β-ray counts measured with a plastic scintillator set at the exit of the IH linac after the ^{138}Xe beam switched-off. The solid curve shows a single-component exponential decay functions with half-life of 14.08 min. The observed β-ray activities clearly decreased with half-life of 14 min.

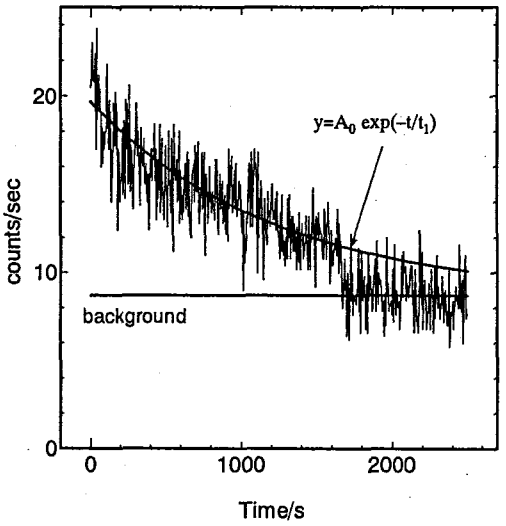

Fig. 2 Decay curve for β-ray counts measured with plastic scintillator placed at exit of the IH linac.

To re-accelerate the low-energy RNBs in the near future by superconducting (SC) booster up to an energy of 5~8MeV/u, we designed a superconducting twin quarter wave resonator (Twin-QWR) [3]. We were preparing to fabricate a prototype twin-QWR in a year.

TRIAC workshop was held at Tokai-site, JAERI, 21-23, September 2004. It aimed at the intense discussion on the physics and the feasibility of each proposed experimental idea using not only the low-energy RNB (< 1.1 MeV/u), but also the higher energy RNB (> 5 MeV/u). There were 34 presentations and 81 participants. The presented subjects covered nuclear structure (15 presentations), material science (5), nuclear astrophysics (4), nuclear reaction mechanism (3) and nuclear chemistry (2) as well as status reports of TRIAC (5). The workshop emphasized the importance of the high-energy RNB and the use of the spin-polarized RNB. There was similar discussion at a symposium in the annual meeting of the Japan Physical Society held on March 2005.

The TRIAC will be available for users from October, 2005. An available machine time for use of RNB is expected to be 50 days in a year. Four experimental proposals listed below were approved by the TRIAC program advisory committee held in January 2005.

(1) A study of the heavy element synthesis in the early universe with using ^{8}Li-RNB (spokesperson, Hironobu Ishiyama, KEK).

(2) Nuclear spectroscopy of spin-polarized nuclei in the region of ^{132}Sn (Yoshikazu Hirayama, KEK).

(3) Spin-polarization of In, Cs, Ba isotopes with a tilted-foil method and measurements of their nuclear magnetic moments (Kensaku Matsuta, Osaka Univ.).

(4) Coulomb excitation spectroscopy of Xe-fragments (Mitsuo Koizumi, JAERI).

References

[1] H. Miyatake and H. Ikezoe, Nucl. Phys. News, Vol. 14 No. 4, 37(2004).

[2] A. Osa et al., in this annual report.

[3] H.Kabumoto et al., JAERI-Review 2004-027, pp13-14.

JP0650012

1.3 SAFETY HANDLING SYSTEM OF A TARGET/ION SOURCE FOR RADIOACTIVE ION BEAM PRODUCTION

S. ICHIKAWA, T. K. SATO and A. OSA

A forced electron beam induced arc discharge (FEBIAD) type ion source and a surface ionization type one have been developed as the ion source for producing heavy neutron-rich radioactive nuclear beam (RNB) at the TRIAC (Tokai Radioactive Ion Accelerator Complex) facility [1]. In the present ion sources, the target of about 2.6g/cm^2 ^{238}U impregnated on a graphite fiber is available [2]. To produce the neutron-rich RNB, we will use a proton beam of 30 MeV on target with an intensity of 3 μA. After an irradiation of 5 days, the dose equivalent at one meter distance from the target/ion source is estimated to be 40 mSv/h. Even one week after the irradiation, the residual level is of the order of 3 mSv/h at the same distance. This makes manual handling or removal of the target/ion source impossible. In addition, the main residual radioactivities are fission products, the risk of dispersion of radioactive elements into the air during a disconnection and/or storage of the target/ion source is present. For this reason, a safety handling system for the target/ion source has been built. The target/ion source and an ion-source carriage are shown schematically in fig.1.

The ion-source housing itself has been designed as a vacuum enclosure. For this purpose, a pneumatic valve was installed at the front end of the housing that permitted closing the housing before removal. The primary beam entrance port on the housing is also sealed with 5 μm HAVAR foil. What the target/ion source is installed into the housing is a "target/ion source module". The housing acts as the vacuum enclosure, so that the risk of dispersion of radioactive elements into the air during disconnection and storage is not present.

The ion-source carriage system makes a linear, circular and up/down motions as well as carriage motion at a storage section. To install the source module, for example, the module is set onto a movable plate with locator pins by means of the ion-source carriage. The movable plate is then pushed forward with a linear-motion carriage as shown in fig.1 and clamped onto the vacuum interface flange by remotely controlled pneumatic actuator mechanism (not indicated in fig.1). The source module is pluged into the vacuum interface flange of the ISOL, and all current feedthroughs, air and water connections (utility interface) of each front end are joined together on a quick connector. The volume between the interface flanges can then be pumped down by remote controlled vacuum pump. This operation is followed by, the connection between the beam entrance on the source module and beam line from the tandem accelerator remotely actuated by a pneumatic device. To remove the source module, the

procedure is reversed, and then transported to a storage cell by the ion-source carriage device.

At present we have three source modules which are recyclable and allow us to cool down the residual activities in the source for about three months and to reach a level sufficiently low enough to refurbish them for reinstallation.

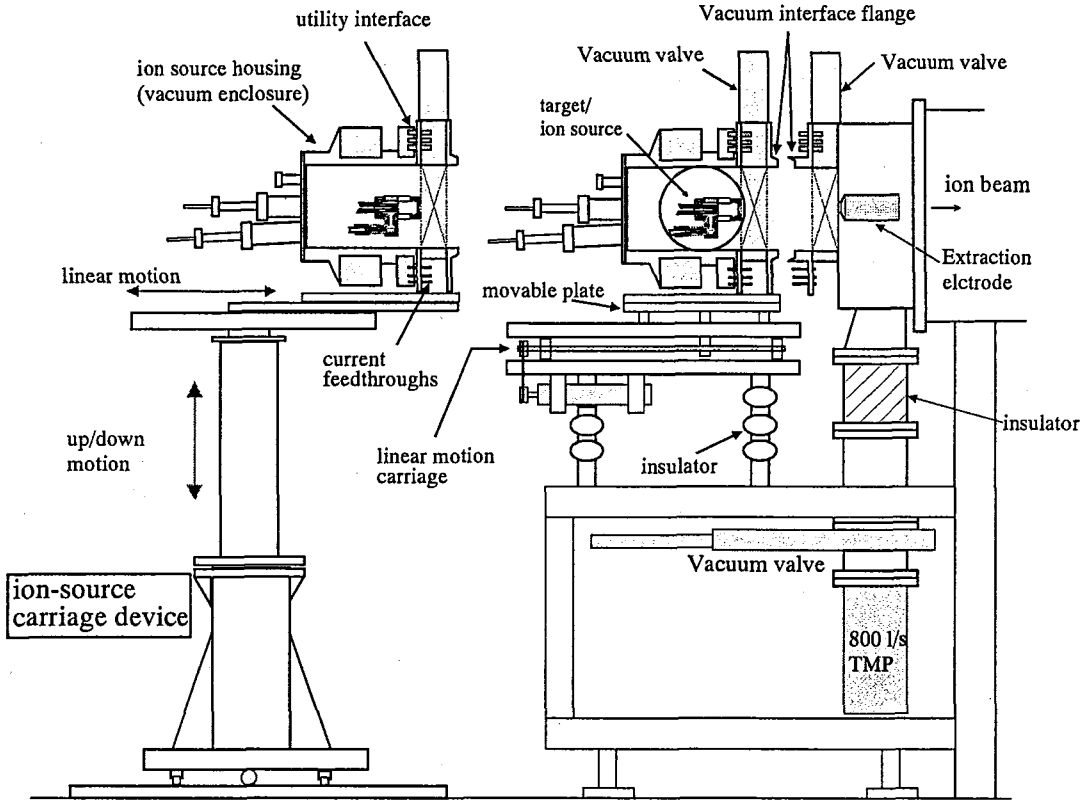

Fig. 1 Schematic view of the target/ion source module and the ion-source carriage.

During irradiation, gaseous radioactivities are produced and pumped away through the pumping systems installed on the extraction and acceleration chambers of ISOL. In order to prevent the gaseous radioactivities flow releasing into the air, the gas from the pumping systems is stored in a vessel for a certain time.

References

[1] H. Miyatake *et al.*, Nucl. Instrum. Meth. B 204 (2003) 746.
[2] S. Ichikawa *et al.*, *ibid.* 204 (2003) 372.

JP0650013

1.4 ION SOURCE DEVELOPMENT FOR THE JAERI-KEK JOINT RNB PROJECT

A. OSA, T.K.SATO, M. MATSUDA, K. TSUKADA, M. ASAI, S.C. JEONG[1)], I. KATAYAMA[1)] and S. ICHIKAWA

According to the JAERI-KEK joint radioactive nuclear beam (RNB) project, we have developed a FEBIAD-type integrated-target-ion source system to produced heavy neutron-rich RNBs with particle-induced fission of ^{238}U [1]. In order to estimate RNB intensities with this ion source, yields of mass-separated fission products were surveyed.

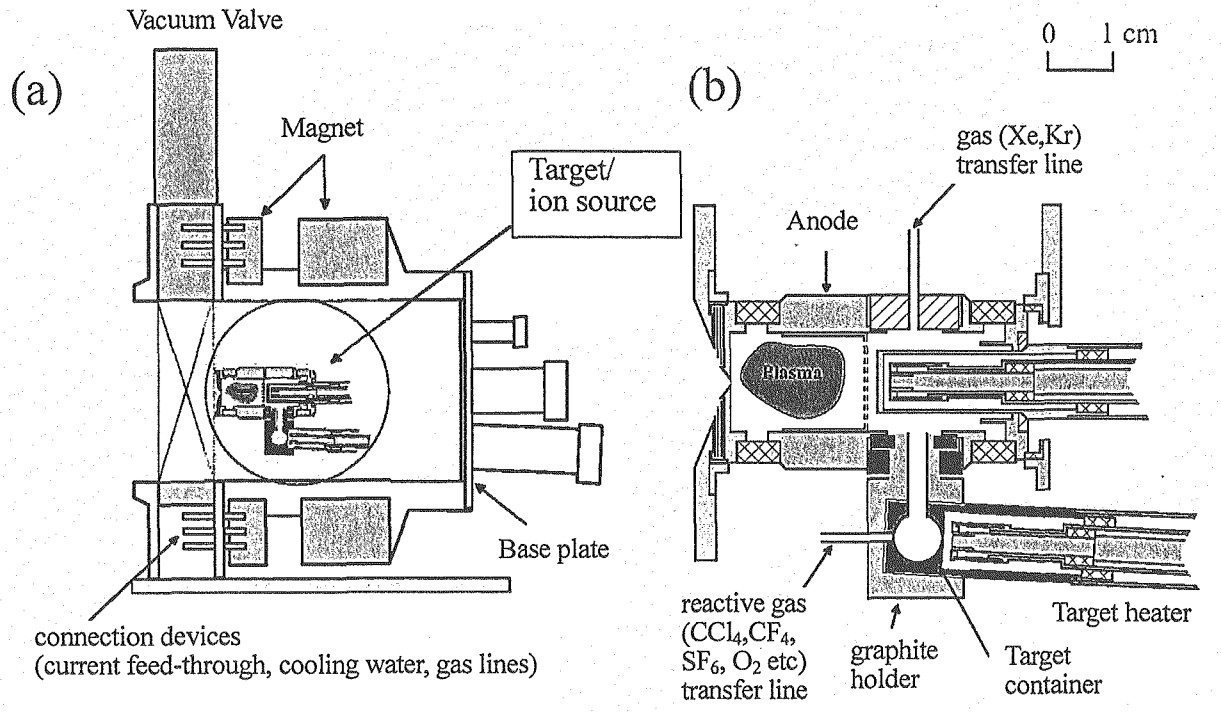

Fig.1. Schematic view of the FEBIAD ion source.

A graphite fiber was chosen as a base material, which showed higher efficiency than a porous one in the experiments of the surface-ionization type integrated-target-ion source system[2]. A uranium carbide target was prepared at a uranium density of 300-mg/cm^{2}U. Graphite fiber (ϕ =11 μm, GC-20, Tokai Carbon Co.) was filled in a target container as a base material and uranyl nitrate solution was impregnated. After drying-out, the target were outgassed and converted to oxide form at 600 °C in argon atmosphere before insertion into the ion source. The target is loaded to the ion source system and sintered as uranium carbide.

The target was bombarded with a 30-MeV proton beam (20 MeV on target) with intensity of about 100 nA. For the separation yield measurements of fission products, the mass separated products were collected on an aluminized Mylar tape in a tape transport system and were periodically

1) High Energy Accelerator Research Organization

transported to a measuring position where an HPGe detector was placed for γ-ray measurements. During the measurements, the condition of the ion source was monitored by the ionization efficiencies of reference stable-isotope-beams that were kept at 15% and 20% for Kr and Xe, respectively.

Separation yields of 15 elements shown in Table 1 and 82 nuclei were derived from γ-ray measurements. At this time, most of RNBs were "cocktail" beams. The separation yield of double magic-nuclei ^{132}Sn was 9.7x10^{3} pps. This ^{132}Sn-beam contained about the same ^{132}Sb-beam. An overall efficiency for radioactive Kr and Xe was derived from the measured yield and the calculated production rate that is based on the independent cross section in the proton-induced fission of ^{238}U [3]. The overall efficiencies of ^{91}Kr, ^{138}Xe and ^{139}Xe were 8.0%, 7.0% and 1.8%, respectively. These are lower than the ionization efficiencies for reference Kr and Xe. These low efficiencies are partly caused by the slow diffusion- and/or effusion-time of fission products from target materials. In addition, these were caused by leakage of fission-product vapor from the graphite holder. When the ionization efficiencies were measured, reference gases were directly fed to the plasma chamber as shown in Fig. 1. On the other hand, the fission-product vapor was fed from the graphite holder that had some clearance to the target container and the plasma chamber.

Table 1 Observed elements in the mass-separated RNBs.

11(IB)	12(IIB)	13(IIIA)	14(IVA)	15(VA)	16(VIA)	17(VIIA)	18(VIIIA)
$_{29}$Cu	$_{30}$Zn	$_{31}$Ga	$_{32}$Ge	$_{33}$As		$_{35}$Br	$_{36}$Kr
$_{47}$Ag	$_{48}$Cd	$_{49}$In	$_{50}$Sn	$_{51}$Sb	$_{52}$Te	$_{53}$I	$_{54}$Xe

		Experiment 1 100-nA 30MeV proton on 300mg/cm^{2}U	
	$T_{1/2}$	Yield(pps)	Efficiency
^{91}Kr	8.6s	5.3 E+04	8.0%
^{138}Xe	14.1m	2.7E+05	7.0%
^{139}Xe	39.7s	3.7E+04	1.8%

References

[1] S. Ichikawa et al., Nucl. Instrum. Methods. B204(2003)372-376.
[2]] T. Sato et al., JAERI-Review 2004-27 pp.9-10.
[3] H. Kawakami, KEK Report 2001-15 Oct. 2001

JP0650014

1.5 STATUS AND DEVELOPMENT OF SNB ION SOURCE FOR TRIAC FACILITY

T.NAKANOYA, M.MATSUDA

Last year we had completed the first phase installation of TRIAC (Tokai Radioactive Ion Acceleration Complex) facility in corporation with KEK. This facility can accelerate radioactive ion beams up to 1.1MeV/u. It has two different ion sources; one is RNB (Radioactive Nuclear Beam) ion source, the other is SNB (Stable Nuclear Beam) ion source. Because of very low intensity of RNB, SNB's are used as pilot beams for accelerating RNB's efficiently. Moreover TRIAC beam line will be connected to JAERI superconducting booster linac in the second phase of the TRIAC. After completing of this project, heavy ion beams would be accelerated up to 5-7MeV/u. In this case, SNB ion source is expected as high intensity stable heavy ion source too.

The SNB ion source is permanent magnet type ECR ion source of 10GHz, 200W. Fig. 1 shows schematic view of the ion source. A same type of ion source has been used to obtain noble gas ion beams at the JAERI tandem accelerator [1]. Last year we had installed SNB ion source and all beam line components. N^{2+} (70eμA) beam was extracted at first beam injection test for TRIAC. The beam was accelerated up to 1.1MeV/u successfully by TRIAC operation group. It worked well as a pilot beam for radioactive ion beam that m/q is 7.

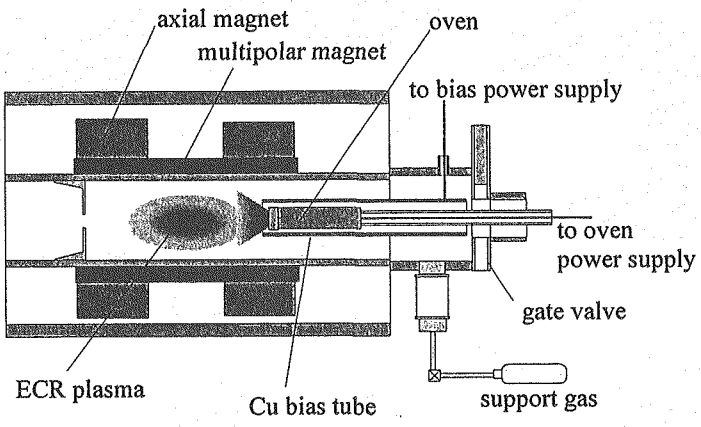

Fig.1 Schematic view of ECR ion source

We have to extend ion species for many kinds of RNB species. It is very important that SNB ion source can produce many ion species not only gaseous elements, especially in the second phase of the project. For obtaining metal ion from ECR ion source, oven method is wildly used. In this method, the oven producing metal vapor is inserted ion source chamber directly. Production of metal ion needs high evaporation pressure over 10^{-1} Pa. In many metal element, such high evaporation pressure require heating them over 1000℃. We had already tested and produced some metal ion species with commercially available oven [2]. But this oven can not heat up to 1200℃ and had some problems that small sample volume, high running cost, and short life time. Therefore we developed a high temperature oven that can easily heat over 1500℃ newly.

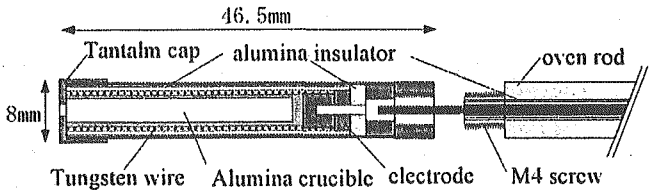

Fig.2 Schematic view of high temperature oven

Fig2. shows schematic view of the high temperature oven. Oven cylinder and oven rod are

connected with screw. Using the screw, connection of two parts is very tight electrically and physically. The crucible volume is about 0.25cm^3. Tantalum cap is used to pretend flow out of melted metal from oven cylinder and protect heater from ECR plasma. Tantalum cap and tungsten heater is easily replaceable. So running cost can be suppressed. The oven is led to plasma chamber through the bias tube after pre-exhausted in load lock chamber.

We tested this oven in a dummy chamber imitating ECR ion source. As a result, this oven succeed heating up to 1650℃ at 50 W. Due to the crucible consist of alumina, it could not raise temperature any more. But it could keep at 1500℃ quite stable for over 10 hours. We measured chamber wall temperature simultaneously to examine the affection of thermal radiation from oven. The temperature is about 50℃, even in the highest temperature point. In actual operating condition, ion source is used under forced air cooling. Therefore, the permanent magnet system will not be affected by thermal radiation from the oven. It seems cupper bias tube functioned as thermal shielding and heat sink effectively.

Next we tested production of many metal ion species using this oven, and obtained 8 metal ion species newly. The results show in fig.3. Such as Mn, Mg which have sufficient evaporation pressures below their melting point showed high intensity and stability. On the other hand, such as Sn, Al showed instabilities on occasions. It is because that melted metal escape from the crucible into tungsten heater will causes short circuit. For stable operations using such elements, more improvement is required.

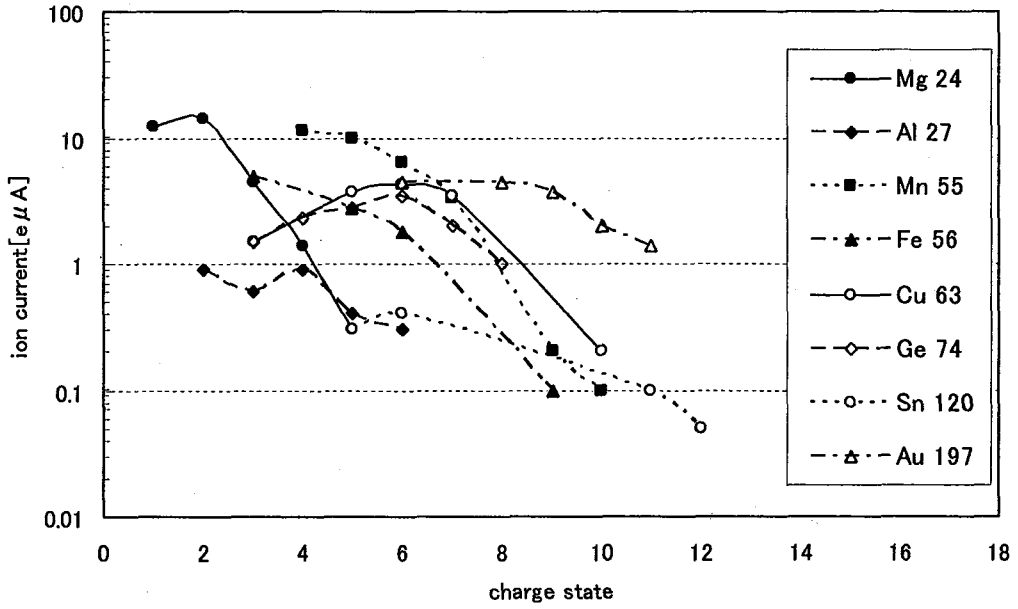

Fig.3 Measured charge distribution and beam current of the metallic ion beam. Natural sample were used for all experiments. Sample form were 1 ϕ wire for Mg,Al,Fe,Cu,Sn,Au and others were powder

References

[1] M.Matsuda, C.Kobayashi, and S.takeuchi Proc. of 14th Int. Workshop on ECR sources
[2] M.Matsuda, T.Nakanoya JAERI-Conf 2003-017

This is a blank page.

2. Nuclear Structure

This is a blank page.

2.1 ALPHA-DECAY SCHEME OF ^{257}No

M. ASAI, K. TSUKADA, M. SAKAMA[1], S. ICHIKAWA, T. ISHII, Y. NAGAME, I. NISHINAKA, K. AKIYAMA, A. OSA, Y. OURA[2], K. SUEKI[3] and M. SHIBATA[4]

Alpha-γ and α-e (internal conversion electron) coincidence spectroscopy for ^{257}No has been performed to establish Nilsson single-particle states in odd-mass $Z > 100$ and $N > 152$ nuclei. The nucleus ^{257}No was produced by the ^{248}Cm(^{13}C, $4n$) reaction. Reaction products were transported by a He jet into a rotating wheel α-γ detection system for α-γ coincidence spectroscopy, and into a gas-jet coupled on-line isotope separator with which the ^{257}No nuclei were ionized, mass-separated, and implanted into a Si detector to measure α-e coincidences. The experimental details are described in Ref. [1,2].

Figure 1(a) shows a γ-ray spectrum in coincidence with α particles of ^{257}No. Three γ transitions of 77.0, 101.8 and 124.1 keV and Fm L X rays were clearly observed. These γ rays were coincident with the 8222 keV α transition. In addition, a weak 136.4 keV γ ray was observed in coincidence with 8167–8195 keV α particles. Figure 1(b) shows an α-coincident electron spectrum. Two prominent electron peaks were observed at 50 and 97 keV, which correspond to the L internal conversion electrons associated with the 77.0 and 124.1 keV transitions, respectively. The M electron peaks were observed as well. The $M1$ multipolarity was assigned to the 77.0 and 124.1 keV transitions from the measured internal conversion coefficients. On the basis of the observed coincidence relationships and the transition energies, we have determined the decay scheme of ^{257}No as shown in Fig. 2.

The spin-parity of the ground state of ^{253}Fm is known to be $1/2^+$ with the $1/2^+[620]$ configuration [3]. Since the 124.1 keV transition has an $M1$ multipolarity, the spin-parity of the 124.1 keV level is either $1/2^+$ or $3/2^+$. On the other hand, the 124.1 keV level is populated by the favored α transition with a hindrance factor of 1.3, indicating that this level is a Nilsson single-particle state whose configuration is the same as that of the ground state of ^{257}No. Among the Nilsson single-particle states with a spin $1/2^+$ or $3/2^+$, only the $3/2^+[622]$ state could lie at such low energy in ^{253}Fm. Therefore, we have assigned the $3/2^+[622]$ configuration to the 124.1 keV level as well as to the ground state of ^{257}No.

Figure 3 shows excitation energies of Nilsson single-particle states in $N = 153$ isotones and ground-state configurations of $N = 155$ isotones. The ground state configuration of ^{257}No is different from that of the lighter $N = 155$ isotones ^{255}Fm and ^{253}Cf. Different α-decay patterns shown in Fig. 3 also indicate the difference in the ground-state configuration. The energy of the $7/2^+[613]$ state in the $N = 153$ isotones increases with increasing proton number, while that of the $3/2^+[622]$ state decreases. This trend can be explained by the crossing between the downsloping $3/2^+[622]$ and the upsloping $7/2^+[613]$ orbitals on the Nilsson diagram. The change of the ground-state configuration between ^{257}No and the lighter $N = 155$ isotones would also result from the gradually increasing quadrupole deformation with increasing proton number.

[1]Department of Radiologic Science and Engineering, The University of Tokushima
[2]Department of Chemistry, Tokyo Metropolitan University
[3]Department of Chemistry, University of Tsukuba
[4]Radioisotope Research Center, Nagoya University

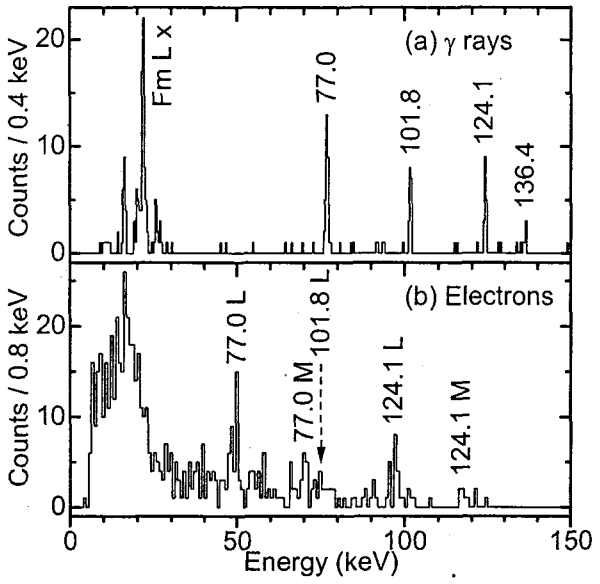

Fig. 1. (a) Gamma-ray and (b) internal-conversion electron spectra observed in coincidence with α particles of ^{257}No.

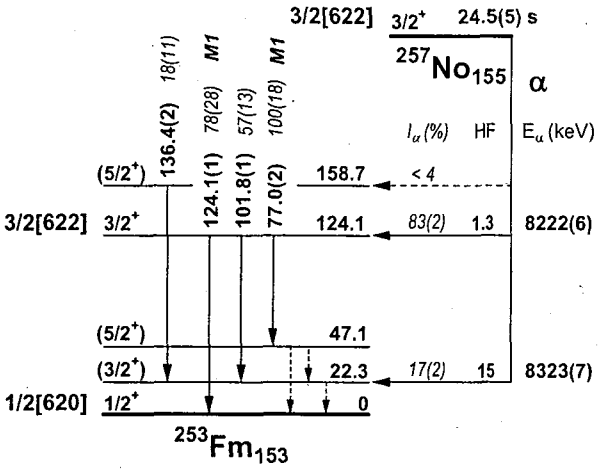

Fig. 2. Proposed decay scheme of ^{257}No.

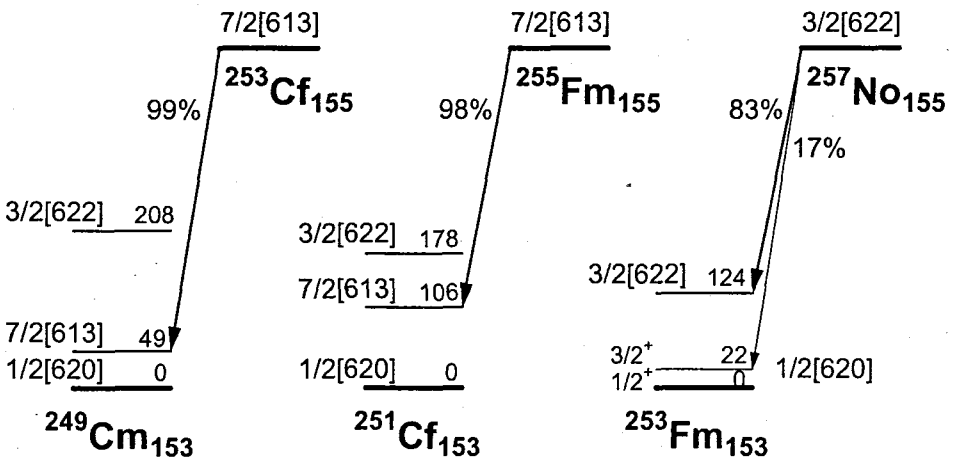

Fig. 3. Alpha decays of $N = 155$ isotones and excitation energies of Nilsson single-particle states in $N = 153$ isotones.

References

[1] M. Asai, K. Tsukada, S. Ichikawa, Y. Nagame, T. Ishii, I. Nishinaka, K. Akiyama, A. Osa, M. Sakama, Y. Oura, K. Sueki and M. Shibata, *Extended Abstracts of the 2nd Int. Conf. on the Chemistry and Physics of the Transactinide Elements, Napa, November 16–20, 2003*, LBNL-53896 Abs. (2003) 20.

[2] M. Asai, M. Sakama, K. Tsukada, T. Ishii, Y. Nagame, I. Nishinaka, K. Akiyama, S. Ichikawa, K. Sueki, Y. Oura and M. Shibata, JAERI-Review 2004-027 (2004) 27.

[3] I. Ahmad, A. M. Friedman, R. F. Barnes, R. K. Sjoblom, J. Milsted and P. R. Fields, Phys. Rev. **164** (1967) 1537.

2.2 OCTUPOLE COLLECTIVITY IN ^{94}Zr

Y. TOH, M. OSHIMA, M. KOIZUMI, A. OSA, Y. HATSUKAWA, M. MATSUDA,
H. KUSAKARI[1], M. SUGAWARA[2] and T. MORIKAWA[3]

In many spherical nuclei the low frequency shape oscillations are of octupole type. Microscopically, they arise as a superposition of $1\hbar\omega$ particle-hole excitations. Given that the measured B(E3) for ^{96}Zr is among the strongest octupole-phonon to ground state transitions observed in nuclei[1,2]. In the simplest single particle model, the ground states of the Zr isotopes have a filled $\pi 2p_{1/2}$ subshell, while the major neutron shell is closed at N=50 in ^{90}Zr, and the $\nu 2d_{5/2}$ subshell is closed at N=56 in ^{96}Zr. Between ^{90}Zr and ^{96}Zr, the low excitation structure is expected to be dominated by neutron $2d_{5/2}$ configurations. The large energy separation due to the presence of shell gaps prevents a static octupole deformation, hence in such nuclei only vibrations are expected to occur, with a large E3 strength concentrated at the lowest 3^- state. The stretched $\pi 2p_{3/2} \rightarrow \pi 1g_{9/2}$ and $\nu 2d_{5/2} \rightarrow \nu 1h_{11/2}$ transitions are responsible for the octupole collectivity in the 28-50 and 50-82 shells, respectively.

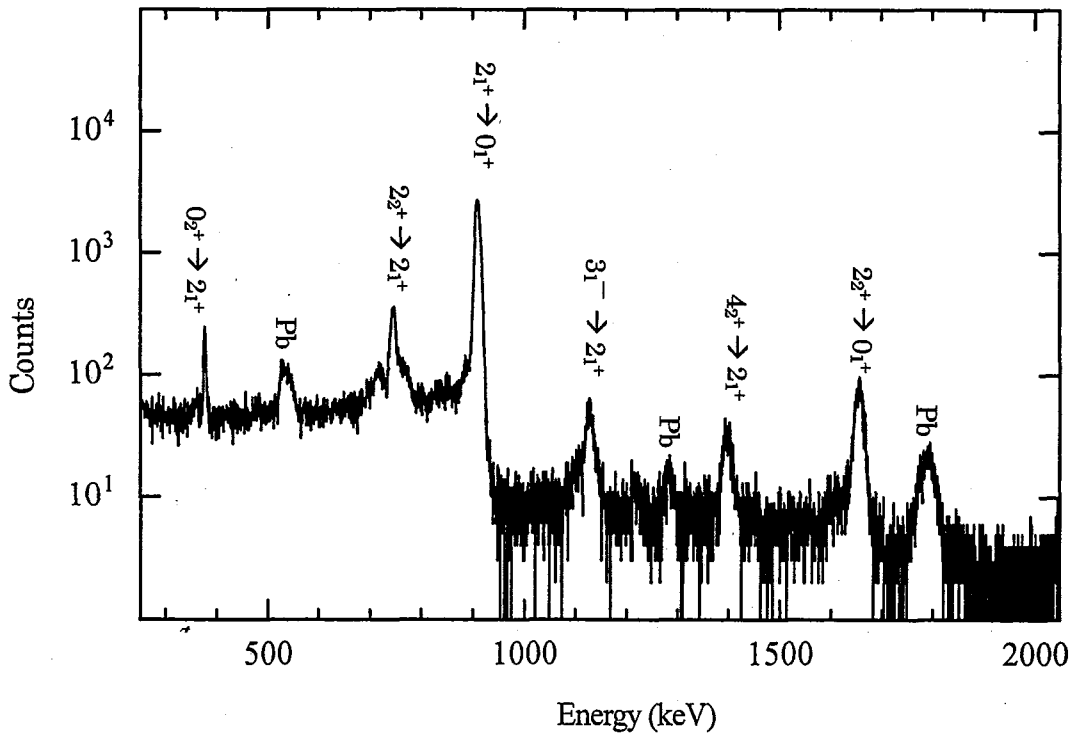

Fig. 1. Doppler-shift corrected γ-ray spectrum of ^{94}Zr Coulomb excitation experiment.

[1]Chiba University
[2]Chiba Institute of Technology
[3]Kyushu University

The ^{94}Zr beam with 300 MeV from the tandem accelerator at the Japan Atomic Energy Research Institute (JAERI) was excited on a self-supporting ^{nat}Pb target of 1.7mg/cm^2 thickness. The γ-ray detector array, GEMINI[3], consisting of 12 HPGe detectors with BGO anti-Compton suppressor shields was used to detect deexcitation γ-rays. A typical energy resolution of the Ge detectors was about 2.2 keV FWHM for the 1.3 MeV γ-rays from ^{60}Co. The Ge detectors were placed at 32°, 58°, 90°, 122° and 148° relative to the incident beam. The scattered beam (^{94}Zr) was detected with a position-sensitive particle detector system[4] with 4 photomultiplier tubes in combination with 2 plastic and 2 Yap Ce scintillators. It covered about 30% of the total solid angle (θ =20° to 67° and 113° to 160°), and the positional resolution was 1.2 mm FWHM near the edge of the detector and 0.5 mm at the center. The information on the particle position was used for Doppler-shift corrections of the γ-rays from ^{94}Zr, simultaneously providing the impact-parameter dependence of the measured γ-transitions. The experimental data were recorded event by event on magnetic tapes when one HPGe detector and one particle detector gave coincident signals.

In ^{94}Zr levels, the 3$^-$ state at 2.1MeV was previously observed in light-ion experiment. An analysis of the Coulomb excitation data using the least-squares search code GOSIA was made to determine E2 and E3 matrix elements. The lifetime, branching ratio and mixing ratio data from other works were included in this analysis. The experimental B(E3) value for the $3_1^- \rightarrow 0_1^+$ transition is seen to be rather large. Further theoretical and experimental studies are needed to elucidate the nature of the 3$^-$ state.

References

[1] D.J. Horen, R. L. Auble, G. R. Satchler, J. R. Beene, I. Y. Lee, C. Y. Wu, D. Cline, M. Devlin, R. Ibbotson, M. W. Simon, Phys. Rev. **C 48**(1993) R2131.

[2] T. Kibedi and R. H. Spear, At. Data Nucl. Data Tables **80**(2002) 35.

[3] K. Furuno, M. Oshima, T. Komatsubara, K. Furutaka, T. Hayakawa, M. Kidera, Y. Hatsukawa, M. Matsuda, S. Mitarai, T. Shizuma, T. Saitoh, N. Hashimoto, H. Kusakari, M. Sugawara, T. Morikawa, Nucl. Instrum. Methods Phys. Res. **A421**(1999) 211.

[4] Y. Toh, M. Oshima, T. Hayakawa, Y. Hatsukawa, J. Katakura, M. Matsuda, H. Iimura, H. Kusakari, D. Nishimiya, M. Sugawara, Y.H. Zhang, Rev. Sci. Instrum.**73**(2002) 47.

JP0650017

2.3 IN-BEAM γ-RAY SPECTROSCOPY OF THE NEUTRON-RICH NUCLEUS ^{240}U

T. ISHII, S. SHIGEMATSU[1], M. ASAI, A. MAKISHIMA[2], M. MATSUDA, J. KANEKO[1], I. HOSSAIN[3], S. ICHIKAWA, T. KOHNO[1] and M. OGAWA[1]

We have measured γ rays in a neutron-rich nucleus of ^{240}U for the first time. The ^{240}U nuclei were produced by the two-neutron-transfer reaction of a 200-MeV ^{18}O beam with a ^{238}U target. Outgoing nuclei were detected with four sets of Si ΔE-E detectors of 20 mm in diameter, placed at 28° with respect to the beam axis, and γ rays emitted by residual nuclei were measured by seven Ge detectors in coincidence with the outgoing nuclei. A E-ΔE plot obtained in the experiment is shown in Fig. 1. Outgoing nuclei were separated not only by the atomic number but by the mass number. The spectra in Fig. 2(a) was obtained by setting the gate on ^{16}O whose total energy E was between 189 and 183 MeV (referred to as a in Fig. 1). Since the incident energy of ^{16}O onto the Si detector is 189 MeV for the ground-state reaction, the decrement of a kinetic energy of ^{16}O, 189MeV $- E$, corresponds to the excitation energy of ^{240}U. The neutron separation energy of ^{240}U is 5.9 MeV. Therefore, ^{240}U nuclei produced by the reaction for the 189-183 MeV range emit no neutrons. Gamma-ray spectra in Figs. 2 (b) and (c) were obtained by the gates of ^{16}O with 183-177 MeV and 177-171 MeV (referred to as b and c in Fig. 1), respectively. The reactions for these energy ranges excite ^{240}U nuclei high enough to evaporate one and two neutrons, respectively. Thus, γ rays in ^{240}U, ^{239}U, and ^{238}U were observed distinctly in Fig. 2.

As shown in Fig. 2(a), γ transitions in the ground-state band of ^{240}U were clearly observed. These γ rays were coincident with each other. Furthermore, interband transitions from the $K^\pi = 0^-$ octupole band to the ground-state band were observed. A level scheme of ^{240}U is shown in Fig. 3. The ground-state band and the $K^\pi = 0^-$ octupole band were established up to 12^+ and 9^-, respectively.

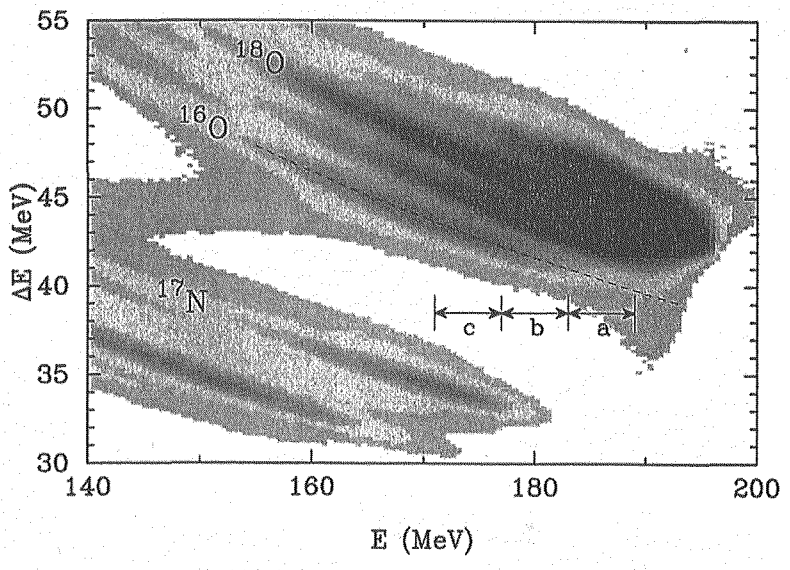

Fig. 1. E-ΔE plot measured by a Si ΔE-E detector in the reaction of a 200-MeV ^{18}O beam with a ^{238}U target. The dashed line represents a calculated energy loss for ^{16}O particles. See the caption of Fig. 2 for the energy ranges of a, b, and c.

[1]Tokyo Institute of Technology
[2]Department of Liberal Arts and Sciences, National Defense Medical College
[3]Department of Physics, Seoul National University

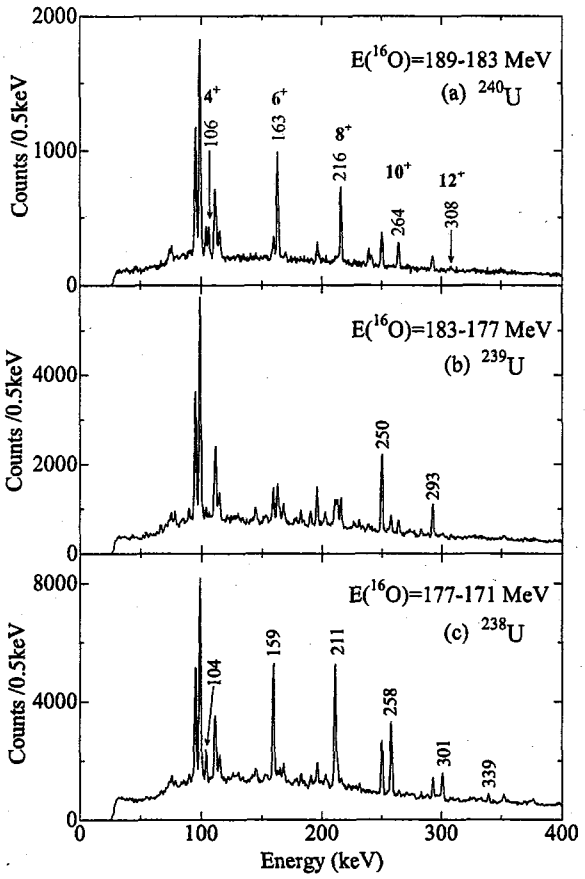

Fig. 2. Gamma-ray spectra obtained by setting the gates on ^{16}O whose total energies are (a) 189-183 MeV, (b) 183-177 MeV, and (c) 177-171 MeV, respectively. These energy ranges are depicted in Fig. 1. Gamma peaks labeled by energies in the spectrum of (a), (b), and (c) are the transitions in ^{240}U, ^{239}U, and ^{238}U, respectively.

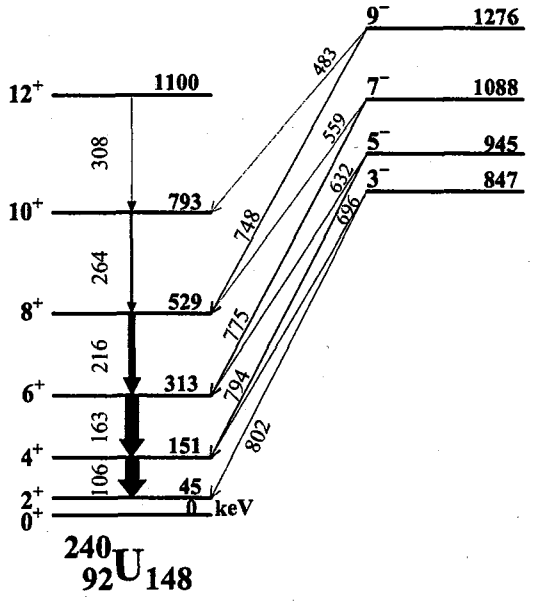

Fig. 3. A level scheme of ^{240}U. The energy of 45(1) keV for the 2^+ level was taken from Ref. 1.

References

[1] B.B. Back *et al.*, Nucl. Phys. **A217** (1973) 116.

JP0650018

2.4 NUCLEAR ISOMERS IN THE Hf-W-Os REGION STUDIED WITH DEEP INELASTIC COLLISIONS

T. SHIZUMA, T. HAYAKAWA, S. MITARAI[1],
T. MORIKAWA[1], T. ISHII

Nuclei in the $A \approx 180$ region are characterized by many high-Ω orbitals close to both the proton and neutron Fermi surfaces [1]. High-$K(=\sum\Omega)$ multi-quasiparticle states formed by stretched coupling of these high-Ω quasiparticles compete with collectively excited states near a yrast line. Transitions depopulating such states often require large K changes, low transition energies, parity change, or combination of these, resulting in the initial state to be an isomer with a comparatively long half-life. However, high-spin studies of the heavier Hf-W-Os nuclei have been limited due to inaccessibility by a fusion-evaporation reaction in combination of stable projectile and target material. In order to populate excited states of these nuclei, we employed nuclear reaction with deep inelastic collisions.

The experiments were carried out at the JAERI tandem and booster accelerator facility. Self-supporting targets of enriched ^{186}W and natural Ta with thickness of 900 μg/cm^2 and 3 mg/cm^2, respectively, were bombarded by a 630 MeV ^{82}Se beam. Projectile fragments were detected by an annular silicon detector, while delayed γ rays emitted by target fragments were measured with four HP Ge detectors using the so-called recoil shadow method. Events were recorded on magnetic tapes when the silicon detector and one or more Ge detectors were fired in coincidence.

Figure 1 shows a partial level scheme of ^{187}W deduced from the present experimental data. A new isomer at 411 keV has been identified. The half-life of the state was found to be 1.55(13) μs. From the comparison with the neighboring nuclei, we assigned the Nilsson configuration of $11/2^+[615]$ to this isomer. A part of the results of the present experiment has been published elsewhere [2].

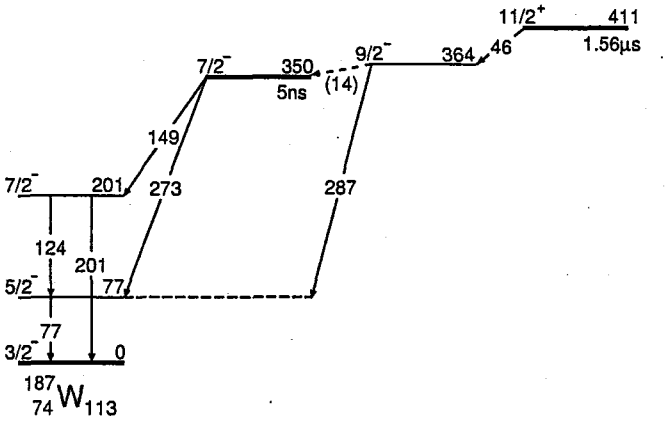

Fig.1 A partial level scheme of ^{187}W.

References

[1] P.M. Walker and G.D. Dracoulis, Nature (London) **399**, 35 (1999).

[2] T. Shizuma *et al.*, Phys. Rev. C, in press (2005).

[1]Kyushu University

JP0650019

2.5 NUCLEAR STRUCTURE OF ^{144}Dy

M. SUGAWARA[1], Y. TOH, M. OSHIMA, M. KOIZUMI, A. OSA,
J. GOTO, A. KIMURA, Y. HATSUKAWA, H. KUSAKARI[2],
Y. H. ZHANG[3], X. H. ZHOU[3], Y. X. GUO[3] and M. L. LIU[3]

In this decade the rotational-like bands consisting of stretched dipole transitions have been observed systematically near the spherical region and interpreted as magnetic rotors. Moreover it was also suggested by Frauendorf[1] that an anti-magnetic rotor might be observed. The anti-magnetic rotor, in which each angular momentum of the proton holes (particles) was coupled to the angular momentum of the neutron particles (holes) with ±90° so as to produce no transverse magnetic moment, was thought to manifest itself as a ΔI=2 band of definite signature which was regular but had very small $B(E2)$ values, and the quests were started at some laboratories. However, there has been only one example of ^{110}Cd known to date for the anti-magnetic rotor, and thus the systematic study is desirable. In the ^{110}Cd case the relevant neutron and proton configurations to create the anti-magnetic rotor are $\nu h_{11/2}^{2}$ and $\pi g_{9/2}^{-2}$ respectively. Here we direct our attention to the ^{144}Dy nucleus which has $\pi h_{11/2}^{2}$ and $\nu h_{11/2}^{-2}$ configurations appropriate for forming the anti-magnetic rotor.

In-beam γ-ray spectroscopy was made on ^{144}Dy through the reaction of ^{92}Mo(^{56}Fe, 2p2n). An enriched ^{92}Mo foil of 7 mg/cm^2 thickness was bombarded with an ^{56}Fe beam of 280 MeV. Emitted γ-rays were detected with an array of 16 HPGe detectors with BGO Compton suppressors and 3 LOAX detectors without BGO shields (GEMINI-II). Total events of 7.0×10^{8} were collected for 3 days of beam time.

Prior to this work, the experimental information was very limited; the ground state band up to the (8^+) state and the existence of three γ-cascades were only known. Two of the three were placed on top of the (8^+) state and the other was arranged to feed into the (4^+) state in the level scheme neither with any spin assignments[2]. Although the data analysis is still in progress, the present results from our data are summarized as follows. Even and odd parity states are extended up to 18^+ and (19^-) states respectively. It is likely that two of the three quadrupole cascades above 10^+ state and one dipole cascade placed upon the negative parity side band are promising candidates for the anti-magnetic rotors and the magnetic rotor respectively.

References

[1] S. Frauendorf, Rev. Mod. Phys. **Vol. 73 No. 2**(2001)463.
[2] National Nuclear Data Center, Brookhaven National Laboratory.

---

[1]Chiba Institute of Technology
[2]Chiba University
[3]Institute of Modern Physics, China

JP0650020

2.6 MEASUREMENT OF β -DECAY ENERGIES USING TOTAL ABSORPTION BGO DETECTOR

H. HAYASHI[1], M. SHIBATA[2], K. KAWADE[1], M. ASAI, T. K. SATO, S. ICHIKAWA, A. OSA, K.TSUKADA, I. NISHINAKA, Y. NAGAME, Y. KOJIMA[3] and A.TANIGUCHI[4]

Measurements of atomic masses of nuclei far from the β-stability line are the most important to check the validity of mass predictions based on various nuclear models. One of the precise methods to determine the atomic masses is to measure β-decay energies (Q_β). A total absorption BGO detector was developed and Q_βs of neutron-rich isotopes were measured without the knowledge of the decay schemes [1-3]. Using the conventional root plot method, the Q_βs were determined with accuracy of about 100 keV. In the present work, more reliable and precise procedure to deduce the Q_βs was studied.

The nuclei of interest were produced with the ^{238}U(p,*f*) reaction by 32 MeV protons and separated by an on-line mass separator (JAERI-ISOL). Radioactive beams were collected on an aluminized Mylar tape in a tape transport system, and moved to a center of the detector after predetermined collecting times. Details of measurement systems and performances of the total absorption BGO detector had been reported [1-3]. Twelve nuclei having precisely measured and well evaluated Q_βs were measured and newly observed ^{162}Eu was measured.

The measured spectra were unfolded with response functions having Gaussian shapes corresponding energy resolution. By assuming a virtual level to which all β-rays feed, Fermi-Kurie plots were applied to the unfolded spectra so as to show a longer straight line as long as possible. In ^{91}Rb as shown in Fig. 1, the ground state (B), a 2500 keV level (C), or a 3500 keV level (D) were assumed as the virtual state. The Fermi-Kurie plot of (C) shows a much longer straight line than the others. Moreover, allowed- or first forbidden-transition shapes were assumed, then a much longer straight line was obtained with the first forbidden. As the result, the Q_β of ^{91}Rb was determined from the Fermi-Kurie plot of (C) with the first forbidden. The Q_βs of the twelve nuclei were deduced with this procedure. As shown in Fig. 2, the reliability of the procedure was confirmed by a comparison between the experimental Q_βs and evaluated ones [5]. It shows this analyzing procedure could deduce Q_βs with the systematic uncertainty of 60 keV, approximately, in the energy range of 2 to 10 MeV. This uncertainty was smaller than the value of 100 keV obtained from the conventional root plot method.

The Fermi-Kurie plot method was applied to analyze a total absorption spectrum of ^{162}Eu, of which no decay scheme was reported, as shown in the inset of Fig. 2. The Q_β of ^{162}Eu was obtained to be 5570(61) keV for the first time. The value is in agreement with the Audi's systematics of 5640(300)

[1]Graduate School of Engineering, Nagoya University
[2]Radioisotope Research Center, Nagoya University
[3]Graduate School of Engineering, Hiroshima University
[4]Research Reactor Institute, Kyoto University

keV [5], the theoretical ones of 5580 keV [6] and 5640 keV [7]. We plan to measure Q_βs of neutron-rich rare-earth isotopes such as $^{163\text{-}166}$Eu using JAERI-ISOL.

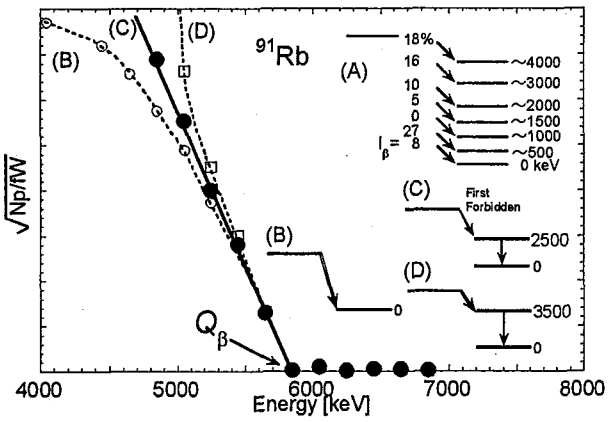

Fig. 1. Open circles, closed circles and open squares are Fermi-Kurie plots of ^{91}Rb according to the assumed virtual levels of (B), (C) and (D), respectively. (A) is the simplified decay scheme that is reported by ref.[4].

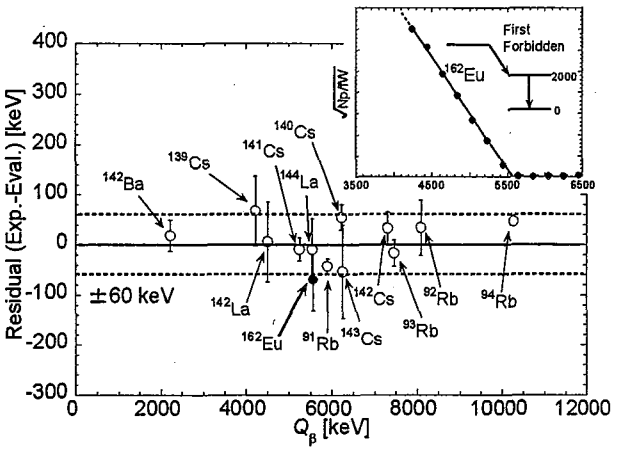

Fig. 2. Comparisons between experimental Q_β and evaluated ones. Open circles and the closed circle are the nuclei that Q_βs are well evaluated and newly observed one, respectively. The inset shows the Fermi-Kurie plot of ^{162}Eu.

References

[1] M. Shibata *et al.*, Nucl. Instrum. Method. **A 459**, (2001) 581.
[2] M. Shibata *et al.*, J. Phys. Soci. Jpn. **71**, (2002) 1401.
[3] M. Shibata *et al.*, JAERI-Review 2003-028, 32.
[4] Coral M. Baglin *et al.*, Nucl. Data Sheets **86**, (1999) 1.
[5] G. Audi *et al.*, Nucl. Phys. **A729**, (2003) 337.
[6] H. Koura *et al.*, RIKEN Accel. Prog. Rep. **36** (2003) 9.
[7] P. Möller et al., At. Data Nucl. Data Tables **59**, (1995) 185.

2.7 IN-BEAM GAMMA-RAY SPECTROSCOPY OF ^{53}Fe

T. MORIKAWA[1], H. KUSAKARI[2], M. OSHIMA, Y. TOH, M. KOIZUMI,
A. KIMURA, J. GOTO, A. OSA, Y. HATSUKAWA, J. KATAKURA,
M. NAKAMURA, and M. SUGAWARA[3]

In the three particle (hole) nuclei of $f_{7/2}$ shell such as ^{43}Sc and ^{53}Fe, there exist the $J^\pi = 19/2^-$ high-spin isomer as the terminating state of $\pi\{1f_{7/2}\}^{1(-2)} \otimes \nu\{1f_{7/2}\}^{2(-1)}$ structure. Since these high-spin isomers are expected to possess a sizable deformation, one would naively expect a collective rotation built on the isomer. Although such a unique nuclear motion has not been known, search of such a state is very interesting. Recently, we have investigated the high-spin yrast structure of ^{43}Sc [1]. A low-energy transition feeding to the high-spin isomer has been newly identified, which could be attributed to a collective excitation of the isomer; the lowness of the transition energy, by comparing with the shell-model calculations, suggests some contribution due to the single-particle orbit(s) other than $\{1f2p\}$ and/or large deformation. To investigate further the high-spin states around/above the '3-particle' isomer and the role of such single-particle orbit(s) in these state, we performed the experiment for ^{53}Fe nucleus which is the particle-hole conjugate of ^{43}Sc nucleus.

The experiment was carried out at the Japan Atomic Energy Research Institute (JAERI). A target of 5.3 mg/cm^2 ^{nat}Ca evaporated on the 7.6 mg/cm^2 Pb backing was bombarded by the 58 MeV ^{16}O beam delivered from the JAERI tandem accelerator. The γ-rays were detected with the GEMINI-II array [2] consisting of 16 HP-Ge detectors with BGO anti-Compton shields. The data acquisition system was triggered by two-fold $\gamma\gamma$ coincidence event in the $\pm$800 ns time window. Our data confirms the all yrast members of $\{f_{7/2}\}^{-3}$ multiplet, including the $J^\pi = 15/2^-$ at 3463 keV and $J^\pi = 17/2^-$ at 4005 keV which have been identified in [3]. In addition, some fast transitions feeding to the $J^\pi = 15/2^-$ and $J^\pi = 17/2^-$ states were newly identified. The data analysis is still in progress.

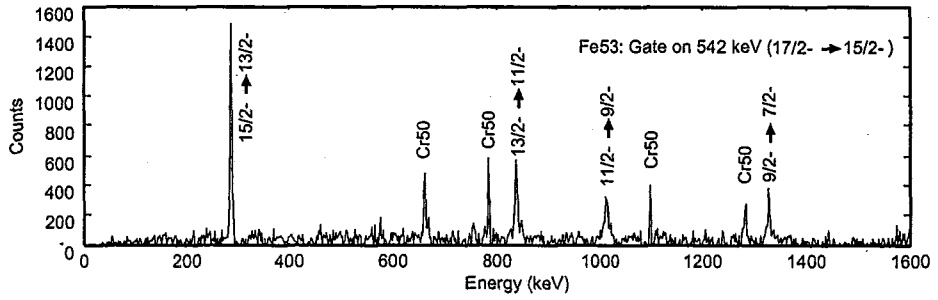

Fig. 1. γ-ray spectrum gated by the 542 keV peak corresponding to the $J^\pi = 17/2^- \rightarrow 15/2^-$ transition in ^{53}Fe. The yrast cascade in ^{53}Fe is seen together with contaminant ^{50}Cr transitions.

References

[1] T. Morikawa et al., Phys. Rev. C **70** (2004) 054323, and references therein.
[2] K. Furuno et al., Nucl. Instrum. Methods **A421** (1999) 211.
[3] S. J. Williams et al., Phys. Rev. C **68** (2003) 011301.

[1]Department of Physics, Kyushu University
[2]Faculty of Education, Chiba University
[3]Chiba Institute of Technology

2.8 VELOCITY DISTRIBUTIONS OF LASER-ABLATED ATOMS FOR LASER SPECTROSCOPY OF RADIOACTIVE NUCLIDES

H. IIMURA, H. WANG[1], H. OHBA, M. SAEKI, M. MIYABE, T. SHIBATA, and H. MIYATAKE[1]

Laser ablation can produce an atomic beam for laser spectroscopy of refractory elements which are not accessible via normal resistance heating method. To apply this technique to radioactive isotopes, it is, however, necessary to improve the sensitivity. A way to achieve the high sensitivity is to use a resonance photo-ionization method with a neutral atomic beam. In this method, the charged ions generated by laser ablation simultaneously with the neutral atoms are background and have to be separated. For this purpose, the difference of velocity distributions between the neutral atoms and ions could be used. So far, however, few measurements have been made to clarify the velocity distribution. In this work, we measured the velocity distribution of atoms generated by laser ablation of a solid target.

The target sample was a neodymium metallic disk. A second harmonic beam from a Nd:YAG laser was focused on the target. With a proper time delay, a XeCl excimer-pumped dye laser beam was introduced perpendicularly to the laser ablation plume. This dye-laser beam passed at a distance of 10 mm above the target. The delay of the dye laser pulse with respect to the YAG laser pulse was varied using a digital pulse generator. The repetition rate of both lasers was 10 Hz. The laser-induced fluorescence (LIF) of Nd atoms was collected by a lens system and transferred to a photomultiplier tube through an optical fiber. A monochromator was used to observe the fluorescence of a specific deexcitation transition. The flux of the ablated atoms was calibrated roughly with a Langmuir probe.

The velocity distributions of neutral and ionized Nd atoms were measured by observing the intensity of LIF as a function of the time delay between the dye laser and the YAG laser. Figure 1 illustrates the temporal evolution of the LIF signal of Nd and Nd^+ under various vacuum conditions. The mean velocities deduced from the peak positions of these curves in a vacuum are 5.3 km/s for neutral atoms, and 7.7 km/s for singly charged ions. The velocity of charged ions is higher than that of the neutral atoms. This could be explained by the Coulomb interaction, i.e., pulling of the outer electrons that were emitted earlier during ablation. It was also found that the difference in the velocity increases with increasing gas pressure. As compared with Ar, He has a weaker effect on reducing the velocities of the ejected ions. It is interesting to notice the change in the fluorescence intensity and in peak shape between the cases of neutral atoms and ions. This is very likely to be due to neutralization of ions through collisions with the gas atoms. Argon has a large mass number, and hence contributes more to the neutralization process compared to helium.

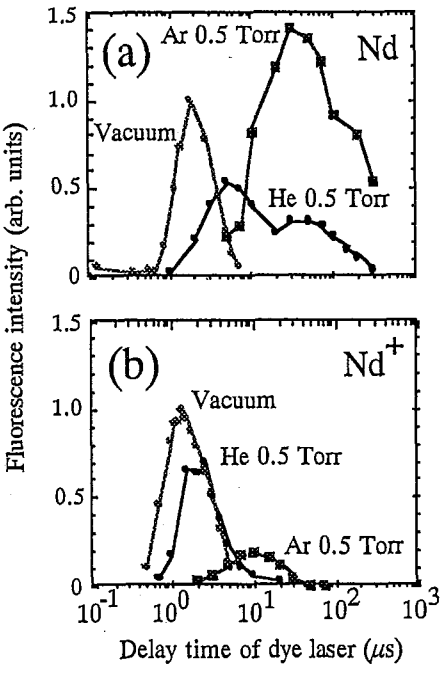

Fig. 1. Temporal evolution of the fluorescence intensities of Nd(a) and Nd^+(b) measured with LIF method in a vacuum and in 0.5 Torr of Ar and He ambient gas.

The ions in the laser ablation plume is to be background when the laser ablation is applied to a resonance photo-ionization spectroscopy. The charge dependence of the velocity distribution found here offers one possible solution for separating the neutral atoms from the charged ions. This is particularly favorable in a gas environment. These data are also important when one performs LIF spectroscopy of radioactive nuclides by using laser ablation.

[1]Institute of Particle and Nuclear Studies, KEK

JP0650023

2.9 LEVEL STRUCTURE OF ^{146}Tb

C.Y. XIE[1], X.H. ZHOU[1], Y. ZHENG[1], Y.H. ZHANG[1], Z. LIU[1], Z.G. GAN[1], T. HAYAKAWA, M. OSHIMA, Y. TOH, T. SHIZUMA, J. KATAKURA, Y. HATSUKAWA, M. MATSUDA, H. KUSAKARI[2], M. SUGAWARA[3], K. FURUNO[4] and T. KOMATSUBARA[4]

The doubly odd nucleus ^{146}Tb has one proton-particle and one neutron-hole with respect to the doubly closed nucleus ^{146}Gd, and its high-spin states should be formed by excitations of valence nucleons. The low-lying states in ^{146}Tb are due to the couplings of one proton-particle with one neutron-hole outside ^{146}Gd. A number of such low-lying states have been identified in the previous in-beam studies [1,2] and in the β-decay studies of ^{146}Dy [3]. These low-lying energy levels can provide important information on the two-body residual interactions between proton-particle and neutron-hole. The higher-lying states should arise from the coupling of the valence proton-particle and neutron-hole to the excitations of the ^{146}Gd core. Here we report on a level scheme for ^{146}Tb up to an excitation energy of 8.39 MeV.

We used the ^{118}Sn(^{32}S, 1p3n) ^{146}Tb reaction to populate the excited states in ^{146}Tb. The ^{32}S beam was provided by the tandem accelerator. The target was an enriched ^{118}Sn metallic foil of 1.8 mg/cm^2 thickness with a 5 mg/cm^2 Pb backing. At the beam energy of 165 MeV, X-γ and γ-γ-t coincidence measurements were carried out with 12 BGO(AC)HPGe detectors, having energy resolutions of 1.9-2.3 keV at 1.33 MeV. To obtain γ-ray anisotropies, these detectors were divided into 3 groups positioned at 32° (148°), 58° (122°), and 90° with respect to the beam direction. Typical γ-ray anisotropies observed for the known γ-rays in this experiment were 1.25 for stretched quadrupole transitions and 0.75 for stretched pure dipole transitions. Therefore we assigned the stretched quadrupole transition and stretched dipole transition to the γ-rays of ^{146}Tb with anisotropies around 1.25 and 0.75, respectively.

Assignments of the observed γ-rays to ^{146}Tb were made based on the coincidence relationships with the known γ-rays [2], and the level scheme of ^{146}Tb is extended up to an excitation energy of 8.39 MeV as shown in Fig. 1, including 41 new γ-rays de-exciting 27 new levels. The spins have been proposed according to the results of the γ-ray anisotropies and the previous conversion coefficient measurements [2].

The level scheme of ^{146}Tb displays irregular level spacings and many parallel decay branches, indicating that the excited states are formed primarily by the excitations of valence nucleons. The ground state in ^{146}Tb has spin and parity of 5$^-$, and its configuration should be the admixture of

---

[1] Institute of Modern Physics, China
[2] Chiba University
[3] Chiba Institute of Technology
[4] University of Tsukuba

the $\pi h_{11/2}\nu d_{3/2}^{-1}$ and $\pi h_{11/2}\nu s_{1/2}^{-1}$ configurations [4,5]. The low-lying states in ^{146}Tb have been well studied, and their configurations have been assigned based on shell model calculations [1,5]. The 10^+ and 11^+ yrast levels were interpreted to be the highest-angular- momentum members of the $\pi h_{11/2}\nu h_{11/2}^{-1}$ multiplet [2]. Obviously, the states above the 11^+ level should involve the excitations of the ^{146}Gd core. In ^{146}Gd, the first-excited state is the 3^- octupole state at 1579 keV, and the octupole excitation was suggested to have the main proton $h_{11/2}d_{3/2}^{-1}$ configuration with the admixture from the neutron $f_{7/2}s_{1/2}^{-1}$ and $h_{9/2}d_{3/2}^{-1}$ contributions [6,7]. Therefore, one would expect in ^{146}Tb a multiplet of negative-parity states of $\pi h_{11/2}\nu h_{11/2}^{-1} \otimes 3^-$ character at excitation energies around 2.5 MeV. The 10^-, 11^-, 12^-, and 13^- levels were suggested to be the members of the $\pi h_{11/2}\nu h_{11/2}^{-1} \otimes 3^-$ septuplet [2]. Further discussions on the configurations at high spins are described in ref. [8].

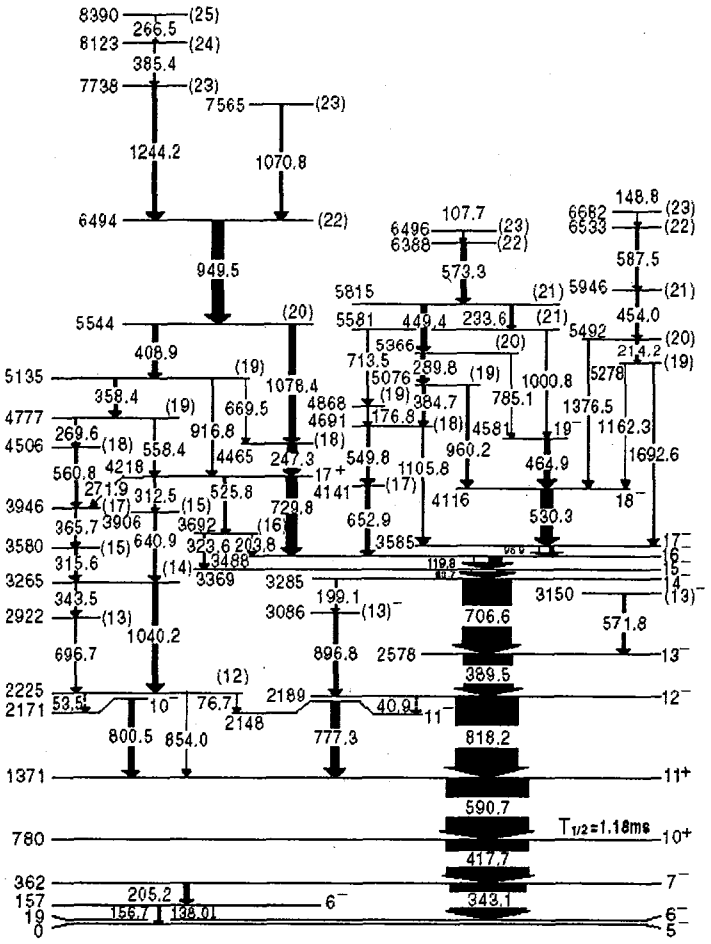

Fig. 1. Level scheme of ^{146}Tb deduced from the present work. The widths of the arrows indicate the relative transition intensities.

References

[1] R. Broda et al.. Z. Phys. A 316, 125 (1984).
[2] R. Collatz et al., Z. Phys. A 359, 113 (1997).
[3] K. Zuber et al., Z. Phys. A 327, 357 (1987).
[4] J. Styczen et al., Proceedings of the Fourth International Conference on Nuclei Far from Stability. Helsingor. Denmark. 7-13 June 1981, Vol. 2 (CERN 81-09, 1981) p. 548.
[5] R. Broda et al., Z. Phys. A 334, 11 (1989).
[6] P. Kleinheinz et al., Z. Phys. A 286, 27 (1978).
[7] S.W. Yates et al., Z. Phys. A 324, 417 (1986).
[8] C.Y. Xie et al., Eur. Phys. J. A19, 7 (2004).

JP0650024

2.10 COULOMB EXCITATION EXPERIMENT WITH INVERSE KINEMATICS

M. KOIZUMI, Y. TOH, M. OSHIMA, A. OSA, A. KIMURA, Y. HATSUKAWA

Coulomb excitation is a useful method to determine electromagnetic properties near the ground state of nuclei [1,2]. The information gives various clues for understanding the low-lying structures. Systematic study revealed nuclear properties and evolutions of nuclear structure [3-10]. We are planning to explore the systematic study beyond the stability with TRIAC facility [11].

Although the method of projectile Coulomb excitation developed at JAERI succeeded for some studies [3-10], it could not be directly applied to the study of radioactive nuclei because scattered radioactive particles will be a source of strong back ground γ-radiation. To avoid the accumulation, inverse kinematics will be a suitable method. The incident beam are scattered forward, and they pass the target chamber through a small opening. For example, the maximum scattering angle is less than 10°, when one use an incident beam of ^{70}Zn and a carbon target.

In order to determine the electromagnetic properties of nucleus, the correlation between Coulomb excitation probability (i.e., de-excitation γ-ray yield) and impact parameter (i.e., recoil angle or scattering angle) should be measured. A particle detector system, therefore, plays an important role in the experiments. Thus, we are developing a particle detector system with position sensitive detectors (PSDs), which is easier to handle than segmented particle detectors. A position sensitive photomultiplier (PS-PMT) and a Si-PSD have been tested. The PSDs were set in a small chamber (about 10 cm in diameter) and placed at the center of the Ge detector array GEMINI-II [12]. In this study, we used 140-MeV ^{70}Zn beam and 150-MeV ^{74}Ge beam. A target of 100-μg/cm^2 carbon was used. Fig. 1 shows calculated kinetic energies of recoiled carbon for each recoil angle, where the incident beam is ^{70}Zn with an energy of 140-MeV and the target is carbon with a thickness of 100 μg/cm^2. The lines connect energies assuming the target is recoiled at the same depth in the carbon target. The kinetic energy of the recoiled particle decreases as the recoil angle increases.

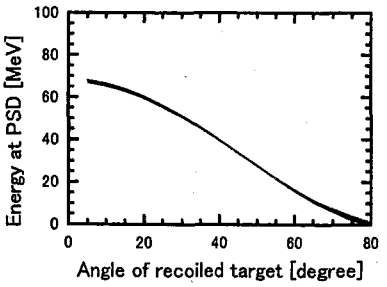

Fig. 1. Kinetic energy of recoiled carbon.

The PS-PMT was a product of Hamamatsu Photonics K.K. (R5900) covered with a scintillator sheet. The size of the PS-PMT is a 28-mm × 28-mm square × 20-mm height with a 22-mm × 22-mm square photocathode. A 5-mm-square wire-grid made up of about 1-mm-width wire was placed in front of the PS-PMT to refer the location. Fig. 2 (a) gives an example of the 2D position spectrum. The position resolution was 0.5-1.0 mm, which is much better than that of the Si-PSD mentioned below. Fig. 2 (b) is a 2D plot of pulse height of PSD v.s. recoil angle in laboratory system. It can be seen that the pulse heights from the area near the center of the detector were higher than those near the edge. The maximum angle for detecting the recoiled particle was 50-55°. Although the cross-section of the Rutherford scattering increases as the recoil angle increase, the particle number detected at the large recoil angle does not increase. This is due to the low kinetic energy of the recoiled particle at larger recoil angle as seen in Fig. 1. With the PS-PMT, we tested some scintillation detectors: a 0.1-mm-thick plastic scintillator, a 0.5-mm-thick YAP-Ce scintillator, and a 0.5-mm-thick LYSO scintillator. We found no

significant differences between those scintillation detectors. After about 1-pnA × 40-h irradiation, we observed no critical radiation damage on the scintillation detectors.

The Si-PSD tested was a product of Hamamatsu Photonics K.K. (S5378) with a large detection area of 45 × 45 mm. The ion beam was 150-MeV $^{74}Ge^{10+}$ with a current of about 0.1 pnA. The position resolution for a recoil angle around 20° was about 1-1.5 mm or worse. Position signal of particles with recoil angle more than 45° was not resolved. After about 4-hour irradiation, the particle signal of recoil angle less than 35° was vanished. This would be caused by the radiation damage on the detector. As seen in Fig. 1, energy deposition on the detector is larger at small recoil angle than that of large recoil angle. The Si-PSD is not suitable for this kind of experiments.

In conclusion, we decided to use the PS-PMT for RI-beam Coulomb excitation experiments. Coincidence events of de-excitation γ-rays and recoiled particles were also taken during the particle detector tests mentioned above. Analysis of the data is in progress. It should be proved that the method is feasible for RI-beam experiments. If the method is found to be efficient, we could apply this method to the study of nuclear structure of stable nuclei as well.

(a) (b)

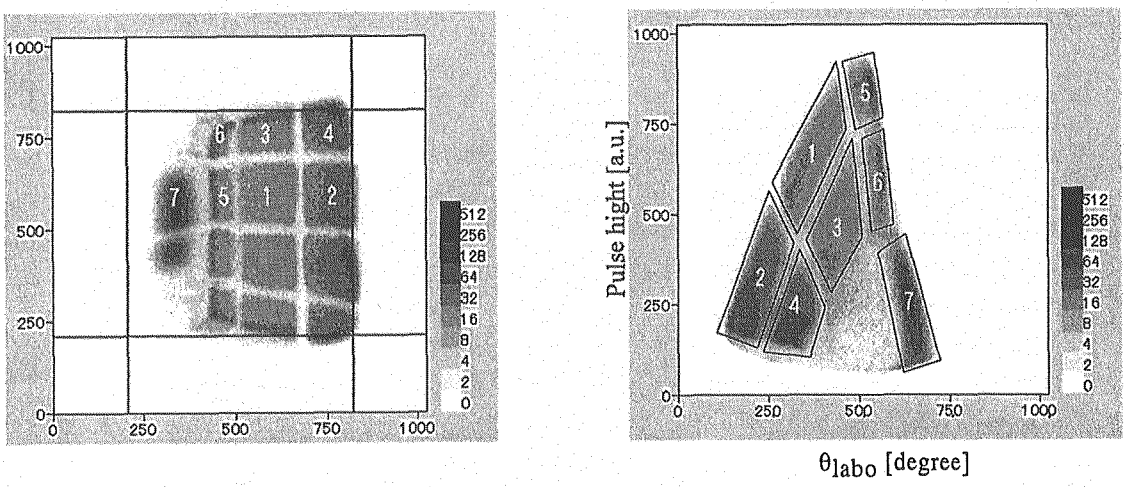

Fig. 2. (a) 2D position spectra. The numbers indicates area number. (b) 2D plot of pulse height v.s. recoiled angle θ_{lab}. The squares correspond to the areas numbered in (a). The area 7 would originate from the back ground noise.

References

[1] K. Alder and A. Winther, Coulomb Excitation (Academic, NewYork, 1966).
[2] K. Alder and A. Winther, Electromagnetic Excitation (North Holland, Amsterdam, 1975).
[3] Y. Toh et al., J. Phys. G **27** (2001) 1475.
[4] Y. Toh et al., Eur. Phys. J. A **9** (2000) 353.
[5] A. Osa, T. Czosnyka, et al., Phys. Lett. B **546** (2002) 48.
[6] M. Zielinska, T. Czosnyka, et al., Nucl. Phys. A **712** (2002) 3.
[7] M. Koizumi, A. Seki, Y. Toh, et al., Eur. Phys. J. A **18** (2003) 87.
[8] M.Sugawara et al., Eur. Phys. J. A **16** (2003) 409.
[9] M. Koizumi, et al., Nucl. Phys. A **736** (2003) 46.
[10] T. Hayakawa, et al., Phys. Rev. C **67** (2003) 064310.
[11] H. Miyatake, et. al., NIM B **204** (2003) 746.
[12] K. Furuno et al., Nucl. Instrum. Methods Phys. Res. A **421** (1999) 211.

3. Nuclear Reactions

This is a blank page.

JP0650025

3.1 EMISSION WAVELENGTH SPECTRA OF CaF_2 SCINTILLATORS BY HEAVY IONS

S.YOSHIDA[1], I. OGAWA[1], S.UMEHARA[1], K.MUKAIDA[1], K.ICHIHARA[1], Y.HIRANO[1], K. MATSUOKA[1], S.MITSUOKA, H.IKEZOE and T.KISHIMOTO[1]

The measurement of neutrino-less double beta($0\nu\beta\beta$) decay is of current interest for the particle physics[1], since neutrinos have distinctive features such as extreme small masses, different mixing properties from quark sector evidenced by the neutrino oscillation experiments[2], and further possibility of being Majorana particle. While the absolute mass scale, being one of the remaining important neutrino properties, can be also given by the spectroscopic measurement on single beta decay, only the discovery of $0\nu\beta\beta$ decay can establish the Majorana nature of neutrino. The measurement of $0\nu\beta\beta$ decay is the realistic experiment to measure the effective Majorana mass in the range of tens meV, so far.
In addition, searching for Weakly Interacting Massive Particles(WIMPs) which may constitute the galactic dark matter are currently being carried out by a number of groups. The direct detection of recoil energy induced by the elastic scattering of WIMPs with target nuclei in the detector[3], enables us to understand the evolution of the universe.
The rate of $0\nu\beta\beta$ decay is expected to be an order of 1 event/10kg/yr of $\beta\beta$ source nuclei. The WIMPs signal rate is also expected to be rare, less than 1 event/day/kg. Thus low background condition and the large scale detector are the crucial requirements for these purposes. CANDLES and ELEGANT VI detectors are suitable for these studies. CANDLES is the binary scintillators complex system, where a large number of undoped CaF_2(CaF_2(pure)) scintillators are immersed in the liquid scintillator[4]. ELEGANT VI system consists of CaF_2(Eu) and CaF_2(pure) scintillators complex[5].
The signals of $0\nu\beta\beta$ decay have the peak at Q-value energy by two electrons, on the other hand the WIMPs signals are due to the nuclear recoils. The main background origins of $0\nu\beta\beta$ decay of ^{48}Ca are the sequential signals of β–α events from uranium and thorium chain(^{212}Bi, ^{214}Bi), while the background of WIMPs search are the low energy β, γ, and X-rays. Therefore the sensitivities of the measurements will be much improved by discrimination between signals due to electron and heavy ions(α, nuclear recoil). We have been studying the pulse shape discrimination(PSD) technique of CaF_2(pure) scintillator. There was a certain difference in pulse shape[6]. The background due to α particle can be reduced by two orders of magnitude by using PSD. In order to improve the reduction factor further, and to understand the origin of pulse shape difference, the wavelength spectra emitted by CaF_2(pure) and CaF_2(Eu) have to be measured by using heavy ion beams and γ(X) rays. The purpose of this study is to compare the emission wavelength spectra of CaF_2 scintillators by heavy ions and γ rays.

The measurements of emission wavelength induced by heavy ions were carried out at JAERI tandem accelerator. The proton and lithium ions were used to irradiate scintillators with the energy of 24.0MeV. To investigate the energy dependence of incident particles, the beam energy was decreased to 12.3, 9.7MeV for proton by Al degrader, and 15.6, 11.0MeV for Li by myler. Scintillation photons emitted by

[1] Department of Physics, Osaka University

irradiating heavy ion beams(proton and Li) were measured by portable spectrometer(USB2000, Ocean Optics) through optical fiber. The six samples were measured. Figures 1 shows the obtained emission spectra of CaF_2(pure) scintillator made by Saint-Gobain Co. Ltd. and CaF_2(Eu) scintillator with Eu concentration of 0.037mol%, which are used in CANDLES and ELEGANT VI systems, respectively. The emission spectra by electron(γ-ray) were preliminary measured by using intense ^{60}Co source at Radiation Lab., Institute for Scientific and Industrial Research, Osaka University, to compare with the ones by heavy ions.

There are large differences in emission spectra between electron and lithium ion. There is additional large bump at the longer wavelength(~500nm) in CaF_2(pure) spectrum induced by lithium ion, comparing with the one by electron. There are also differences at longer(~600nm) and shorter(~300nm) wavelength in CaF_2(Eu) spectrum. The property of CaF_2(pure) is emerged in the large LET particles for CaF_2(Eu) scintillator. It should be noted that there is no definite difference in pulse shape of CaF_2(Eu). These differences indicate possibility to identify the particle by wavelength information. The use of photo-diode or multialkali-PMT readout of CaF_2 scintillator enables us to discrimination between alpha and electron signals.

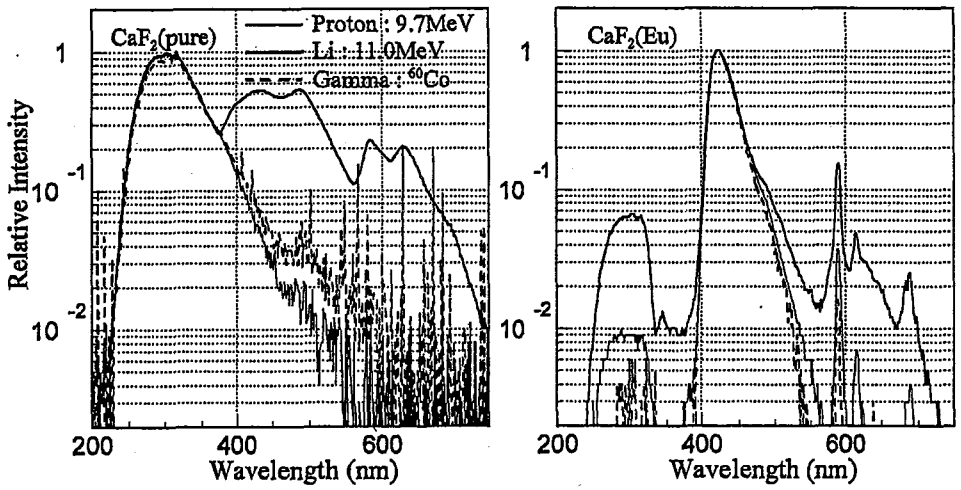

Fig.1 Emission wavelength spectra of CaF_2(pure)(left) and CaF_2(Eu)(right) scintillators, respectively. All of spectra were not corrected by them although the efficiency of spectrometer depends on wavelength, since relative intensities is relevant to the particle identification.

References

[1] M. Doi, T. Kotani and E. Takasugi, Prog. Theor. Phys. Suppl. **85**(1985) 1.

[2] S. Fukuda et al, Phys. Rev. Lett. **86**(2001) 5651, Q.R. Ahmad et al, Phys. Rev. Lett. **89**(2002) 011301, K. Eguchi et al, Phys. Rev. Lett. **90**(2003) 021802, M.H. Ahn et al, Phys. Rev. Lett. **90**(2003) 041801.

[3] A. Drukier, K. Freese and D.N. Spergel, Phys. Rev. **D33**(1986) 3495.

[4] S. Yoshida et al, Nuclear Physics B(Proc. Suppl.) **138**(2005)214--216

[5] Ogawa I. et al, Nuclear Physics A**730**(2004)215.

[6] S. Umehara et al , Proceedings of International Conference on Neutrinos and Dark Matter in Nuclear Physics(NDM03), ppXII-23 (2003).

JP0650026

3.2 MEASUREMENT OF THE ^{8}Li(α, n)^{11}B REACTION AROUND T_9=1

H. ISHIYAMA[1], S. K. DAS[3], T. HASHIMOTO[1], T. ISHIKAWA[2], H. MIYATAKE[1], Y. X. WATANABE[1], Y. HIRAYAMA[1], N. IMAI[1], M. H. TANAKA[1], Y. FUCHI[1], N. YOSHIKAWA[1], S. C. JEONG[1], H. KAWAKAMI[1], I. KATAYAMA[1], T. NOMURA[1], S. MITSUOKA, K. NISHIO, M. MATSUDA, S. ICHIKAWA, H. IKEZOE, T. FURUKAWA[4], H. IZUMI[4], Y. MIZOI[3], M. TERASAWA[5], P. K. SAHA[3], T. FUKUDA[3], K. NAKAI[2], T. SHIMODA[4]

It has been discussed that the r (rapid neutron capture)-process may occur in so-called "hot-bubble" under explosive conditions in the supernova, where nuclear reactions involving light neutron-rich nuclei are expected to play an important role as the r-process starting point [1]. We are trying to obtain systematic nuclear cross section data of (α, n) reactions using low energy (E = 1-2 MeV/u) light neutron-rich radioactive nuclear beams (RNB). The excitation function of the ^{8}Li (α, n) ^{11}B reaction in the energy region of E_{cm} = 0.7 – 2.5 MeV has been already measured at the Tandem facility of JAERI [2-4], followed by a new measurement for the excitation function in the lower energy region around T_9 = 1 (= 10^9 k).

The ^{8}Li-beam was produced via the ^{9}Be (^{7}Li, ^{8}Li) reaction. The produced ^{8}Li-beam was separated from the primary ^{7}Li-beam with the JAERI recoil mass separator (RMS). The energy of ^{8}Li was adjusted to be 12.5 MeV at the exit of the RMS (15.1 MeV in the previous experiment). A detector system consists of a Multi-Sampling and Tracking Proportional Chamber (MSTPC) and a large solid angle neutron detector array. The MSTPC has high detection efficiency of almost 100%, and can measure three-dimensional tracks of charged particles as well as the energy losses along their trajectories. The MSTPC is surrounded by a neutron detector array, which consists of 28 pieces of BC408 plastic scintillators covering 31.4% solid angle of 4π. (See the reference [2] for more details of the experimental setup.) The ^{8}Li-beam was injected into the MSTPC filled with the gas of He + CO_2 (10%) which works as counter gas and gas target. In this experiment, the gas pressure was set to be 140 Torr (220 Torr in the previous experiment) so as to cover the energy region of Ecm = 0.2 – 1.5 MeV. When a nuclear reaction takes place inside the MSTPC, the energy loss (dE/dx) changes largely due to the change of the relevant atomic numbers. Therefore, the reaction position can be determined by detecting the "sudden" dE/dx change (ΔE), and the reaction energy can be evaluated by

[1] Institute of Particle and Nuclear Studies, KEK
[2] Tokyo University of Sciences
[3] Osaka Electro-Communication University
[4] Osaka University
[5] CNS

summing up the energy losses inside the MSTPC. In order to select reaction events, the energy loss difference (ΔE) was set to be 40 keV. The reaction event thus selected was checked with the kinematical conditions by using all information on its reaction energy, scattering angle and the energy of ejected nuclei and neutron.

Fig. 1 shows the reaction energy distribution of the selected ^{8}Li (α, n) ^{11}B reaction events. The excitation function of the ^{8}Li (α, n) ^{11}B reaction can be determined at the energy region of Ecm = 0.5 – 1.7 MeV, corresponding to the Gamow peak energy T_9 = 1 – 3 by correcting for the detection efficiencies as well as the analysis efficiencies. Further analysis is in progress.

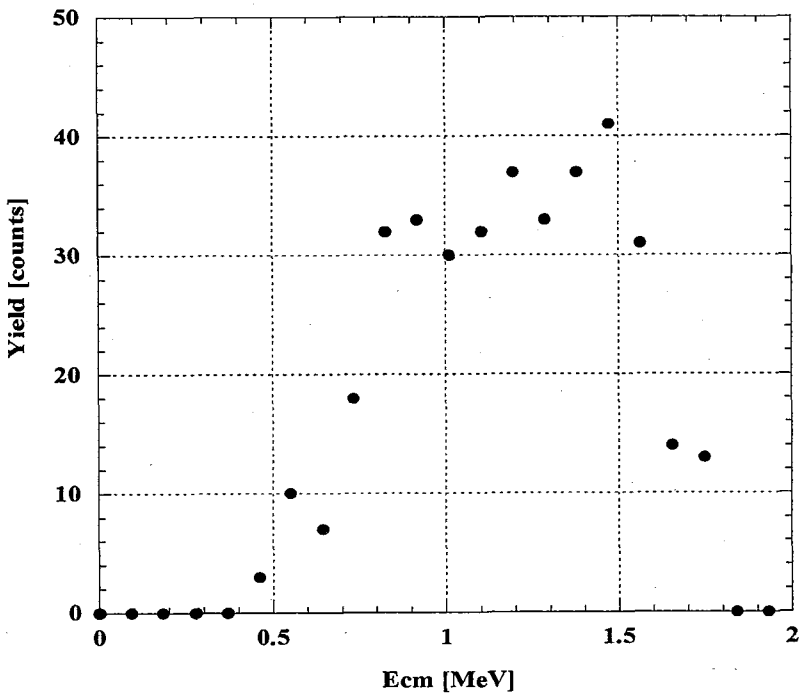

Fig.1 Reaction energy distribution of the selected ^{8}Li(α, n) ^{11}B reaction events.

References

[1] M. Terasawa, et al., Nucl. Phys. A688(2001)581c.
[2] H. Ishiyama, et al., America. Insti. Phys. 704(2003)453.
[3] T. Hashimoto, et al., Nucl. Phys. A746(2004)330.
[4] H. Miyatake, et al., Nucl. Phys. A738(2004)401.

JP0650027

3.3 IDENTIFICATION OF NEW NEUTRON-RICH Eu ISOTOPES

T. K. SATO, A. OSA, K. TSUKADA, M. ASAI, H. HAYASHI[1],
M. SHIBATA[1], and S. ICHIKAWA

Three new neutron-rich rare-earth isotopes $^{163\text{-}165}$Eu produced in the proton-induced fission of ^{238}U were identified using the JAERI-ISOL with a surface ionization type integrated-target-ion source. The assignment of these isotopes was based upon the observation of Gd *K* x rays in the β-coincident x/γ spectra measured for the separated mass fraction.

A ^{nat}U target was used in the form of uranium carbide which contained 620 mg/cm^2 ^{nat}U. The target was bombarded with the 30 MeV proton beams (20 MeV on target) with the intensity of about 200 nA. Fission products were diffused-out from the target, and then ionized in the ion source. The $^{163\text{-}165}$Eu isotopes were mass-separated as metallic ions. The mass-separated ions of interest were implanted into an aluminum-coated Mylar tape in a tape transport system, and periodically transported to a measuring position. The measuring position was equipped with a sandwich-type plastic scintillator for β-ray measurements, a short coaxial Ge detector (ORTEC LOAX) and a 35% Ge detector (ORTEC GAMMA-X). β–γ and γ–γ coincidences between these detectors were recorded event by event together with time information used in a half-life analysis.

Figure shows a β-coincident x/γ-ray spectrum gated by Gd K_α x-ray at mass 164 fraction. Gd *K* x rays from the β decay of ^{164}Eu as well as the γ rays with energies of 71.6 and 164.8 keV are clearly observed. The 71.6 and 164.8 keV γ rays were assigned to the $2^+ \rightarrow 0^+$ and $4^+ \rightarrow 2^+$ transitions in the ground state band of daughter nucleus ^{164}Gd, respectively, by considering their energies[1].

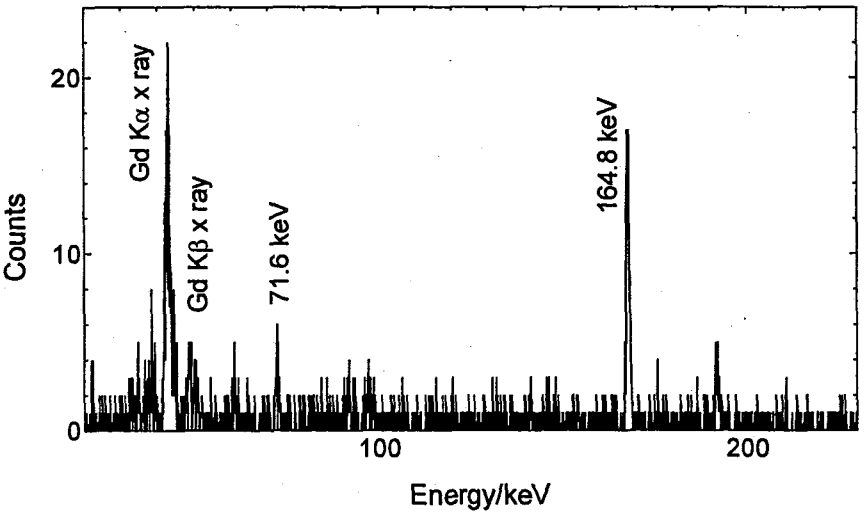

Fig. β and x–ray–coincident x/ γ–ray spectrum for the mass164 fraction.

The isotopes $^{163, 165}$Eu were identified by observing the *K* x rays of Gd in the mass 163 and 165 fractions, respectively. The tentative half-lives of these isotopes measured with the Gd *K* x rays show fairly agreements with theoretical values predicted by the gross theory. Further analyses of half-lives and γ-ray transitions for these new isotopes are in progress.

Reference

[1] E. F. Jones et al. J. Phys. G: Nucl. Part. Phys. **30** (2004) L43-48.

[1]Nagoya University

JP0650028

3.4 BARRIER DISTRIBUTIONS FOR HEAVY-ION FUSION REACTIONS

H. IKEZOE, S. MITSUOKA, K. NISHIO, K. TSURUTA, Y. WATANABE[1], S. C. JEONG[1], and K. SATOU[2]

The barrier distribution of the heavy-ion fusion reaction is an important quantity to investigate the reaction mechanism between heavy projectile and target nuclei in super heavy-element synthesis. We measured the barrier distributions from the quasi-elastic backward scattering of ^{48}Ti, ^{56}Fe and ^{64}Ni projectiles on ^{208}Pb target. A thin ^{208}Pb target of 100μg/cm^2 with carbon backing (30μg/cm^2) was bombarded by ^{48}Ti, ^{56}Fe and ^{64}Ni beams from the JAERI-tandem and superconducting booster accelerators. Quasi-elastic events were measured at the scattering angles 162°, 168° and 172° by using three solid state detectors. The beam energy was changed by the step of about 1.5 MeV. The quasi-elastic events were integrated after subtracting a deep-inelastic event which becomes dominant at high bombarding energy, and normalized by the Rutherford cross sections.

The measured cross sections and the first derivatives of the cross sections for the reaction ^{64}Ni + ^{208}Pb are shown in Fig.1 as functions of center-of-mass energy E_{cm}. The peak position of the barrier distribution coincides with the center of the 1n evaporation channel reported in Ref. [1] and lower by the amount of 4 MeV than the recent measurement of RIKEN [2]. The Bass barrier of 241.5 MeV is about 5 MeV higher than the present peak position. The data analysis is in progress.

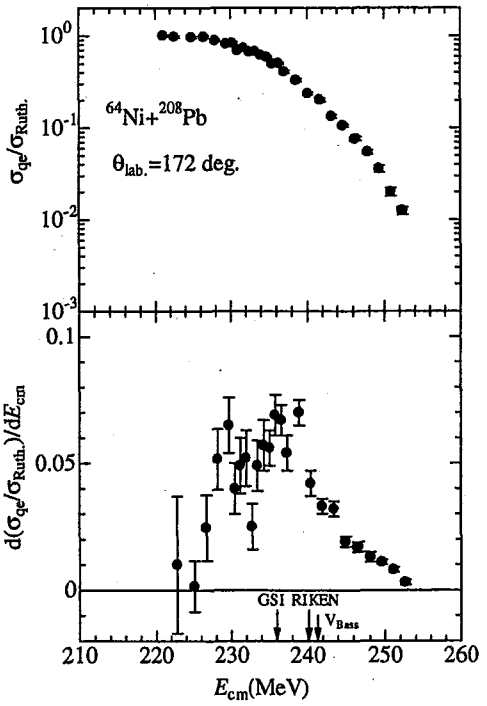

Fig. 1 Measured cross section and the first derivative of the cross section as a function of E_{cm} for the reaction ^{64}Ni + ^{208}Pb. The Bass barrier and the peak positions for the 1n evaporation channel measured at GSI and RIKEN are shown by arrows.

References

[1] S. Hofmann, Rep. Prog. Phys. 61, 639 (1998).
[2] K. Morita et. al., Eur. Phys. J. A 21, 257 (2004).

[1]Institute of Particle and Nuclear Studies, KEK.
[2]Tandem Accelerator Complex, Research Facility Center for Science and Technology, University of Tsukuba.

JP0650029

3.5 EXPERIMENTAL STUDY OF FUSION REACTIONS USING ACTINIDE NUCLEI

K. NISHIO, H. IKEZOE, S. MITSUOKA, S.ICHIKAWA, Y. NAGAME, K. TSUKADA, M. ASAI, K. TSURUTA, K. SATOU[1], and T. OHSAWA[2]

Search for the superheavy elements (SHEs) close to the doubly magic nucleus $^{298}114$ is one of the most fascinating motivations in nuclear physics [1,2,3]. Recent discussions suggest that the deformation of actinide target has an important role in the fusion process [2] and the collision of projectile to the equatorial side of the target nucleus results in larger fusion probability. Recently, we have shown in the reaction of $^{16}O + ^{238}U$ [4] that the collision of projectile ^{16}O with the tips of ^{238}U also results in complete fusion. As a next step, we started to measure the evaporation residue cross sections for $^{30}Si + ^{238}U$. On the basis of Z_1Z_2 systematics, the $^{30}Si + ^{238}U$ system (1288) is still located in the light system, so that we expect complete fusion even for the tip collisions. In this case, the Coulomb barrier height is about 13 MeV smaller than the Bass barrier, opening the 4n channel products ^{264}Sg (new isotope) in sub-barrier region. The calculation using the HIVAP code [5] combined with the coupled channel code [6] determining the fusion cross section predicts 50 pb at $E_{c.m.}$=133 MeV.

The experiment is going on by using the JAERI-Recoil Mass Separator with modified set up for the focal plane detectors. To detect the α decay and/or spontaneous fission with high efficiency, we designed a new silicon detector array (Fig.1). The sided detectors (B) consist of eight silicon strip detectors (PIN Diode 60×60 mm^2). This can detect escaped α particles. In the spontaneous fission, we can determine the total kinetic energy of fragments by coinciding the signals from the stop detector (A) and one of the side detectors (B). The detection efficiency is estimated to be 90 %.

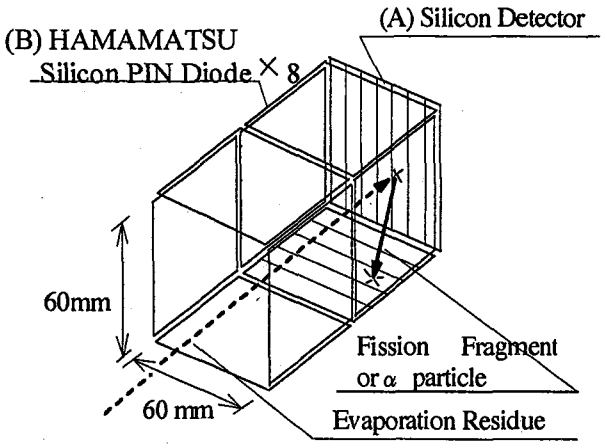

Fig.1 Detector array at the JAERI-RMS

References

[1] S. Hofmann and G. Münzenberg, Rev. Mod. Phys. **72** (2000) 733.
[2] Yu. Ts. Oganessian *et al.*, Phys. Rev. C **70** (2004) 64609; Yu. Ts. Oganessian *et al.*, Phys. Rev. C **69** (2004) 54607.
[3] K. Morita *et al.*, J. Phys. Soc. Japan, **73**, (2004) 2593.
[4] K. Nishio *et al.*, Phys. Rev. Lett. **93** (2004) 162701.
[5] W. Reisdorf and M. Schaedel, Z. Phys. A **343** (1992) 47.
[6] K. Hagino *et al.*, Compu. Phys. Commu. **123** (1999) 143.

[1] Tsukuba University
[2] Kinki University

JP0650030

3.6 BARRIER DISTRIBUTION OF QUASI-ELASTIC BACK-SCATTERING OF ^{48}Ti, ^{56}Fe AND ^{64}Ni ON ^{208}Pb

S. MITSUOKA, H. IKEZOE, K. NISHIO, K. TSURUTA, S.C. JEONG[1], Y.X. WATANABE[1]

Two methods of Pb/Bi-based cold fusion and actinide-based hot fusion have been successfully used to produce superheavy elements so far, but unfortunately the production rates are close to the present experimental limit of the order of one atom per a few months. It is of critical importance to select the optimum reaction conditions for the projectile and target combination as well as the incident energy for the maximum production cross sections. In particular, for optimum preparation of experiments searching for elements 113 and 114 by cold fusion, it is needed to learn more about the measured excitation functions of elements 104 to 112 produced by Ti, Cr, Fe, Ni and Zn induced sub-barrier fusion reactions.

In order to experimentally extract the fusion barrier distribution, one can take usually the second derivative of the product $E\sigma_{fus}(E)$ of the fusion excitation function σ_{fus}(E) with respect to the center-of-mass energy E, that is $d^2(E\sigma_{fus})/dE^2$. This method is normally used to interpret the barrier distribution in terms of coupling between inelastic excitation and nucleon transfer channels. This, however, requires the excitation function of fusion cross sections to be measured with high precision and with small energy steps. Here, we adopted a newly proposed procedure of taking the first derivative of the ratio of quasi-elastic cross section σ_{qel} to the Rutherford cross section σ_R, that is $-d(\sigma_{qel}/\sigma_R)/dE$. This has an attractive experimental advantage that i) less statistics are required for data by taking the first derivative rather than the second derivative, and ii) cross sections for some effective energies in narrow range can be obtained at a single beam energy by taking into account the centrifugal correction for measurements at several backward angels.

We measured the excitation functions of quasi-elastic scattering in the reactions of ^{48}Ti+^{208}Pb, ^{56}Fe+^{208}Pb and ^{64}Ni+^{208}Pb, relating to cold fusion for elements 104, 108 and 110, respectively. For precise measurements at backward angles, a strip target of ^{208}Pb (100 μg/cm^2 in thickness, 98.4% enriched) with 3 mm width in horizontal plane was prepared by sputtering onto a carbon foil (30 μg/cm^2). Beam energies from the tandem-booster accelerator were varied in a range of *Ec.m.* = 175-255 MeV with 1.5 MeV step. Back-scattered quasi-elastic was detected by SSDs at laboratory angles of 172, 168 and 162 degrees and Rutherford scattering was monitored at 30, 42 and 55 degrees with respect to the beam axis. The cross section of quasi-elastic scattering was obtained by summing elastic, inelastic scattering and transfer yields, but excluding deep-inelastic scattering by using a code LINDA. Analysis of the measured excitation functions by comparing with coupled channel calculations or experimental data for superheavy elements is in progress.

---

[1] Institute of Particle and Nuclear Studies, KEK

4. Nuclear Chemistry

This is a blank page.

JP0650031

4.1 REVERSED-PHASE EXTRACTION CHROMATOGRAPHY OF Zr AND Hf IN THE TBP/HCl SYSTEM -MODEL EXPERIMENTS FOR CHEMICAL CHARACTERIZATION OF ELEMENT 104, RUTHERFORDIUM-

H. HABA,[1] K. TSUKADA, K. AKIYAMA, M. ASAI, A. TOYOSHIMA, Y. ISHII, I. NISHINAKA, T. ICHIKAWA, T. SATO, S. ICHIKAWA, Y. NAGAME, W. SATO,[2] K. MATSUO,[2] Y. KITAMOTO,[2] Y. TASHIRO,[2] A. SHINOHARA,[2] J. SAITO,[3] M. ITO,[3] T. IKEZAWA,[3] S. GOTO,[3] H. KUDO,[3] K. MORISHITA,[4] M. ARAI,[4] A. YOKOYAMA,[4] Y. OURA,[5] and K. SUEKI[6]

The extraction behavior of the first transactinide element, rutherfordium (Rf), into tributylphosphate (TBP) has been investigated together with its lighter group-4 homologues Zr and Hf [1–3]. From the extractability into TBP, we can obtain information such as chloride complexation and hydrolysis, and stability of TBP complexes. Czerwinski *et al.* [1] first examined the extraction behavior of Rf, Zr, and Hf into 0.25 M TBP in benzene in 8–12 M HCl. The results showed that extraction for these elements increases or remains high as a function of HCl concentration and that the extractability decreases in the order of Zr > Rf > Hf. Kacher *et al.* [2] performed some additional extractions of Rf into TBP/benzene with Ti, Zr, and Hf, and revised the extraction sequence by Czerwinski *et al.* [1] as Zr > Hf > Rf > Ti around 8 M HCl. Thereafter, a reversed-phase chromatographic separation of Rf, Zr, and Hf at 8 M HCl was performed by Günther *et al.* [3] using microcolumns containing TBP on an inert support, and the conflicting order of Zr > Rf > Hf was obtained. On the other hand, we investigated the adsorption behavior of Rf, Zr, and Hf on the strongly basic anion-exchange resin from 4.0–11.5 M HCl using the Automated Ion-exchange separation apparatus coupled with the Detection system for Alpha spectroscopy (AIDA) [4]. It was found that the adsorption behavior of Rf on the anion-exchange resin is similar to that of Zr and Hf, and that the adsorption order is Rf > Zr > Hf. Using AIDA, we had planned to perform the reversed-phase extraction chromatography of Rf in the TBP-HCl system to clarify the conflicting results mentioned above [1–3]. Recently, we developed a TBP resin for microcolumns of AIDA and investigated its performance by batch method using radiotracers ^{89}Zr and ^{175}Hf [5]. In this work, we have conducted on-line extraction chromatography of short-lived ^{85}Zr (7.86 min) and ^{169}Hf (3.24 min) as a model experiment for ^{261}Rf (78 s).

Isotopes of ^{85}Zr and ^{169}Hf were simultaneously produced in the ^{nat}Ge(^{18}O,*xn*) and ^{nat}Gd(^{18}O,*xn*) reactions, respectively, using a 94-MeV ^{18}O beam delivered from the JAERI tandem accelerator. The ^{nat}Gd target of 370 μg cm^{-2} thickness and 5 mm diameter was electrodeposited on a 2.7 mg cm^{-2} Be backing, and then

[1] Cyclotron Center, RIKEN
[2] Department of Chemistry, Graduate School of Science, Osaka University
[3] Department of Chemistry, Faculty of Science, Niigata University
[4] Department of Chemistry, Faculty of Science, Kanazawa University
[5] Department of Chemistry, Graduate School of Science, Tokyo Metropolitan University
[6] Department of Chemistry, University of Tsukuba

on the resulting ^{nat}Gd target, the ^{nat}Ge target of 660 μg cm^{-2} thickness was deposited by vacuum evaporation. Beam intensity was approximately 0.3 particle μA. Reaction products recoiling out of the target were transported by a He/KCl gas-jet system to AIDA. The 20 wt.% TBP/CHP20Y resin [5] was filled in the 1.6 i.d. × 7.0 mm microcolumns. After the aerosol collection for 180 s, ^{85}Zr and ^{169}Hf were first fed into the column with 160 μL of hot conc. HCl and the effluent was discarded. Then, 7.0, 7.2, 7.5, 7.7, and 8.0 M HCl were fed into the column at a flow rate of 1.0 mL min^{-1}, and the effluent fractions were separately collected in 7 polyethylene tubes. The remaining Zr and Hf in the column were eluted with 230 μL of 4.0 M HCl. These fractions were assayed by γ-ray spectrometry with Ge detectors.

As an example, cumulative eluted radioactivities of ^{85}Zr and ^{169}Hf at 7.0, 7.5, and 8.0 M are shown in Fig. 1 as a function of effluent volume. A good separation between Zr and Hf is achieved, and the eluted radioactivities at a fixed effluent volume decrease with an increase of HCl concentration, [HCl]. This reflects the variation of distribution coefficients (K_d) on the TBP/CHP20Y resin in 6.0–11.9 M HCl: the K_d values of Zr are larger than those of Hf, and both increase steeply with [HCl] from 6.0 M to 11.9 M [5]. Because of the short half-life (78 s) and low production yield (2 atoms min^{-1}) of ^{261}Rf, it is unrealistic to determine the elution curve for ^{261}Rf. Therefore, we will measure radioactivities in the two effluent fractions as indicated in Fig. 1: 200 μL of HCl solutions of interest (Fraction 1) and 230 μL of 4.0 M HCl to strip remaining Rf from the column (Fraction 2). From the radioactivities A_1 and A_2 observed in Fractions 1 and 2, respectively, the percent extraction (%Ext.) on the TBP/CHP20Y resin can be evaluated using %Ext. = $100A_2/(A_1 + A_2)$. In Fig. 2, the %Ext. values of Zr and Hf at the 200 μL effluent volume are shown as a function of [HCl]. The %Ext. values are 50% at ~7.2 M for Zr and ~7.8 M for Hf, where a difference in the extractability between Rf and its homologues Zr and Hf may be clearly found. In the near future, we will conduct the extraction experiment of ^{261}Rf produced in the ^{248}Cm(^{18}O,5*n*) reaction.

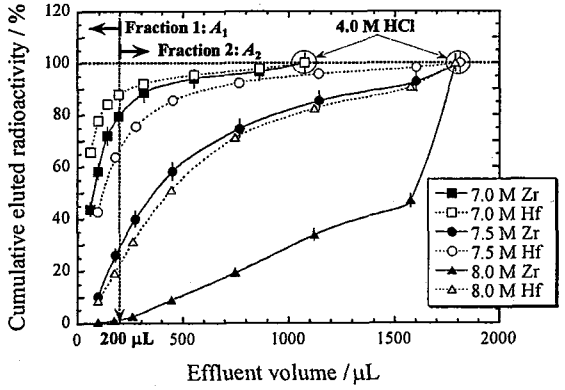

Fig. 1. Cumulative eluted radioactivities of ^{85}Zr and ^{169}Hf from the 20 wt.% TBP/CHP20Y column at a flow rate of 1.0 mL min^{-1} as a function of the effluent volume.

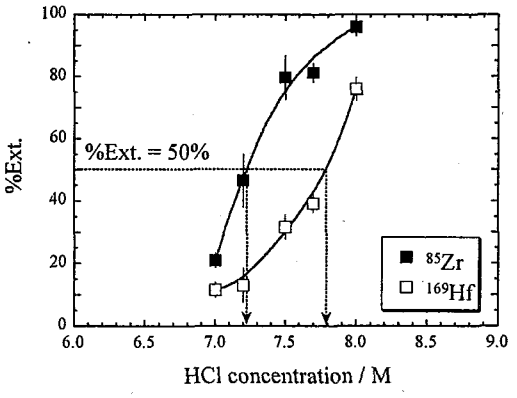

Fig. 2. Variation of the percent extraction (%Ext.) of ^{85}Zr and ^{169}Hf at the effluent volume of 200 μL from the 20 wt.% TBP/CHP20Y column as a function of the HCl concentration.

References

[1] K. R. Czerwinski *et al.*: Radiochim. Acta **64**(1994)29.
[2] C. D. Kacher *et al.*: Radiochim. Acta **75**(1996)127.
[3] R. Günther *et al.*: Radiochim. Acta **80**(1998)121.
[4] H. Haba *et al.*: J. Nucl. Radiochem. Sci. **3**(2002)143.
[5] H. Haba *et al.*: RIKEN Accel. Prog. Rep. **38**(2005)107.

4.2 FLUORIDE COMPLEXATION OF RUTHERFORDIUM IN HF/HNO_3 SOLUTION

A. TOYOSHIMA, K. TSUKADA, M. ASAI, H. HABA,[1] K. AKIYAMA,[2] Y. ISHII, I. NISHINAKA, T. SATO, M. HIRATA, T. ICHIKAWA, Y. NAGAME, W. SATO,[3] Y. TANI,[3] H. HASEGAWA,[3] K. MATSUO,[3] D. SAIKA,[3] Y. KITAMOTO,[3] A. SHINOHARA,[3] M. ITO,[4] J. SAITO,[4] S. GOTO,[4] H. KUDO,[4] K. MORISHITA,[5] A. YOKOYAMA,[5] M. SAKAMA,[6] K. SUEKI,[2] Y. OURA,[7] H. NAKAHARA,[7] M. SCHÄDEL,[8] W. BRÜCHLE,[8] and J. V. KRATZ[9]

Previously, we have reported that the anion-exchange behavior of rutherfordium, Rf, in the 1.9-13.9 M HF solution is quite different from those of the group-4 homologues, Zr and Hf [1]. The present study aims to further understand the fluoride complexation of Rf. In this report, our recent result on anion-exchange experiments of Rf in mixed HF and nitric acid (HF/HNO_3) solution is presented.

The isotope ^{261}Rf (78 s) was produced in the ^{248}Cm(^{18}O,5*n*) reaction at the JAERI tandem accelerator. The ^{248}Cm target of 645 μg/cm^2 thickness was prepared by electrodeposition onto 1.80 mg/cm^2 Be backing foil. The average beam intensity was 220 pnA. Reaction products recoiling out of the target were transported by a He/KCl gas-jet technique to the the Automated Ion-exchange separation apparatus coupled with the Detection system for Alpha spectroscopy (AIDA). Two different-sized columns, 1.6 mm i.d.×7.0 mm and 1.0 mm i.d.×3.5 mm, filled with anion-exchange resin (MCI GEL CA08Y) were used alternatively for studying a wide range of chromatographic behaviors. After the collection for about 125 s, ^{261}Rf was dissolved in various concentrations of HF/HNO_3 solution and was subsequently fed onto the column. Effluent from the column was collected on a Ta disc and prepared for α-spectrometry by evaporation to dryness. A fraction of the isotope adsorbed on the column was then stripped by the 4 M HCl solution. The effluent was collected on another Ta disc and was evaporated to dryness. The pair of discs was then subjected to α-spectroscopy with 600 mm^2 PIPS detectors. In anion-exchange chromatography of Zr and Hf, the isotopes ^{85}Zr (7.86 min) and ^{169}Hf (3.42 min) were simultaneously produced in the ^{nat}Ge(^{18}O,*x*n) and ^{nat}Gd(^{18}O,*x*n) reactions, respectively. The isotopes transported by the gas-jet system were collected on the deposition site of AIDA. ^{85}Zr and ^{169}Hf were then dissolved in various concentrations of HF/HNO_3 solution and fed onto the column at the same flow rates as those with Rf. Effluent from the anion-exchange column was fractioned in 7 aliquots which were separately collected in 7 polyethylene tubes. A fraction of the isotopes remaining in the column was stripped with 4.0 M HCl solution and collected in another polyethylene tube. The eight tubes were subjected to γ-ray measurements using a Ge detector in order to obtain their distribution coefficients (K_d). For batch experiments, the radioisotopes ^{88}Zr and ^{175}Hf were produced in the ^{89}Y(*p*,2*n*) and ^{175}Lu(*p*,*n*) reactions, respectively. Procedures in the batch experiments were similar to those in Ref. [1].

[1] Cyclotron Center, RIKEN
[2] Department of Chemistry, University of Tsukuba
[3] Department of Chemistry, Osaka University
[4] Department of Chemistry, Niigata University
[5] Department of Chemistry, Kanazawa University
[6] School of Health Sciences, University of Tokushima
[7] Department of Chemistry, Tokyo Metropolitan University
[8] Gesellschaft für Schwerionenforschung
[9] Institut für Kernchemie, Universität Mainz

In Fig. 1, the variations of the K_d values for the three elements, Rf, Zr and Hf, are together shown as a function of nitrate ion concentration ($[NO_3^-]$). The K_d values were obtained in the constant concentration of fluoride ion ($[F^-]=3.0\times10^{-3}$ M). The K_d values of ^{85}Zr and ^{169}Hf under the dynamic condition agree well with those of ^{88}Zr and ^{175}Hf under the static one. The K_d values of ^{261}Rf were evaluated from its adsorption behavior. It is found that while the K_d values of Zr and Hf are identical with each other and the slopes in the $\log K_d$-$\log[NO_3^-]$ plot are -2.0±0.1, the K_d values of Rf are much smaller than those of Zr and Hf and the slope in the plot is -2.2±0.2. In Fig. 2, the variations of the K_d values for Rf, Zr and Hf at a few constant $[NO_3^-]$ are shown as a function of $[F^-]$. The K_d values of ^{88}Zr and ^{175}Hf vary in the same trend; they start to increase at around $[F^-]=1\times10^{-5}$ M, reach the plateau at around $[F^-]=1\times10^{-3}$ M, and start to decrease at around $[F^-]=5\times10^{-3}$ M. On the other hand, the K_d values of ^{261}Rf start to increase from $[F^-]=5\times10^{-4}$ M. It is found that the K_d values of Rf start to increase at about two-orders higher $[F^-]$ than those of Zr and Hf do.

Considering into account a chemical reaction that an anionic complex replaces to nitrate ion on the anion-exchange resin, it is found that the -2.2±0.2, -2.0±0.1 and -2.0±0.1 slopes for Rf, Zr and Hf, respectively, shown in Fig. 1 represents some complexes of the three elements with -2 charges are increasingly driven out of the resin with an increase of $[NO_3^-]$. For Zr and Hf, it is well-known that hexafluoro-complexes, $[ZrF_6]^{2-}$ and $[HfF_6]^{2-}$, respectively, are formed in a HF solution. Thus, the -2.0±0.1 slopes for Zr and Hf shown in Fig.1 means that their hexafluoro-complexes are driven out of the resin. The increases of the K_d values for Zr and Hf shown in Fig. 2 are reasonably understood by the formation of the hexafluoro-complexes from the pentafluoro-complexes. Assuming that hexafluoro-complex of Rf, $[RfF_6]^{2-}$, is formed in the same way as those of Zr and Hf, the -2.2±0.2 slope for Rf shown in Fig.1 indicates that $[RfF_6]^{2-}$ is driven out of the resin, and the increase of the K_d values for Rf shown in Fig. 2 represents that $[RfF_6]^{2-}$ is increasingly formed from its pentafluoro-complex at more than $[F^-]=5\times10^{-4}$ M. The differences of the $[F^-]$ range that the K_d values increase reflect differences of the reactivity for the formation of the hexafluoro-complexes of the group-4 elements. It is, therefore, concluded that the formation of $[RfF_6]^{2-}$ is much weaker than those of $[ZrF_6]^{2-}$ and $[HfF_6]^{2-}$.

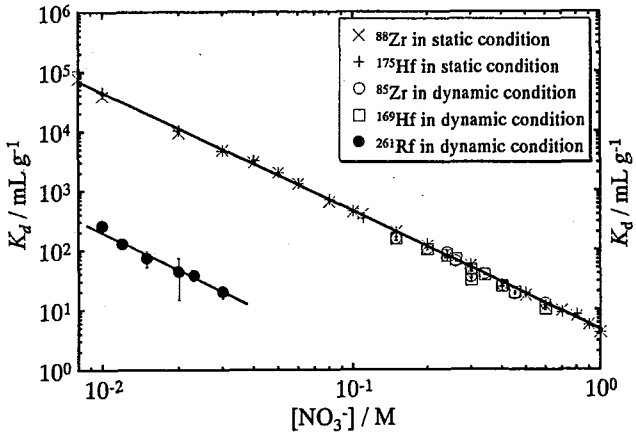

Fig. 1. Variations of the K_d values of ^{88}Zr, ^{175}Hf, ^{85}Zr, ^{169}Hf, and ^{261}Rf at a constant fluoride-ion concentration of 3.0×10^{-3} M as a function of nitrate-ion concentration.

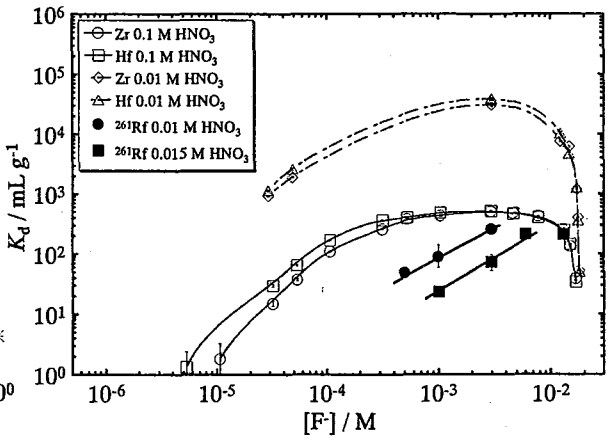

Fig. 2. Variations of the K_d values of ^{88}Zr, ^{175}Hf, and ^{261}Rf as a function of fluoride-ion concentration.

Reference

[1] H. Haba *et al.*, J. Am. Chem. Soc. **126**(2004) 5219.

5. Nuclear Theory

This is a blank page.

JP0650033

5.1 QGP PHASE TRANSITION IN A MOLECULAR DYNAMICS APPROACH

Y. AKIMURA, [1] T. MARUYAMA, N. YOSHINAGA, [2] and S. CHIBA

Quarks are thought to be one of the most fundamentally particles and they are confined in hadrons(baryon and mesons) in normal environment. In high density and/or high temperature situation, however, quarks are predicted to undergo a phase transition so that they are released from hadrons to quarks so called quark gluon plasma(QGP)[1]. Many efforts are devoted to extract quarks from hadrons with experimental and theoretical supports. In this report, we give our recent results of the theoretical study about the baryon-quark phase transition in a framework of the molecular dynamics(MD).

The total wave function in MD is given as a direct product of n single particle quark Gaussian wave packets in coordinate and momentum spaces and state vectors χ with a fixed flavor, a color and a spin orientation,

$$\Psi = \prod_{i=1}^{n} \frac{1}{(\pi L^2)^{3/4}} \exp\left[-\frac{(\mathbf{r}_i - \mathbf{R}_i)^2}{2L^2} + \frac{i}{\hbar}\mathbf{P}_i\mathbf{r}_i\right]\chi_i, \tag{1}$$

where $n = 3A$ (A is the baryon number), L is the fixed width of wave packets chosen to 0.33fm, and $\mathbf{R}_i$ and $\mathbf{P}_i$ are the center of the wave packet of i-th quark in coordinate and momentum spaces, respectively. We solve the cooling equations which is the Newtonian equations with friction terms to search for the energy minimum configuration.

The effective Hamiltonian H is given as follows[2, 3].

$$H = H_0 + V_{\text{Pauli}} - T_{\text{spur}}, \tag{2}$$

where V_{Pauli} is a phenomenological potential instead of using antisymmetlized wave function, T_{spur} is a spurious zero point energy of the center-of-mass motion of clusters and H_0 is the original Hamiltonian expressed as

$$H_0 \equiv \left\langle \Psi \left| \sum_{i=1}^{n} \hat{T}_i + \hat{V}_{\text{color}} + \hat{V}_{\text{meson}} \right| \Psi \right\rangle, \tag{3}$$

$$\left\langle \Psi \left| \hat{T}_i \right| \Psi \right\rangle = \frac{\mathbf{P}_i^2}{2m} + \frac{3\hbar^2}{4mL^2} + m, \tag{4}$$

where V_{color} consists of color-dependent linear and one gluon exchange terms and V_{meson} consists of σ, ω and ρ meson exchange potentials in Yukawa-type. The parameters in the meson exchange potentials are adjusted to reproduce well-known properties of nuclear matter. The value of the constituent quark mass m for u or d quarks is 300 MeV.

We have compared two kinds of matters with different u-d compositions: ud(matter containing the same number of u and d quarks which corresponds to symmetric nuclear matter) and udd(d quarks twice the number of u quarks; neutron matter). The ground state energies of ud and udd matters are shown by solid lines in Fig. 1. The vertical axis indicates the energy per baryon. For comparison, the case of cooling with baryon-constraint is shown by thin dashed lines. The energy by normal cooling agrees with that by cooling with baryon-constraint at low density. This means that quarks are confined as baryons. Around $5\rho_0$(ρ_0

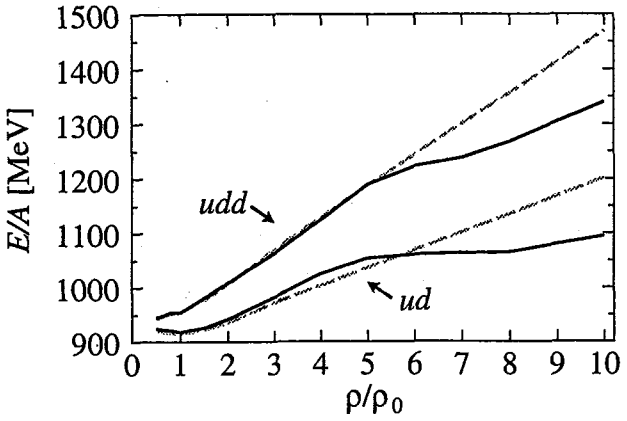

Figure 1: Density dependence of energy per baryon for *ud* and *udd* matter. The dashed lines indicate the cases of cooling with baryon-constraint and solid lines normal cooling.

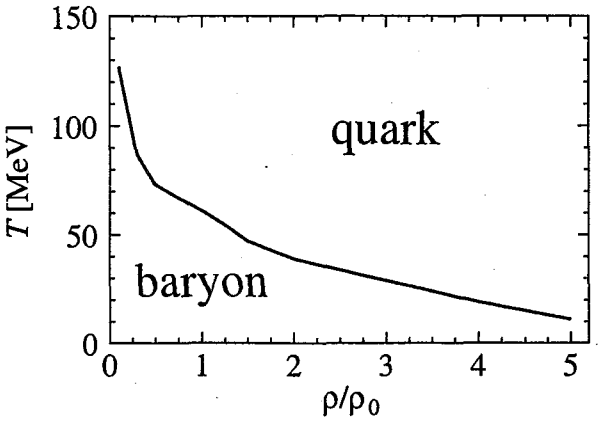

Figure 2: Phase diagram with the density and temperature for *ud* matter.

is the normal nuclear saturation density), a baryon-quark transition occurs and the energy decreases. This critical density agrees with that predicted by other models.
We extend above MD to finite temperature systems by using the Nosé-Hoover method [4]. Fig. 2 shows a phase diagram in the temperature-density plane for *ud* matter. Baryon phase is realized at lower side of density and temperature, and quark phase is realized at higher side.
Note that it is necessary to include $\bar{q}q$ creation/annihilation process for the high temperature simulation. Lack of the chiral symmetry restoration and the asymptotic freedom are also open problems.

References

[1] J. C. Collins and M. J. Perry, Phys. Rev. Lett. **34** , 1353 (1975).

[2] Y. Akimura, T. Maruyama, N. Yoshinaga and S. Chiba, Nucl. Phys. **A**, 749, 329 (*nucl-th*/0411008)

[3] Y. Akimura, T. Maruyama, N. Yoshinaga and S. Chiba, submitting to European Physical Journal **A**. (*nucl-th*/0505029)

[4] W. G. Hoover, Phys. Rev. **A31**, 1695 (1985).

[1] Department of Physics, Saitama University and Jaeri
[2] Department of Physics, Saitama University

JP0650034

5.2 DISAPPEARANCE OF THE MAGIC STRUCTURE IN ^{30}Na AND ITS IMPACT ON THE SHELL STRUCTURE

Y. UTSUNO, T. OTSUKA[1], T. MIZUSAKI[2] and M. HONMA[3]

Recently, it has much attracted theoretical interest where the N=20 magic structure disappears. In the so-called ``island of inversion" picture [1], the region with the disappearance was restricted to nine N≥20 nuclei, whereas a recent Monte Carlo shell-model (MCSM) calculation [2] has indicated that certain N=19 isotopes including Na have the ground state dominated by the intruder state, from a comparison with experimental [3] electromagnetic moments. In the present study [4], at first we confirm the dominance of the intruder state at N=19 from the viewpoint of the energy levels and the $E2$ transition probability. We then examine what the dominance of the intruder state in the N=19 isotope ^{30}Na means in terms of the N=20 shell gap on the basis of the MCSM calculation. The numerical computations were carried out in part with the Helios computer system in the JAERI Tandem.

Figure 1 compares the energy levels of ^{30}Na between experiment [5] and the MCSM and the *sd*-shell calculations. The latter calculation naturally results in the dominance of the normal state. Experimentally [5], there is a rather low excited state strongly connected to the ground state with the $E2$ transition. In the *sd*-shell calculation, as the ground state is not so deformed, all of the $E2$ excitations from the ground state are very weak. On the other hand, the MCSM calculation reproduces the experimental feature very well as a result of the disappearance of the magic structure in this nucleus.

To examine the impact of the present result on the shell structure in neutron-rich nuclei, we artificially widen the shell gap from the original interaction, shifting the strength of the monopole interaction with a control parameter x as $\delta V^{T}_{0d5/2,\,0d3/2}(x) = -0.3x, +0.7x$ MeV for T=1 and 0, respectively, where V^{T}_{ij} denotes the monopole interaction between i and j orbits with isospin coupled to T. Figure 2 shows some quantities as functions of the shell gap. As presented in Figs. 2 (a) and (b), both the quadrupole moment and the magnetic moment of ^{30}Na suddenly deviate from values close to the experimental values at the shell gap ~ 4 MeV. This coincides with the sudden transition of the dominant ground-state component from the intruder state to the normal state as indicated in Figs. 2 (c) and (d). Compared with the cases of ^{29}Na and ^{31}Na, the transition in ^{30}Na occurs very sharply and the dominance of the intruder state in this nucleus is thus a rather sensitive probe for the shell gap. The present result supports the argument that the shell evolution [6] occurs in neutron-rich nuclei due to the spin-isospin dependence of the effective interaction.

[1]Department of Physics and CNS, University of Tokyo
[2]Institute of Natural Sciences, Senshu university
[3]Center for Mathematical Sciences, University of Aizu

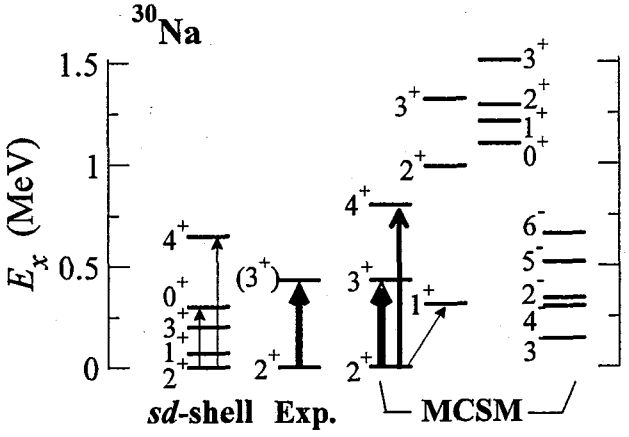

Fig. 1. Energy levels and B($E2$) values compared between the experiment [5] and the calculations in ^{30}Na. The width of the arrow illustrates the $E2$ strength excited from the ground state.

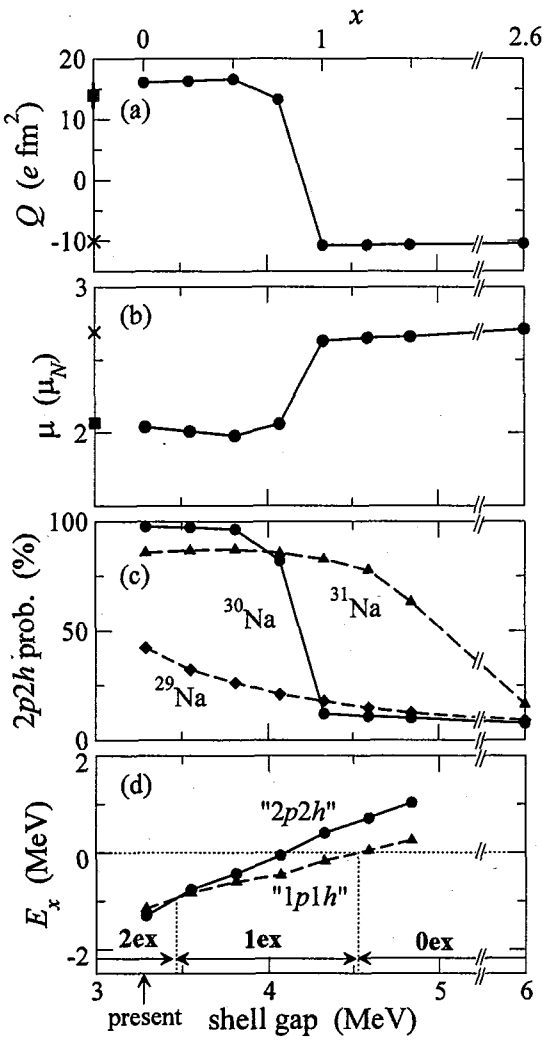

Fig. 2. (a) Quadrupole moment and (b) magnetic moment of ^{30}Na as functions of the shell gap. The moments by the experiment [3] and the *sd*-shell model are the squares and the crosses, respectively. (c) *2p2h* probabilities in the (positive-parity) ground states of $^{29\text{-}31}$Na. (d) Energies of the *2p2h*- and *1p1h*-dominant lowest states of ^{30}Na (denoted by "*2p2h*" and "*1p1h*", respectively) measured from the *0p0h*-dominant lowest state. The range of the shell gap giving the *npnh* ground state (n=0, 1, 2) is indicated by *n*ex.

References

[1] E.K. Warburton, J.A. Becker, B.A. Brown, Phys. Rev. C **41** (1990) 1147.
[2] Y. Utsuno, T. Otsuka, T. Mizusaki, M. Honma, Prog. Theor. Phys. Suppl. **146** (2002) 488.
[3] M. Keim, AIP Conf. Proc. **455** (1998) 50; M. Keim et al., Euro. Phys. J. A **8** (2000) 31.
[4] Y. Utsuno, T. Otsuka, T. Mizusaki, M. Honma, Phys. Rev. C **70** (2004) 044307.
[5] B.V. Prityckenko et al., Phys. Rev. C **66** (2002) 024325.
[6] T. Otsuka, R. Fujimoto, Y. Utsuno, B.A. Brown, M. Honma, T. Mizusaki, Phys. Rev. Lett. **87** (2001) 082502.

JP0650035

5.3 NUCLEAR PASTA STRUCTURE

T. MARUYAMA, T. TATSUMI,[1] D. M. VOSKRESENSKY, [2]
T. TANIGAWA [3] and S. CHIBA

One of most interesting features in the low-density nuclear matter is the existence of non-uniform structure, called "nuclear pasta" [1, 2]. At low densities, nuclei in matter are expected to be crystalized so as to minimize the long range Coulomb energy. The stable nuclear shape changes from sphere to cylinder, slab, cylindrical hole, and to spherical hole with increase of the matter density. Finally they melt into uniform matter at a certain density close to the saturation density. The favorable nuclear shape is determined by a balance between the surface and Coulomb energies. Though the treatment of Coulomb interaction is very important, the screening of the Coulomb interaction by the localization of electrons has been rather simplified in the previous works.

We adopt a relativistic mean-field plus Thomas-Fermi model for the study of nuclear matter. It reproduces the binding energies of finite nuclei, once the parameters are chosen to fit the properties of nuclear matter at the saturation density. Using the Wigner-Seitz approximation for the non-uniform nuclear matter, we carefully include the Coulomb interaction and solve the Poisson equation in accord with the differential equations of motion for meson fields. The baryon and electron densities are determined in a way *fully consistent with the Coulomb potential* [3]. We solve the following coupled equations of motion for baryon densities ρ_a $(a = n, p)$, baryon chemical potentials μ_a $(a = n, p)$, the sigma, omega and rho meson mean-fields σ, ω_0, R_0, and the Coulomb potential $V_{\rm Coul}$,

$$\nabla^2\sigma(\mathbf{r}) = m_\sigma^2\sigma(\mathbf{r}) + \frac{dU}{d\sigma} - g_{\sigma N}(\rho_n^{(s)}(\mathbf{r}) + \rho_p^{(s)}(\mathbf{r})), \quad (1)$$

$$\nabla^2\omega_0(\mathbf{r}) = m_\omega^2\omega_0(\mathbf{r}) - g_{\omega N}(\rho_p(\mathbf{r}) + \rho_n(\mathbf{r})), \quad (2)$$

$$\nabla^2 R_0(\mathbf{r}) = m_\rho^2 R_0(\mathbf{r}) - g_{\rho N}(\rho_p(\mathbf{r}) - \rho_n(\mathbf{r})), \quad (3)$$

$$\nabla^2 V_{\rm Coul}(\mathbf{r}) = 4\pi e^2 \rho_{\rm ch}(\mathbf{r}), \quad (4)$$

$$\mu_n = \sqrt{k_{{\rm F},n}^2(\mathbf{r}) + m_N^*(\mathbf{r})^2} + g_{\omega N}\omega_0(\mathbf{r}) - g_{\rho N}R_0(\mathbf{r}) = \mu_B, \quad (5)$$

$$\mu_p = \sqrt{k_{{\rm F},p}^2(\mathbf{r}) + m_N^*(\mathbf{r})^2} + g_{\omega N}\omega_0(\mathbf{r}) + g_{\rho N}R_0(\mathbf{r}) - V_{\rm Coul}(\mathbf{r}) = \mu_B - \mu_e, \quad (6)$$

$$\rho_e(\mathbf{r}) = -(\mu_e - V_{\rm Coul}(\mathbf{r}))^3/3\pi^2, \quad (7)$$

with the scalar densities $\rho_a^{(s)}(\mathbf{r})$ $(a = n, p)$, and the charge density $\rho_{\rm ch}(\mathbf{r}) = \rho_p(\mathbf{r}) + \rho_e(\mathbf{r})$.

In symmetric nuclear matter (in this case the last equality in (6) does not apply), we observ the "nuclear pasta" structures with various geometries at sub-nuclear densities. Figure 1 shows some examples of pasta structure (droplet, rod, slab, cylindrical hole). Note the nonuniform electron distribution which is an evidence of the proper treatment of the Coulomb interaction and electron density.

EOS of the nuclear pastas is shown as a function of the averaged density in the upper panel of Fig. 2. The energy $E - m_B$ includes the kinetic energy of electrons, which makes the total pressure positive. The lowest-energy configuration is selected among various geometrical structures for a given averaged density. The most favorable configuration changes from the

[1] Department of Physics, Kyoto Univeristy
[2] Moscow Institute for Physics and Engineering
[3] Japan Society for the Promotion of Science, JAERI

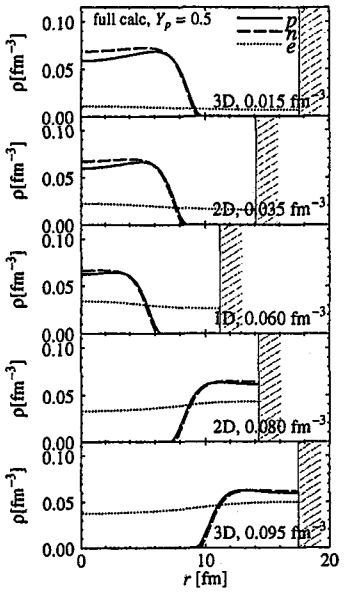

Figure 1: Density profile of symmetric nuclear matter. "3D" etc. means the geometrical dimension. The hatches in the figure show cell boundaries.

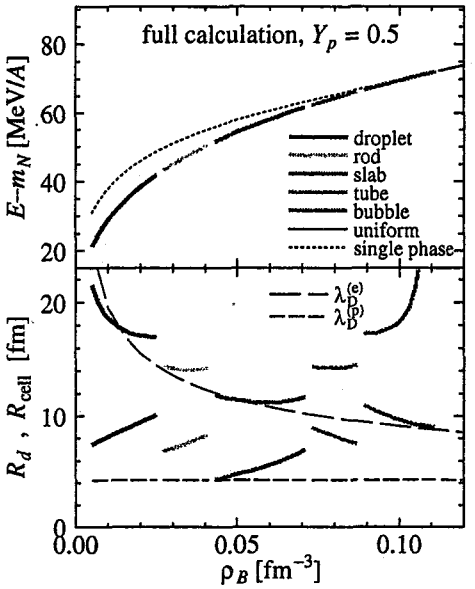

Figure 2: Binding energies per nucleon and the cell size for symmetric nuclear matter.

droplet to rod, slab, tube, bubble, and to the uniform one (the dotted thin curve) with increase of the density. We can see that the appearance of the nuclear pastas results in a softening of the EOS: the energy per baryon gets lower up to about 15 MeV/A compared to the uniform case. The lower panel in Fig. 2 show the cell sizes $R_{\rm cell}$ and structure sizes R_d as functions of the averaged density. Dashed curves show the Debye screening lengths of electron and proton calculated as $\lambda_D^{(e)} = \left(-4\pi e^2 \frac{d\rho_e^{\rm av}}{d\mu_e}\right)^{-1/2}$, $\lambda_D^{(p)} = \left(4\pi e^2 \frac{d\rho_p^{\rm av}}{d\mu_p}\right)^{-1/2}$, respectively, where $\rho_p^{\rm av}$ is the proton density averaged over the nuclear lump and $\rho_e^{\rm av}$ is the electron charge density averaged inside the cell. Numerically, the cell sizes $R_{\rm cell}$ for droplet, rod, and slab configurations are shown to be close to the Debye screening length of electron. The structure size R_d, on the other hand, is smaller than $\lambda_D^{(e)}$. This means that the Debye screening effect of electrons inside these structures should not be pronounced. For bubble $\lambda_D^{(e)}$ is substantially smaller than the cell size and the electron screening should be significant. The value $\lambda_D^{(p)}$ is shorter than R_d, which means that the rearrangement of proton density is essential for the structures of the nuclear pastas, as it is indeed seen from the increase of proton density at the surface (see Fig. 1).

In neutron-star matter (nuclear matter in beta-equilibrium), we have observed only the proton-enriched droplet in the neutron sea. We have also examined the effect of the Coulomb screening. Since the electron density is not so large, the screening effect is not remarkable for the equation of state.

References

[1] D. G. Ravenhall, C. J. Pethick and J. R. Wilson, Phys. Rev. Lett. **50**, 2066 (1983).

[2] M. Hashimoto, H. Seki and M. Yamada, Prog. Theor. Phys. **71**, 320 (1984).

[3] T. Maruyama, T. Tatsumi, D.N. Voskresensky, T. Tanigawa and S. Chiba, Phys. Rev. C, in press.

JP0650036

5.4 POSSIBILITY OF CHARGE POLARIZATION FOR PROJECTILE AND TARGET IN ENTRANCE CHANNEL OF HEAVY-ION REACTIONS

T. ICHIKAWA and A. IWAMOTO

For synthesis of superheavy elements, heavy-ion fusion reactions have been used extensively with Pb, Bi and actinide targets [1]. In heavy-ion reactions, the Coulomb-repulsion force increases linearly with increasing the product of the proton numbers of the target and projectile $Z_T \times Z_P$ which takes a very large value for cold-fusion reactions. In this case, it is expected that charge distributions of the colliding nuclei are changed to some extent. The resulting charge distributions induced by this polarization decrease the interacting Coulomb energy between the colliding partners, whereas their own self energies increase due to increase of the symmetry energy. Thus, the extent of the static charge polarization of the target and projectile is determined by a competition between the interacting Coulomb and the self energies.

A charge displacement between protons and neutrons is observed in the giant-dipole resonance (GDR) of nuclei. To explain this phenomena on the basis of the macroscopic picture, Myers et al. [2] introduced a realistic model combining both surface- and volume-charge vibrations with the droplet model. This model well reproduces a macroscopic trend of resonance energies for all mass regions. A superposition of a surface- and volume-charge components is essential in GDR. Thus, we assume that the resulting charge displacements between protons and neutrons in the projectile and the target are a sum of the surface- and volume-charge components. According to this picture, we calculate the total energy of a nucleus when charge polarizations occur and estimate a change of the fusion barrier in entrance channel by minimizing this total energy. The total energy consists of a sum of the interaction-Coulomb and -nuclear energy and the self energy of the target and projectile. The self energy includes the change of the symmetry energy, which is estimated with the droplet model [2,3].

Figure 1 shows a potential energy for a system ^{48}Ca+^{208}Pb calculated with a nuclear interaction energy E_N of Krappe-Nix-Sierk (KNS) model [4]. The solid and dashed lines denote the potential energy for spherical nuclei with and without the charge polarization, respectively. According to the increase of the Coulomb repulsion with the approach of the projectile to the target, the charge polarization of the target and projectile increases and results in the decrease of the Coulomb barrier height. In Fig. 1, the barrier height $B_f^{(sph)}$ at $R = 11.89$ fm with a uniform charge distribution is 182.56 MeV and the barrier height $B_f^{(pol)}$ at $R = 11.92$ fm with a charge polarization is 181.64 MeV. Thus, the decrease of the barrier height ΔB_f is -0.93 MeV. The same calculation for the system ^{197}Au+^{197}Au tells us that the decrease of the potential energy ΔE at the touching configuration $R = 13.50$ fm is -5.33 MeV. For this system, due to the increase of the Coulomb repulsion, the decrease of the Coulomb potential energy coming from the charge polarization becomes significantly larger.

The decrease of the Coulomb barrier height for the entrance channel of various reactions leading to the synthesis of superheavy elements is presented in Fig. 2. The solid line denotes the decrease of the Coulomb barrier height from the one with the uniform-charge distribution. As a comparison, we also calculate the decrease of the Coulomb barrier height by minimizing the

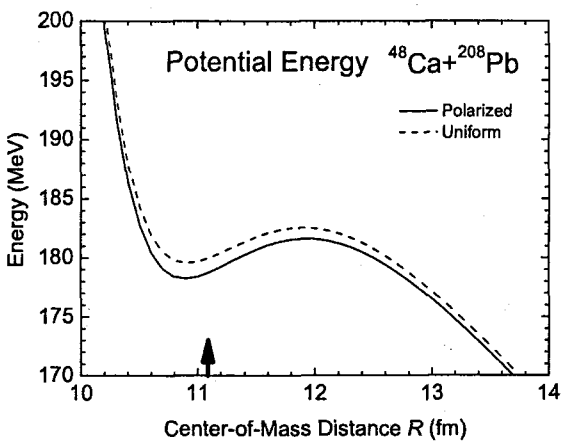

Figure 1: Potential energy for charge-polarized and uniform $^{48}Ca+^{208}Pb$ system. The solid arrow denotes the touching distance of the target and projectile.

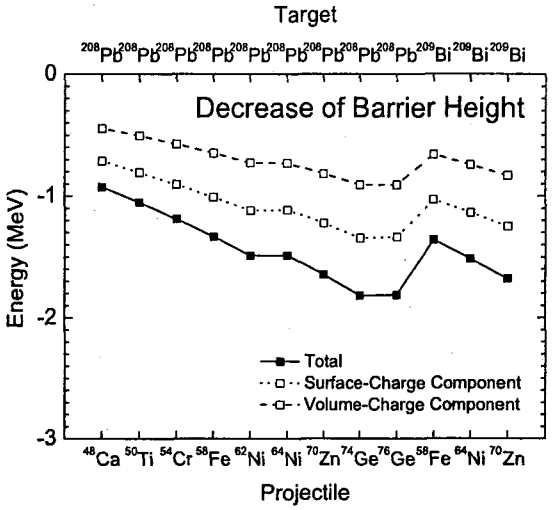

Figure 2: Decrease of Coulomb-barrier height in the entrance channel for various reactions leading to the synthesis of superheavy elements.

total energy when a surface- or volume-charge polarization occurs individually. The dashed and dotted lines denote the decrease of the Coulomb barrier height restricted only to the volume- and surface-charge component, respectively. It is clearly seen that the presence of both surface- and volume-charge components is important. For the systems $^{74,76}Ge+^{208}Pb$, the Coulomb barrier decreases by 1.82 MeV. When we estimate the barrier height in the entrance channel for the synthesis of superheavy elements, the charge polarization gives a non-negligible contribution. Thus, the effect of the charge polarization is important for a determination of the bombarding energy in the cold-fusion reactions leading to the superheavy elements.

References

[1] S. Hofmann and G. Münzenberg, Rev. Mod. Phys. **27**, (2000) 733.
[2] W. D. Myers and W. J. Swiatecki, T. Kodama, L. J. El-Jaick and E. R. Hilf, Phys. Rev. C **15**, (1977) 2032.
[3] W. D. Myers and W. J. Swiatecki, Ann. Phys. **55**, (1969) 395.
[4] H. J. Krappe, J. R.Nix and A. J. Sierk, Phys. Rev. C **20**, (1979) 992.

6. Atomic Physics and Solid State Physics

This is a blank page.

6.1 MEASUREMENT OF SELF-DIFFUSION COEFFICIENTS IN Li IONIC CONDUCTORS BY USING SHORT-LIVED RADIOTRACER OF ^{8}Li

S.C. JEONG[1], I. KATAYAMA[1], H. KAWAKAMI[1], H. ISHIYAMA[1], Y. WATANABE[1], N. IMAI[1], Y. HIRAYAMA[1], H. MIYATAKE[1], M. SATAKA, S. OKAYASU, H. SUGAI, S. ICHIKAWA, K. NISHIO, T. NAKANOYA, S. MITSUOKA, Takashi HASHIMOTO, Takanori HASHIMOTO[2], M. YAHAGI[2], K. TAKADA[3], M. WATANABE[3], T. ISHIKAWA[4]and A. IWASE[5]

For the effective use of the short-lived radioactive beams to be available at TRIAC (Tokai Radioactive Ion Accelerator Complex), we have developed a radiotracer method for diffusion studies in solids, by using a α-emitting radiotracer of ^{8}Li ($T_{1/2}$=0.84s) [1]. The method has been applied to measure the self-diffusion coefficients of Li in β-LiGa in order to study the influence of the lattice defects on the Li diffusion in Li ionic conductors.

The β-LiGa is one of the Li intermetallic compounds with the NaTl structure composed of two interpenetrating sub-lattices, each forming a diamond lattice with a homogeneity range of around stoichiometric atomic ratio of Li, 44~54% at. % Li. The Li compounds have been considered as possible electrode materials in Li ionic batteries because of their high diffusion coefficients at room temperature for Li ions [2]. In order to understand the motion of Li as an ionic conductor, the defect structure in the compounds has been intensively studied via the measurement of electrical resistivity and density by help of the standard x-ray diffraction analysis [3]. The high diffusion coefficient in the Li compounds is associated with the constitutional vacancy concentration on the Li sub-lattice, which is relatively large as compared to the usual metal alloy. The thermodynamic behavior of the Li vacancy has also been inferred from the anomalous electrical resistivity ("100K" anomaly) observed at around 95K near the critical composition corresponding to the Li-deficient region of β-LiAl [4], which is considered as an order-disorder transition of vacancies on the Li sub-lattices [5].

In order to observe the order-disorder transition of the vacancies on Li-sites in terms of self-diffusion of Li, a detailed measurement has been performed below room temperature for

[1] Institute of Particle and Nuclear Studies, KEK
[2] Aomori University
[3] National Institute of Materials Science (NIMS)
[4] Tokyo University of Science
[5] Osaka Prefecture University

the β-LiGa of 44 at. % Li, most Li-deficient in the β-phase of LiGa. Indeed, a sudden change in the Li self-diffusion coefficients is observed around 240 K as shown in Fig.1, at which the anomalous electrical resistivity has been observed [6].

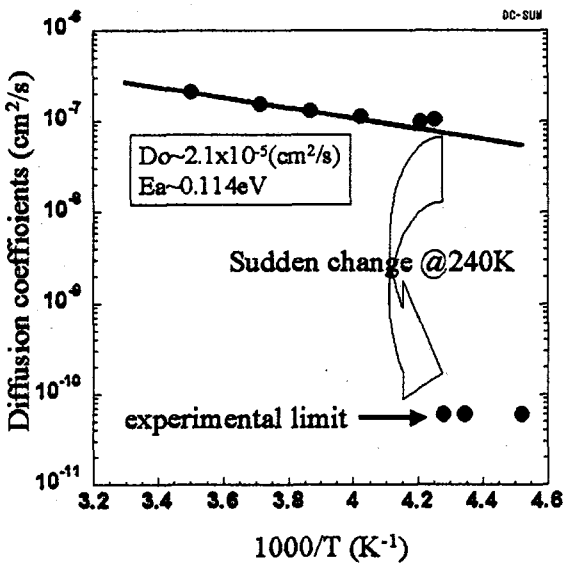

Fig.1: Arrhenius plot of the diffusion coefficients measured in β-LiGa (44 at. % Li). The solid line is resulting from the data fitted with a single exponential of $Do \cdot exp(-Ea/kT)$, where Do is the pre-factor (frequency factor) and Ea is activation energy for diffusion.

The figure shows the temperature dependence of Li diffusion coefficients in β-LiGa (44 at. % Li) obtained by using short-lived radiotracer of ^{8}Li. Around 240K, a sudden change in the value of the diffusion coefficients is observed. In the region of higher temperature, the diffusion coefficients follow Arrhenius behavior. In the lower temperature, the diffusion coefficients are observed as a constant, which is the lower limit of diffusion coefficients accessible by our method: For diffusion coefficients less than about 10^{-10} cm^2/s, any significant effect in the $\tilde{\alpha}$-particle yields due to the diffusing ^{8}Li could not be observed because of the short life-time of the radiotracer.

Around the transition temperature, the time structure of the normalized α-particle yields could not be explained in terms of one component of diffusion, i.e. one diffusion coefficient, implying that the diffusion coefficients would not be singly determined in the transition region. Further investigation will be done in this respect.

References.

[1] S.C. Jeong et al., Nucl. Instrum. And Meth. B230 (2005) 596.
[2] C.J. Wen and R.A. Huggins, J. Electrochem. Soc. 128 (1981) 1636.
[3] K. Kuriyama, H. Hamanaka, S. Kaido, and M. Yhagi, Phys. Rev. B54 (1996) 6015.
[4] K. Kuriyama et al., Phys. Rev. B 24 (1981) 6158.
[5] T.O. Brun, S. Susman, R. Dejus, B. Granelli, and K. Sköld, Solid State Commun. 45 (1983) 721.
[6] H. Hamanaka et al., Solid State Ionics 113 (1998) 19.

JP0650038

6.2 HIGH-RESOLUTION ZERO-DEGREE ELECTRON SPECTROSCOPY OF HIGHLY CHARGED OXYGEN IONS(Ⅱ)

K. KAWATSURA[1], K. TAKAHIRO[1], M. SATAKA, M. IMAI[2],
K. KOMAKI[3], H. SUGAI and H. SHIBATA[2]

High-resolution Coster-Kronig (C-K) electron spectra from highly excited states in high-energy collisions of Si, S, Cl, Ar and Ti ions with He and C-foil targets have been widely investigated experimentally and theoretically by our group [1-6]. Recently, we have measured high-resolution Auger and C-K electron spectra produced in 32 MeV O^{q+} (q = 1-5) + He collisions [7,8]. The experiments were performed at the tandem accelerator facility of JAERI-Tokai. The details of the experimental set up for zero-degree electron spectroscopy have been described in Refs. [1,2]. The primary O^{q+} (q = 1-5) ion beams were produced by using the ECR ion source (ECRIS) installed at the high-voltage terminal of the tandem accelerator.

In the present, the high-resolution C-K electron emission spectra in collisions of 32 MeV O^{3+} ions with a He gas target have been investigated using zero-degree electron spectroscopy [8]. Figure 1 shows zero-degree electron spectrum around the cusp energy region. It is well known that the O^{3+} projectiles give rise to a strange looking crown shaped or trident-like structure around the cusp peak, made up of three clear peaks [9]. The central peak at 1.090 keV is the cusp peak primarily due to electron loss to the continuum. Each peak on either side of the cusp corresponds to the autoionization line from highly excited O^{3+} ions produced in the collision with He.

The energies of these autoionization lines in the projectile rest frame are determined with high resolution. Figure 2 shows the ejected electron spectrum of autoionization lines from excited O^{3+} ions, where energy scale refers to the projectile rest frame transferred from the laboratory frame as shown in Fig. 1, using the cusp energy of t = 1.090 keV. These autoionization lines for O^{3+} ions are more complicated than for O^{4+} ions [7]. Here we calculate autoionization lines arising from the Rydberg states from ground state and metastable state O^{3+} ion via single-electron excitation. Vertical bars indicate the line positions obtained by Eq. (1) given in Ref. [7], where n is the principal quantum number. The C-K transitions at low energy region are found to originate in $1s^22s2p(^3P)nl - 1s^22s^2(^1S)\varepsilon l$ (n = 5-11). The crown shaped peak observed in the previous work [9] is confirmed to be due to the configuration $1s^22s2p(^3P)5s$, where the transition energy is 0.0144 eV, using the quantum defect theory of Eq. (2) given in Ref. [7]. For n = 5 to 7, a clear angular momentum distribution is observed, where the maximum intensity is attributed to the relatively high angular momentum l = 2 or 3, though the lines from the low angular momenta l = 0 and 1 are also observable [8].

[1] Department of Chemistry and Materials Technology, Kyoto Institute of Technology
[2] Department of Nuclear Engineering, Kyoto University
[3] Institute of Physics, Graduate School of Arts and Sciences, University of Tokyo

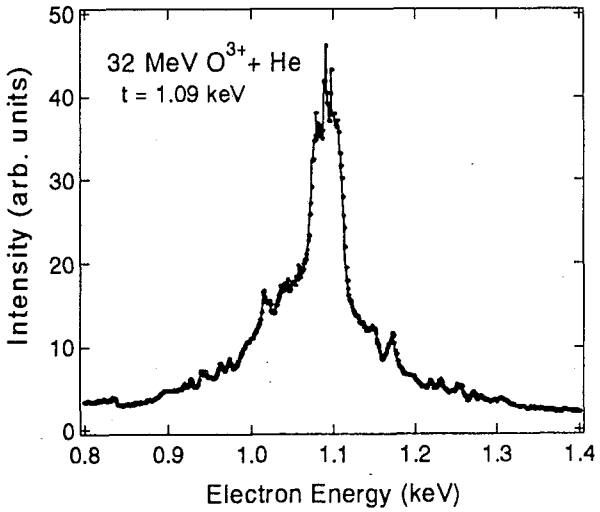

Fig. 1. Zero-degree electron spectrum around the cusp energy (t = 1.090 keV) in the collisions of 32 MeV O^{3+} + He. Energy scale refers to the laboratory frame.

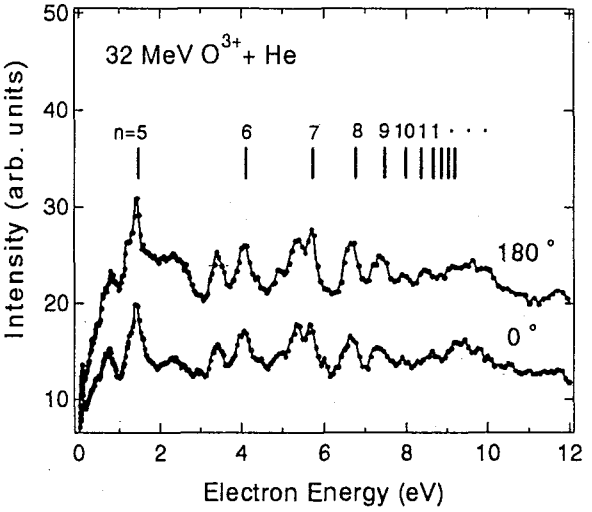

Fig. 2. Zero-degree Coster-Kronig electron spectra around the cusp region in the collisions of 32 MeV O^{3+} + He. Energy scale refers to the projectile rest frame.

In summary, we have measured ejected electron spectra for 32 MeV O^{q+} (q = 1-5) ions on a He target, though only the spectrum from 32 MeV O^{3+} + He collisions is shown. It is found that the $1s^2 2s2pnl$ states with relatively high angular momenta are produced in the O^{3+} ion collisions, while the $1s^2 2pnl$ states with lower ones in the O^{4+} ion collisions [7]. The electron energies for $1s^2 2s2pnl$ C-K transitions are also discussed and compared with the quantum defect theory [8]. However, higher-resolution measurements using a wide variety of charge states (q = 1-6) of O^{q+} ions on a He target are still needed for more detailed analysis on excitation and ionization processes in high energy collision regime. This work was supported in part by the JAERI Tandem co-operation program.

References

[1] K. Kawatsura *et al.*, Nucl. Instr. and Meth. **B48** (1990) 103.
[2] K. Kawatsura *et al.*, Nucl. Instr. and Meth. **B53** (1991) 421.
[3] K. Kawatsura *et al.*, Nucl. Instr. and Meth. **B124** (1997) 381.
[4] M. Sataka *et al.*, J. Phys. B: At. Mol. Opt. Phys. **35** (2002) 267.
[5] M. Sataka *et al.*, Phys. Rev. **A65** (2002) 052704.
[6] M. Imai *et al.*, Nucl. Instr. and Meth. **B193** (2002) 674.
[7] K. Kawatsura *et al.*, Nucl. Instr. and Meth. **B205** (2003) 528.
[8] K. Kawatsura *et al.*, in Abstracts of SHIM2005 (Aschaffenburg, 2005).
[9] T.J.M Zouros *et al.*, Nucl. Instr. and Meth. **B99** (1995) 27.

JP0650039

6.3 CHARGE STATE DISTRIBUTION OF SULFUR IONS AFTER PENETRATION OF C-FOIL TARGETS(Ⅱ)

M. IMAI[1], M. SATAKA, K. NISHIO, H. SUGAI,
K. KAWATSURA[2], K. TAKAHIRO[2], K. KOMAKI[3], and H. SHIBATA[1]

Charge state evolution is one of the most important aspects in ion-solid interactions. Various processes, such as electron capture, ionization, vacancy production and the consequent phenomena like energy loss and stopping, are closely related with the projectile charge state evolution in the target. Equilibrium charge state distributions for various collision systems after passing gaseous or solid target have been extensively investigated and compiled [1], although the charge state distribution somewhat changes upon exiting the target foil. Charge state distributions before its equilibrium have also been studied experimentally as well as theoretically. We also have been performing another experiment to derive the charge state distributions of 2.0 MeV/u sulfur ions after penetration of thin carbon foils of 0.9 – 10 μg/cm^2, which cover the non-equilibrium region. [2]

The present experiments were performed at the LIR1–3 beam line of the 20UR Tandem Accelerator Facility. A beam of 2.0 MeV/u (64 MeV) S^{6+} ion was provided from the tandem accelerator within 0.1% of energy accuracy, using a calibrated energy analyzing magnet. A post-stripper C-foil of ~20 μg/cm^2 in thickness was placed after the energy analyzing magnet to produce higher charge state fraction of S^{10+}, S^{11+} and S^{13+} ions. The energy losses at the post-stripper foil were estimated to be at most 0.7% by our separate measurement of cusp electron energies with zero-degree electron spectroscopy. The primary S^{6+} or post-stripped S^{10+}, S^{11+} and S^{13+} ion beam was directed by a switching magnet to self-support carbon target foils of 0.9, 1.1, 1.5, 2.0, 3.0, 4.7, 6.9 and 10 μg/cm^2 in thickness. The charge state distributions after foil penetration were measured using the heavy ion magnetic spectrometer ENMA [3] and position-sensitive gas chamber detector. The vacuum condition inside the spectrometer was maintained below 10^{-6} Pa to eliminate the background charge exchange collisions with residual gas, which was confirmed by measurements without target foil.

Charge state distributions of 2.0 MeV/u S^{6+} ion through the carbon foil targets are shown in fig. 1(a) with calculations by ETACHA code [4]. Typical errors for the charge fractions are estimated to be 20% for the smallest fractions around 1.0×10^{-5} and less than 0.5% for the largest fractions around 0.3. Mean charge state $\bar{q} = \sum_q qF(q)$ and charge distribution width $d = \left[\sum_q (q-\bar{q})^2 F(q)\right]^{1/2}$ for S^{6+}, S^{8+}, S^{10+} and S^{12+} ions, where q and $F(q)$ are charge state and its fraction, respectively, are plotted in fig. 2. The ETACHA code proves to reproduce the general feature of the evolution of the mean charge state and the distribution width, although the present energy is lower than the assumed energy range of

[1] Department of Nuclear Engineering, Kyoto University
[2] Department of Chemistry and Materials Technology, Kyoto Institute of Technology
[3] Institute of Physics, Graduate School of Arts and Sciences, University of Tokyo

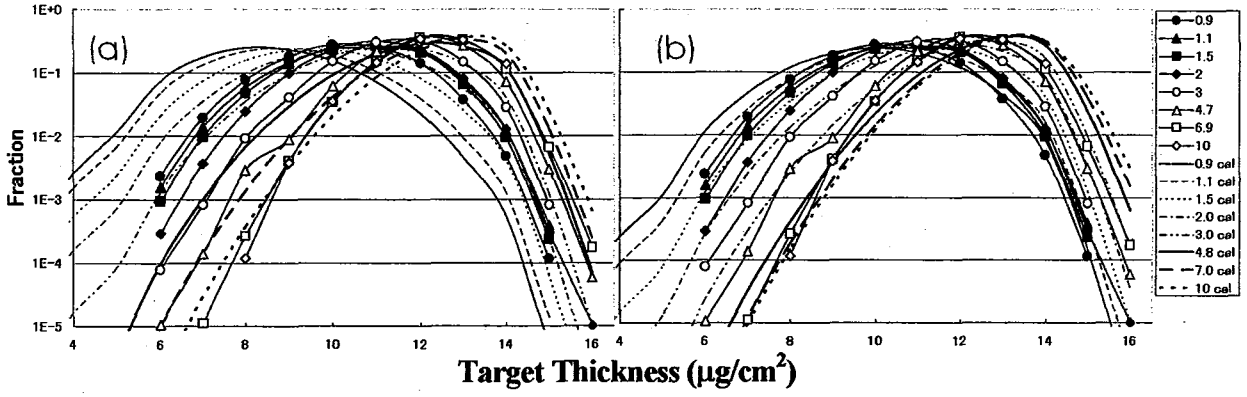

Fig. 1 Charge state distribution of 2.0 MeV/u S^{6+} ion incident through carbon foil targets of 0.9 – 10 μg/cm^2; (a) Present data with ETACHA calculation and (b) with modified ETACHA results..

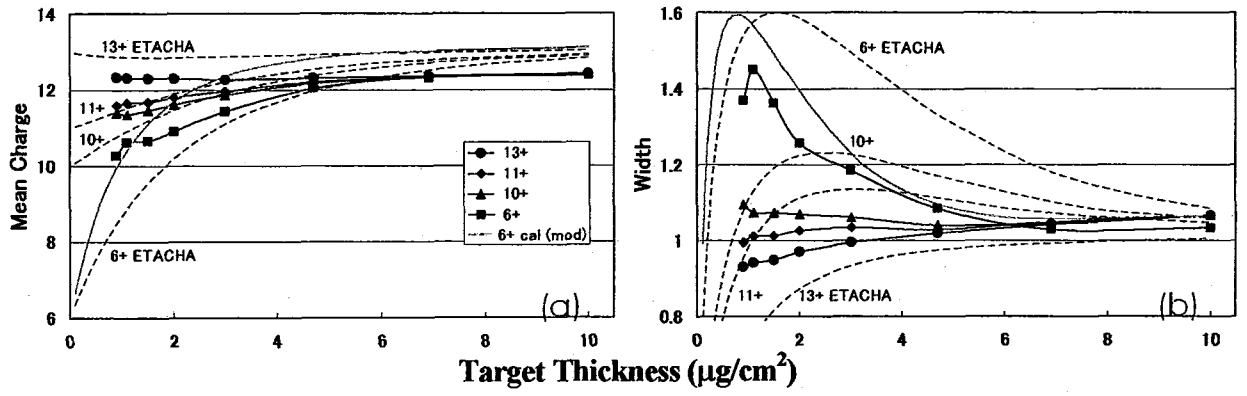

Fig. 2 (a) Mean charge state and (b) distribution width for 2.0 MeV/u S ion passing through C-foil. The dashed and full lines are ETACHA and modified ETACHA results, respectively.

the code (over 10 MeV/u), except for that the near equilibrium mean charge falls on a bit larger value (5%) and that the calculated mean charge and distribution width change roughly twice slower then the experiment. This implies the actual cross sections of the electron capture and loss processes are roughly a factor of 2 larger than those adopted in the calculation. A modified calculation using 2 times larger cross section input has been performed for S^{6+} ion penetration [5], whose results are shown in figs. 1(b) and 2. It can be seen that the charge distribution for thinner (0.9 – 1.5 μg/cm^2) target region is well improved, indicating that the scenario of the ETACHA simulation satisfactorily explains the experiment in MeV/u region and a better agreement can be achieved if larger cross section inputs are employed.

References

[1] A. B. Wittkower and H. D. Betz, At. Data Nucl. Data Tables **5**, 5 (1973); K. Shima *et al.*, At. Data Nucl. Data Tables **34**, 357 (1986); K. Shima *et al.*, At. Data Nucl. Data Tables **51**, 173 (1992).

[2] M. Imai *et al.*, Nucl. Instrum. Method **B230**, 63 (2005).

[3] Y. Sugiyama *et al.*, Nucl. Instrum. Method **A281**, 512 (1989).

[4] J. P. Rozet *et al.*, J. Phys. **B22**, 33 (1989); Nucl. Instrum. and Method **B107**, 67 (1996).

[5] M. Imai *et al.*, Materials Science Symposium, Jan 2005; to be published in JAERI-Conf series.

JP0650040

6.4 HEAVY-ION IRRADIATION EFFECT FOR THE SUPERCONDUCTING PROPERTIES OF OVER-DOPED $YSr_2Cu_3O_{7\pm\delta}$ SUPERCONDUCTOR

H.KITÔ[1], T.WADA[1], S.OKAYASU and M.SATAKA

The multilayered structures of the $M_mA_2OQ_{n-1}$-$Cu_nO_{m+2+2n\pm\delta}$ or M-$m2(n-1)n$ superconductive cuprates are constructed of continuous piling of different blocks. *i.e.* the superconductive CuO_2-$(Q\text{-}CuO_2)_{n-1}$ infinite layer block and non-superconductive AO-$M_mO_{m\pm\delta}$-AO blocking block. For the practical applications of high critical temperature (T_c) oxide superconductors such as superconducting magnets, the critical current density (J_c) must be high enough in applied magnetic fields, which requests the introduction of effective pinning centers. One of the methods of introducing pinning centers is heavy-ion irradiation. Especially, Cu- based blocking superconducting cuprates could be promising candidates for the application of the next generation because of high T_c, high J_c and high irreversibility field (H_{irr}) [1]. Generally, for Cu-, T*l*- and Hg- based superconductive cuprates, partial substitution of the larger Ba by the smaller Sr in the AO layer of non-superconductive AO-$M_mO_{m\pm\delta}$-AO blocking block and over-doped level have been shown to shift the H_{irr} line to the higher magnetic field, [2, 3, 4, 5]. $YSr_2Cu_3O_{7\pm\delta}$ (YSCO) is an end member of Sr substitution for Ba site in $YBa_2Cu_3O_{7\pm\delta}$ and the crystal structure of YSCO is same as that of $YBa_2Cu_3O_{7\pm\delta}$. We research on the J_c and the H_{irr} for the under-doped, the optimized and the over-doped YSCO superconductor that pinning centers were introduced by heavy-ion irradiation.

The polycrystalline YSCO samples were prepared by the solid state reaction method using the high-pressure apparatus utilizing internal oxidizing agents (2 GPa, 1323 ~1373 K for 2 hours). Nominal compositions were $YSr_2Cu_3O_{6.9}$ for the under-doped, $YSr_2Cu_3O_{7.0}$ for the optimized and $YSr_2Cu_3O_{7.1}$ for the over-doped. Lattice parameters are determined to be a = 0.37901(7) nm and c = 1.1381(4) nm for the under-doped, a = 0.37885(5) nm and c = 1.13950(19) nm for the optimized, a = 0.37886(3) nm and c = 1.13892(15) nm for the over-doped by X-ray powder diffraction. Polycrystalline samples were cut and polished into thin discs less than 100 μm in thickness. The polycrystalline samples were irradiated with Au^{15+} ions (200 MeV energy) at the fluence of 1×10^{11} ions/cm^2 at room temperature using a Tandem accelerator at JAERI. The ion range were estimated from the range-energy relations proposed by Ziegler. For the heavy-ion irradiated YSCO samples, the length of the ion tracks was determined by the stopping powers calculated using TRIM 2000 codes. The tracks of the Au^{15+} ion of 200 MeV were 12.2 μm for the under-doped, 12.1 μm for the optimized and 12.0 μm for the over-doped, these values being smaller than the thickness of these samples, so that all of the irradiated ions stop inside of the samples.

The intragrain J_c was determined from *M-H* curves using Bean's critical state model and the maximum value of H_{irr} was determined by extrapolating J_c curves to a 10^2 A/cm^2 criterion. Figure 1 show the heavy-ion irradiation effect of the magnetic field dependence of J_c at 5K for the under-doped, the optimized and

[1]National Institute of Advanced Industrial Science and Technology (AIST)

the over-doped YSCO. In comparison with J_c of unirradiated YSCO, for the under-doped state, irradiated YSCO is decreasing clearly. For the optimized state, J_c of irradiated YSCO does not change and for the over-doped state, J_c of irradiated YSCO is slightly increasing. Figure 2 show H_{irr} versus 1-T/T_c of the under-doped, the optimized and the over-doped for the irradiated YSCO. The optimized and over-doped levels have been shown to shift the H_{irr} line to the higher magnetic field than that of the under-doped level. This is suggested that H_{irr} versus T/T_c characteristics improved with the increase in excess oxygen.

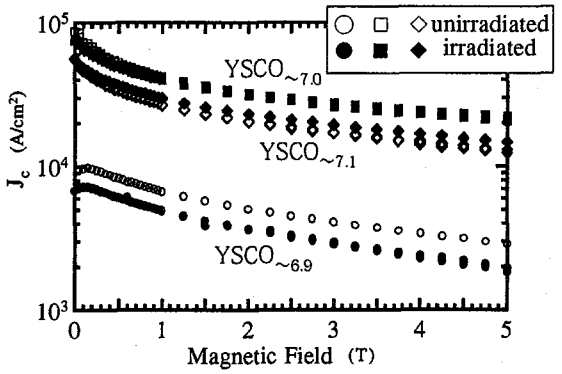

Fig. 1. The heavy-ion irradiation dependence of the J_c at 5K for the under-doped, the optimized and the over-doped YSCO.

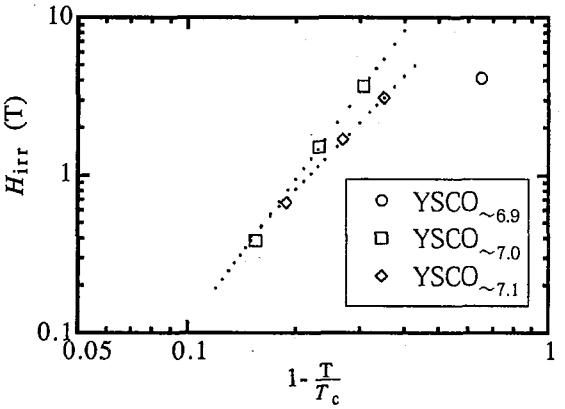

Fig. 2. H_{irr} versus 1-T/T_c of the under-doped, the optimized and the over-doped for the irradiated YSCO.

References

[1] H.Ihara: Kotaibuturi **35**(2000) 301 (in Japanese).

[2] T.Nakane, Y.Yasukawa, E.S.Otabe, T.Matsushita, M.Karppinen and H.Yamauchi: Physca **C338**(2000) 25.

[3] T. Nabatame, J. Sato, Y. Saito, K. Aihara, T.Kamo, S.Matsuda: Physica C **193** (1992)390.

[4] S. Lee, N.P. Kiryakov, D.A. Emelyanov, M.S. Kuznetsov, Y.D. Tretyakov, V.V. Petrykin, M. Makihana, H.Yamauchi, Y. Zhuo, M.Z. Kim, S.I. Lee: PhysicaC **305** (1998)57.

[5] H. Yamauchi, M. Karppinen, K. Fujinami, T. Ito, H. Suematsu, K. Matsuura and K. Iwasa: Supercond. Sci. Technol. **11** (1998) 1006.

6.5 VORTEX OBSERVATION IN Tl-BASED SUPERCONDUCTORS WITH A SCANNING SQUID MICROSCOPY

S. OKAYASU, S. SATAKA, A.IYO[1] and Y. TANAKA[1]

Thallium-based superconductor $TlBa_2Ca_2Cu_3O_x$ (Tl-1223) has the superconducting transition temperature, Tc, over 100K. Due to high-Tc and strong pinning properties, this material is a candidate for practical applications, such as superconducting wires, for high-Tc superconductor usage. To investigate the pinning properties of this material, a comparison of vortex images between pristine and Au-irradiated thin film sample is presented.

Thin film sample preparation will be shown in elsewhere[1]. High energy 200MeV-Au ion irradiation was accomplished at room temperature up to the dose $1x10^{10}$ ions/ cm^2, corresponding the matching field B_=0.2 Tesla. The superconducting transition temperature Tc is 102 K for both cases. Vortex imaging is obtained with a commercial scanning SQUID microscope SQM-2000 (Seiko nano technology)[2]. Measured temperatures are from 4 K to 120 K under a residual magnetic field (~1_T). The scanned area of the sample is 200_mx200_m and spatial sampling is every 2_m step.

As shown in the figure, vortex images for both cases, pristine sample and Au-irradiated one, can be observed just below the Tc. Due to the strong pinning, melting from vortex solid state to liquid state can not be observed. In spite of highly thermal fluctuations around 100 K, vortex arrangements are almost the same for both cases for all temperature range. This also suggests the existence of strong pinning centers. For pristine sample, some shadings of magnetic field other than vortices can be observed. They look like pairs of vortex-antivortex, but they are observed even above Tc. Thus the shadings come from the convexo-concave structure of the film surface, not superconducting origin. Some vortices, however, always stand by the shadings, and the convexo-concave structure must be one of strong pinning centers of this material. For Au-irradiated sample, on the other hand, no shadings of magnetic field on the surface is observed. The convexo-concave structure is smoothened by the irradiation, and the columnar defects play a role of pinning center on behalf of the structure.

[1]AIST, Tsukuba, Ibaraki 305-8577, Japan

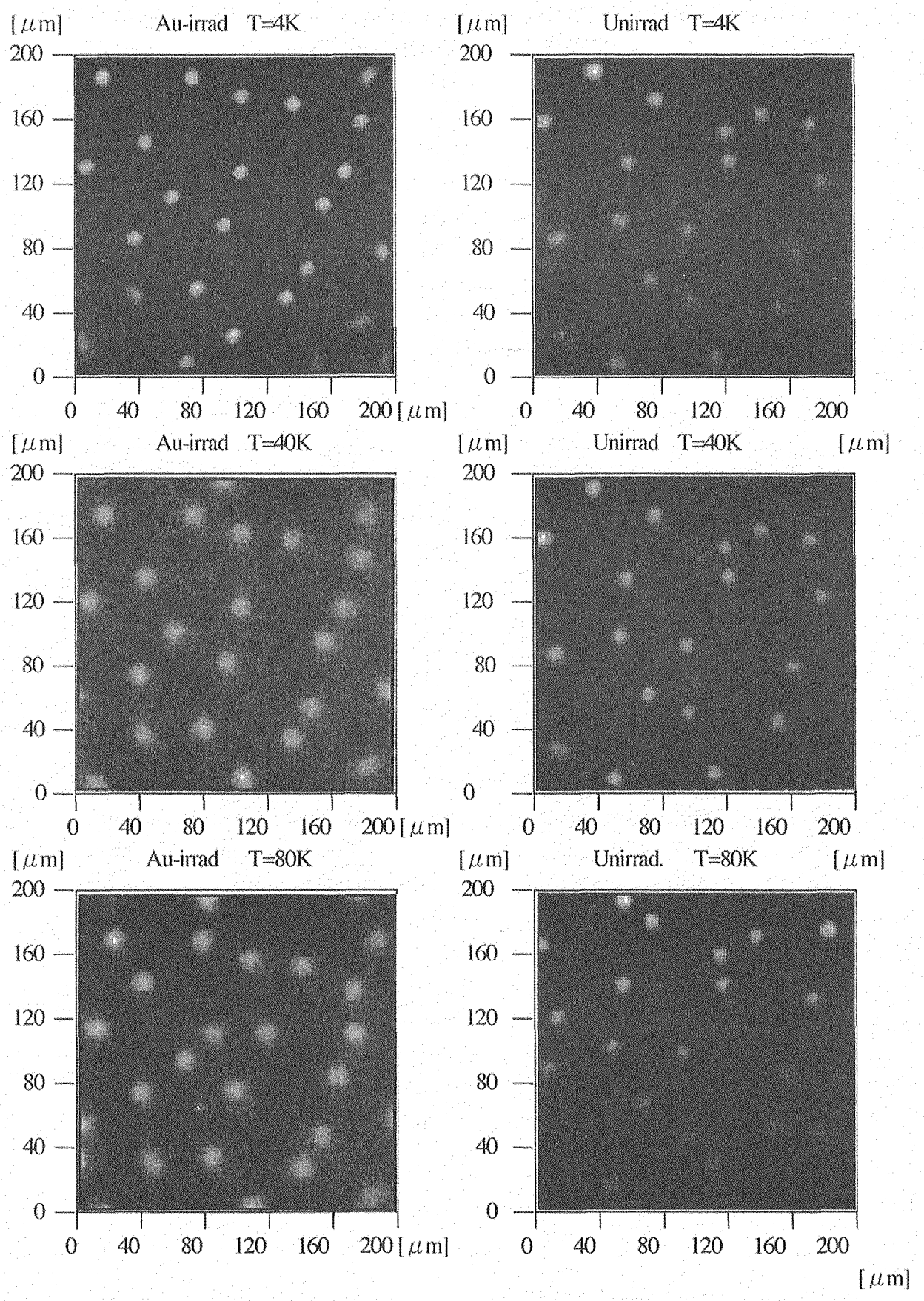

Fig.1 Voltex imaging Tl-1223 pristine and Au-irradiated thin film

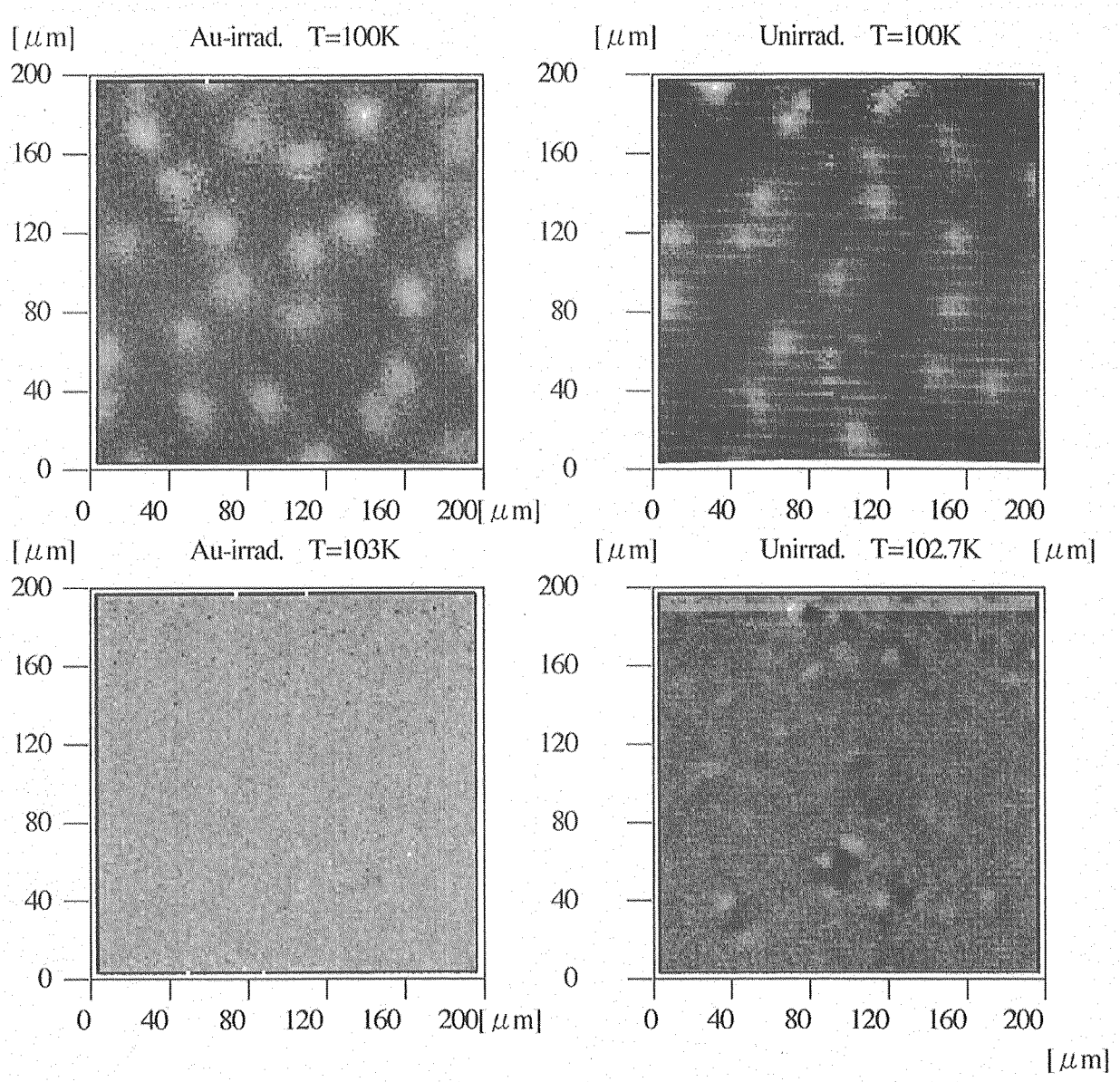

Fig.1 Voltex imaging Tl-1223 pristine and Au-irradiated thin film

Reffrences

[1] S. Athinarayanan et al., IEEE TRANSACTIONS ON APPLIED SUPERCONDUCTIVITY 13(2003)2913.

[2] T. Nishio et al., Physica C 412-414(2004) 379-384

This is a blank page.

7. Radiation Effects in Materials

This is a blank page.

7.1 ION BEAM MIXING AT Bi-SiO_2 INTERFACES

A. IWASE[1], R. NAKATANI[1], Y. CHIMI and N. ISHIKAWA

We have reported that atomic mixing is realized at Bi-Al_2O_3 interface by swift heavy ion induced electronic excitation [1]. In this report, we show that the electronic mixing at Bi-metal interface strongly depend on oxide substrates.

Bismuth was evaporated on SiO_2 substrates in a vacuum. The thickness of Bi later was about 100 nm. The specimens were irradiated with 200 MeV Xe or 200 MeV Au ions at room temperature up to the fluence of $1x10^{14}/cm^2$ using 20 MV tandem accelerator at JAERI-Tokai. As the thickness of Bi layers on SiO_2 substrates was much smaller than the projected range of the ions, all of irradiating ions passed completely through the Bi-SiO_2 interface. To examine the irradiation-induced atomic mixing, the concentration profiles at the interfaces for irradiated and unirradiated specimens were obtained by means of Rutherford Backscattering Spectrometry (RBS) with 2.4 MeV α-particles.

In Fig. 1, we plott the RBS spectra for unirradiated Bi-SiO_2 specimens and those irradiated with 200 MeV Xe or 200 MeV Au ions. The figure shows that even 200 MeV Au ion irradiation cannot induce any atomic mixing at Bi-SiO_2 interface. It has been reported that the threshold value of the electronic stopping power, Se, for amorphous track formation is 1.8 keV/nm for SiO_2[2], which is much smaller than the threshold value for Al_2O_3 (about 20 keV/nm[3]).

Then, we conclude that the atomic mixing under swift heavy ion irradiation cannot be described only by the sensitivity of interface-forming materials to electronic energy deposition. After the energy transfer from highly excited electronic system to the lattice system, some kind of chemical reaction may occur between interface-forming materials. If such a chemical reaction occurs under the irradiation, it should affect the final state of atomic mixing. To explain the difference in atomic mixing between Bi-Al_2O_3 and Bi-SiO_2 interfaces, we have to consider some factors which dominate chemical reactions, such as mixing enthalpy, diffusivity and so on.

1 Osaka Prefecture University

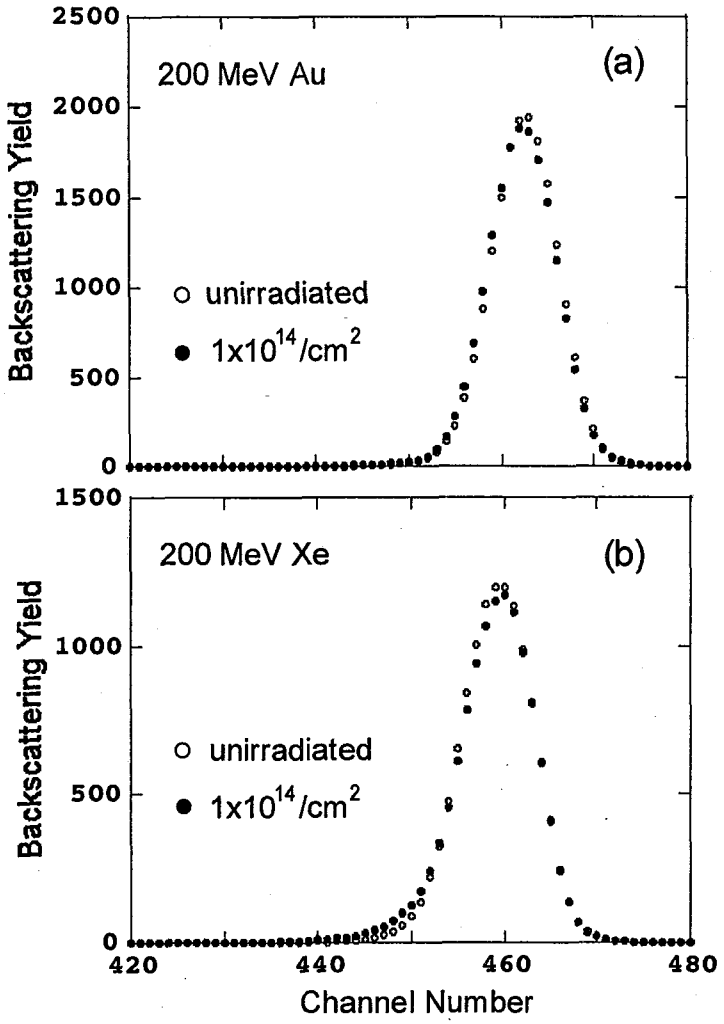

Fig. 1 RBS spectra for unirradiated Bi-SiO_2 specimens and for those irradiated with 200 MeV Au ions (a) or 200 MeV Xe ions (b).

References

[1] R. Natkatani, R. Taniguchi, Y. Chimi, N. Ishikawa, M. Fukuzumi, Y. Kato, H. Tsuchida, A. Iwase, JAERI-Review 2004-027, 78-79(2004).

[2] F. Studer, M. Hervieu, J. M. Constantini, M. Toulemonde, Nucl. Instr. Meth. B122, 449(1997).

[3] S. M. M. Ramos, N. Bonardi, B. Canut, S. Bouffard, S. Della-Negra, Nucl. Instr. Meth. B143, 319(1998).

JP0650043

7.2 ATOMIC DISORDERING AND STRUCTURAL CHANGE IN $MgAl_2O_4$ IRRADIATED WITH 350 MeV Au IONS

T. YAMAMOTO[1], M. SHIMADA[1], K. YASUDA[1], S. MATSUMURA[1], Y. CHIMI AND N. ISHIKAWA

Magnesium aluminate spinel ($MgO{\cdot}nAl_2O_3$) is one of the promising materials for the inert matrix of Rock-like oxide fuels, and will be exposed to fast neutrons, alpha particles, fission products (FPs) and so on. The high-density electron excitation caused by high energy FPs (typically 70 ~ 100 MeV) is known to induce columnar defects (latent tracks), and changes atomic configurations in the materials. In the present work, we investigated changes in microstructure and atomic configurations inside and around ion tracks induced by swift heavy ions, through the HRTEM and HARECXS (high angular resolution electron channeling X-ray spectroscopy [1]) techniques.

Single crystals of near-stoichiometric spinel ($MgO{\cdot}1.1Al_2O_3$) were cut into disks of 3 mm diameter and mechanically polished to about 120 μm thickness. The center of disks was dimpled and ion-milled with 5 keV Ar^+ ions to be electron transparency. The specimens were annealed in air at 1673 K for 2 h to remove defects produced by ion-milling. These prepared specimens were irradiated with 350 MeV Au^{28+} ions by Tandem accelerator in JAERI at room temperature to fluence of 1.0×10^{15}- 5.0×10^{15} ions/m^2. According to SRIM calculation, 350 MeV Au^{28+} ions deposit their energy mostly in electronic system, and the electronic stopping power S_e is estimated to be 34 keV/nm at the incident surface of specimens. The knock-on displacements are evaluated to be less than 10^{-4} dpa at the maximum fluence of 5.0×10^{15} ions/m^2. Followed by the irradiation, HRTEM observations and HARECXS experiments were performed. In HARECXS experiments, characteristic X-rays of Mg-K, Al-K and O-K were measured as a function of incident beam direction between -4g and 4g (g=400) Bragg conditions. Theoretical fittings of the experimental profiles were performed with ICSC program [2] to determinate atomic configurations.

Figure 1 illustrates HRTEM images of a specimen irradiated with 5.0×10^{15} ions/m^2. The ion tracks show square shapes, with about 2.5 nm on side length. Strong strain contrasts are observed in some regions between ion tracks. Furthermore, spacing of lattice fringes inside some ion tracks is seen to be half of the spacing of the matrix. This indicates that a phase transformation is induced from spinel structure by high-density electronic excitation. Figure 2 shows experimental and simulated HARECXS profiles obtained from the unirradiated and irradiated specimens. The profiles describe the variation of X-ray intensity as a function of incident beam angle along 400 direction. The theoretical calculation was performed on an assumption that the atomic configuration of the concerned region is uniform. The profiles, therefore, describe an average atomic configuration of irradiated and unirradiated regions. In figure 2, X-ray intensity decreases and becomes to be flat with increasing fluence. This indicates that the disordering progresses with irradiation. The volume fraction and diameter of disordered region were

[1]Kyushu University

evaluated from the profiles shown in figure 2. In this evaluation, the disordered region was assumed to have a random cation configuration. The estimated values of disordered region increase almost proportionally with the fluence. The value of diameter is identical within the experimental error and about 12 nm. This value is about 5 times lager than that observed by HRTEM (see Fig. 1), suggesting that the atomic disordering occurs far beyond the observable ion tracks.

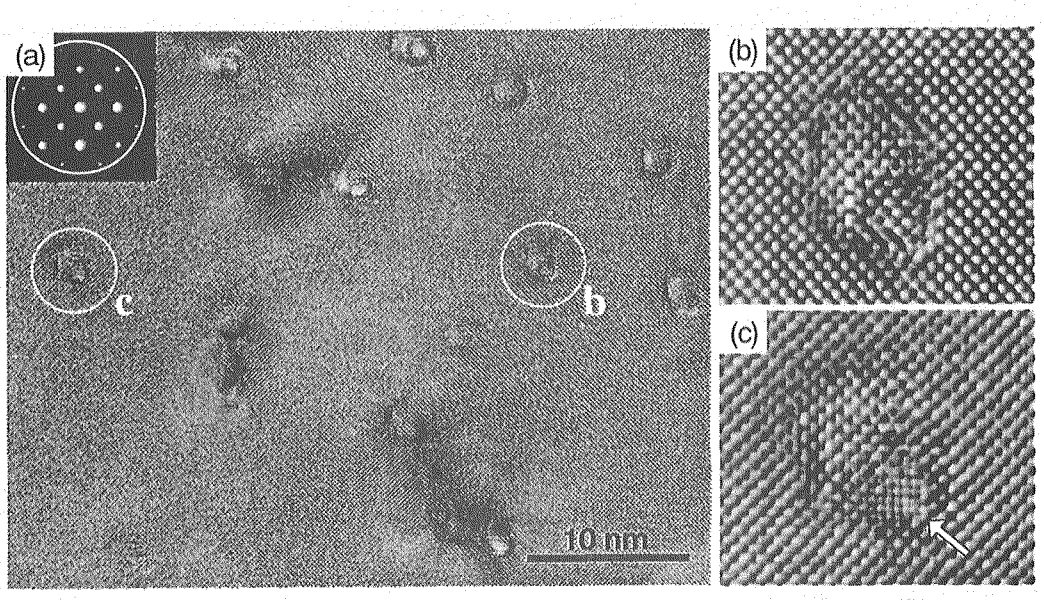

Fig. 1 (a) HRTEM image of the specimen irradiated with 5.0×10^{15} ions/m^2, which is taken along the irradiation direction. (b) and (c) Enlarged images of ion tracks in (a).

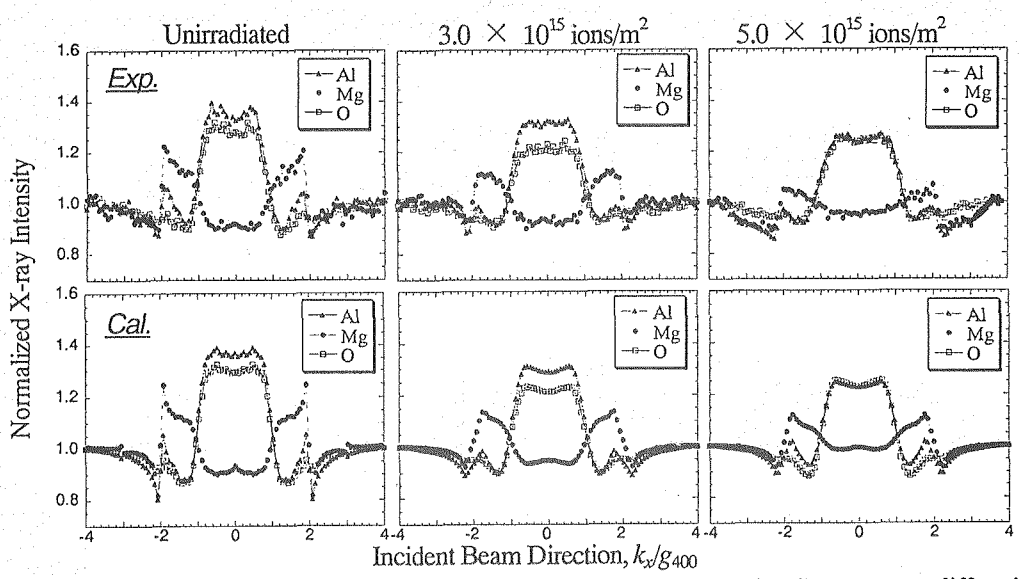

Fig. 2 Experimental and calculated HARECXS profiles. Horizontal axis expresses diffraction condition. Here, $k_x/g_{400}=1$ corresponds to the exact Bragg condition of 400.

References

[1] S. Matsumura, T. Soeda, M. Shimada and N. J. Zaluzec. , MRS symp. Proc. , 589 (2001) 129.

[2] M. P. Oxley and L. J. Allen, J. Appl. Cryst. , 36 (2003) 940.

7.3 STRUCTURAL CHANGE IN ANATASE TiO_2 THIN FILMS IRRADIATED WITH HIGH-ENERGY HEAVY IONS

N. ISHIKAWA, S. YAMAMOTO, Y. CHIMI

So far the structural change due to high-density electronic excitation effects has been extensively investigated for oxide superconductors irradiated with high-energy heavy ions, and in this system linear increase in lattice parameter as a function of ion-fluence has been always observed [1]. It is clear that formation of amorphous tracks along ion-paths is the origin of the lattice expansion, but it is not obvious in other oxide systems how the formation of tracks influences crystallographic structure of the lattice. In this study TiO_2 thin films with anatase structure have been irradiated with 230MeV Xe ions, and the change in X-ray diffraction (XRD) pattern has been investigated by varying the ion-fluence.

TiO_2 thin films with the thickness of 0.3μm were deposited on $SrTiO_3$ (001) by a pulsed laser deposition method. Before irradiation, two XRD peaks at 2_=37.7° and 80.4°, assigned to the (004) and (008) planes of TiO_2, respectively, are observed. After the irradiation up to the fluence of $1x10^{12}$ ions/cm^2, shift of XRD peaks has hardly been observed, indicating that there is no detectable increase in (average) c-axis lattice parameter within experimental error. After the irradiation up to the fluence of $3x10^{12}$ ions/cm^2, slight increase in c-axis lattice parameter is detected. Change in FWHM (Full width at half maximum) has hardly been observed up to the fluence of $3x10^{12}$ ions/cm^2. These results are in contrast to the results obtained for oxide superconductors which shows increase in lattice parameter and FWHM as well as a function of ion-fluence. The present results can be explained as the following. For TiO_2 system the track region along an ion-path is damaged due to the high-density electronic excitation, while the influence to the unirradiated region of the specimen is very small.

Intensities of the (004)-peak and (008)-peak decrease monotonically as a function of ion-fluence up to $3x10^{12}$ ions/cm^2 as shown in Fig.1. The decrease in the intensity can be explained by the formation of tracks which do not contribute to XRD. The fluence dependence of XRD intensity follows an exponential function as demonstrated in Fig.2. By assuming that the tracks occupy part of the specimen volume according to the Poisson law, the XRD intensity can be expressed by

$$I(\Phi)=I_o\exp(-A\Phi), \qquad (1)$$

where $I(\Phi)$ is the intensity of XRD peak as a function of ion-fluence Φ, I_o the $I(\Phi=0)$, and A

the area of tracks which do not contribute to XRD. By fitting the intensity data with the equation (1), the diameter of the track can be estimated to be $D=2x(A/\pi)^{0.5}$ =9.6nm, which is comparable with the track size reported for other oxides[2]. It is necessary to confirm track size directly by using a transmission electron microscope or an atomic force microscopy. Nevertheless, it should be noted that the track size measurement using XRD has been successfully applied for mica [3] and polivinylidene fluoride [4].

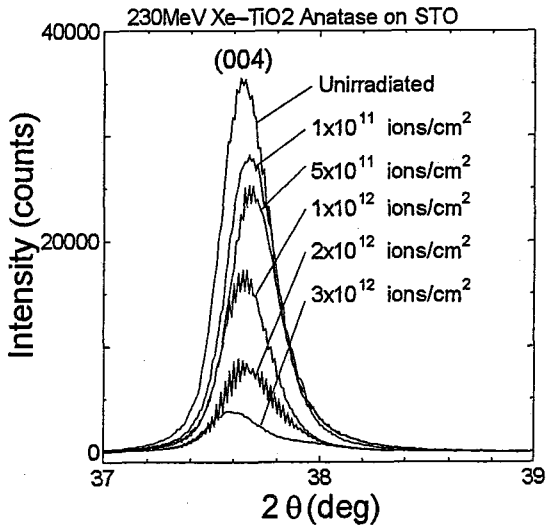

Fig.1. Evolution of (004) peak of TiO_2 thin films by the irradiations with 230MeV Xe ions.

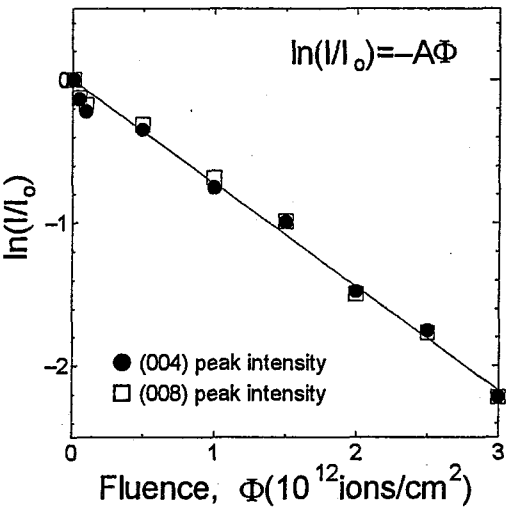

Fig.2. Intensity of XRD peaks for TiO_2 thin films plotted as a function of ion-fluence. The straight line is a fit to equation (1) assuming Poisson law.

References

[1] N. Ishikawa, A. Iwase, Y. Chimi, O. Michikami, H. Wakana, T. Hashimoto, T. Kambara, C. Müller and R. Neumann, Nucl. Instr. and Meth. B 193 (2002) 278.

[2] M. Toulemonde, S. Bouffard and F. Studer, Nucl. Instr. and Meth. B 91 (1994) 108.

[3] V. Chailley, E. Dooryhée, S. Bouffard and E. Balanzat, Nucl. Instr. and Meth. B 91 (1994) 162.

[4] V. Chailley, E. Balanzat and E. Dooryhee, Nucl. Instr. and Meth. B 105 (1995) 110.

JP0650045

7.4 ELECTRONIC EXCITATION EFFECTS IN CeO_2 UNDER IRRADIATION WITH HIGH ENERGY IONS

T. SONODA[1], M. KINOSHITA[1], N. ISHIKAWA, Y. CHIMI, M. SATAKA and A. IWASE[2]

In order to progress high burnup extension of LWR fuels, formation and growth mechanism of a crystallographic re-structuring in the periphery region of high burnup fuel pellets, as named "rim structure" [1] should be clarified. This structure is characterized by the existence of highly dense small sub-grains whose size is approximately 200 nm, and the accumulation of small pores with average size around 1 μm. The structure shall be formed by the accumulation and mutual interactions of radiation damages, fission products (FPs) and electronic excitations deposited partially by nuclear fissions [2].

In order to separate each of the processes as radiation damages, FPs and the effects of electric excitation, clarify the mutual interactions among them, and understand the formation mechanism of this restructuring, 70 – 210 MeV FP ions (Xe, I, Zr) irradiation examinations on CeO_2, as a simulation of fluorite ceramics of UO_2, have been done at JAERI-Tandem facility. Microstructural evolutions in the specimen are observed in a 300kV FE-TEM (HF-3000) at CRIEPI.

High dense electronic excitation effects by high energy ions irradiation produce a typical radiation damage, "ion tracks", in CeO_2. Table 1 summarizes the mean diameter of ion tracks under irradiation with several FP ions. This table suggests that the affected area of electronic excitation by fissions in CeO_2 seems to be around 5 ~ 7 nm ϕ, because the fission energies of Median light FPs and Median heavy FPs are around 95 MeV and 67 MeV, respectively. Fig. 1 shows the square of the mean diameter of ion tracks as a function of electronic stopping power (S_e). The dotted line in this figure indicates the estimated value derived from Szenes model [3], which is based on Thermal spike model [4]. In this figure, the square of track diameter tends to be proportional to S_e. This result suggests that the diameter of ion tracks, i.e. affected area by high-energy fission products, will be estimated by S_e. Fig. 2 indicates the mean diameter of ion tracks by 100 MeV Xe ion irradiation as a function of irradiation temperature (°C). This figure shows that the mean diameter was in decrease around 8% at 400°C relatively, though the inner-structure of ion tracks and microstructural evolution in CeO_2 were not so changed. This result indicates the temperature range from R.T. to 400°C will not affect on the annealing of ion tracks.

In order to clarify the overlapping effect of ion tracks, high fluence irradiation up to 1 x 10^{15} ions/cm^2 have been done, and observed microstructural exchanges by SEM/TEM. After overlapping of ion tracks by irradiation of 210 MeV Xe^{14+} to a fluence over 5 x 10^{12} ions/cm^2, the elliptical deformation of diffraction spots is observed, but the diffraction spots maintained at fluence up to 1 x 10^{13} ions/cm^2. These results indicate that the structure of CeO_2 is still crystalline, not amorphous. Fig. 3 shows the SEM image of grain surface in CeO_2 under irradiation with 210 MeV Xe^{14+} to a fluence of 1 x 10^{15} ions/cm^2. In this figure, surface roughness is observed and the characteristic size of the roughness, as shown in the line AB and A'B' in Fig.3 (a), is around 1 μm. Similar surface roughness has also been observed in LWR fuels. This result suggests that this roughness is occurred by the mutual interaction between the overlapping of high-dense electronic excitation and the accumulation of radiation damage.

---

[1] Sector, Nuclear Power Generation Technology, Nuclear Technology Research Laboratory, Central Research Institute of Electric Power Industry (CRIEPI)
[2] Research Institute for Advanced Science & Technology, Osaka Prefecture University

ION	Charge	Irradiation Energy (MeV)	Irradiation Temp. (℃)	Mean Diameter of Ion Track (nm)
Xe	14+	210	Room	9.30 ±0.12
	13+	150	Room	8.71 ±0.07
	10+	100	Room	7.91 ±0.09
	14+	80	Room	5.68 ±0.07
	14+	100	300℃	7.44 ±0.11
	14+	100	400℃	7.31 ±0.07
I	7+	80	Room	5.14 ±0.07
	7+	70	Room	～ 4.6
Zr	9+	100	Room	7.56 ±0.16

Table 1. Mean diameter of ion tracks under several FP ions and temperature in CeO_2

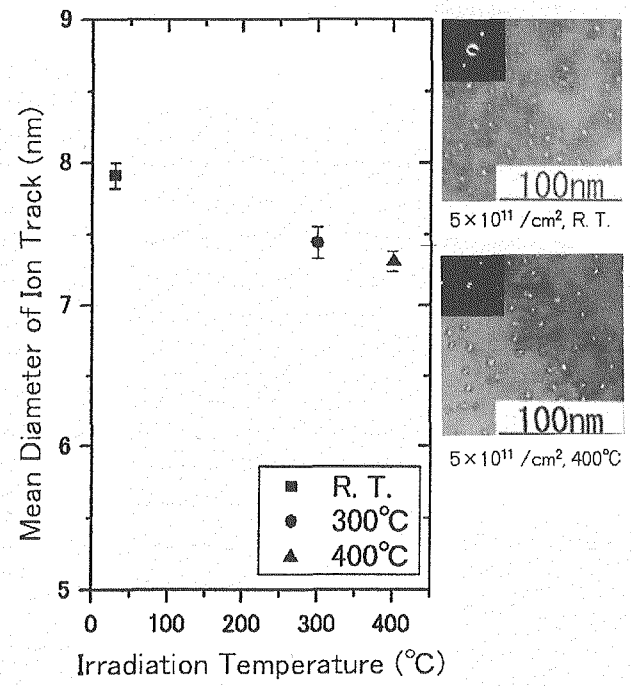

Fig 2. Mean diameter of ion tracks by 100 MeV Xe ion irradiation as a function of irradiation temperature (℃).

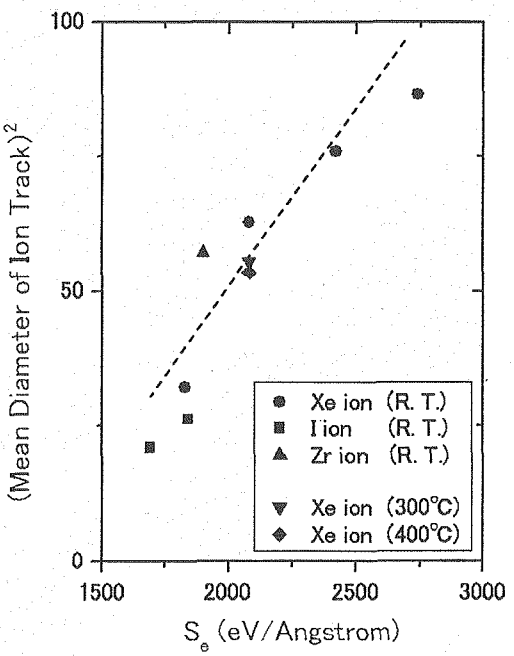

Fig 1. Square of the mean diameter of ion tracks as a function of electronic stopping power (S_e). Dotted line indicates the estimated value by Szenes model [3].

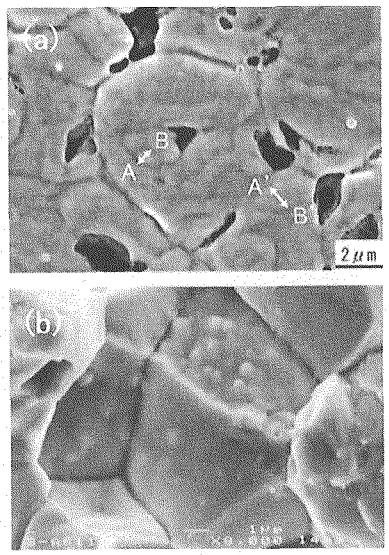

Fig. 3. SEM image of grain surfaces in CeO_2 under irradiation with 210 MeV Xe to a fluence of 1 x 10^{15} ions/cm^2 (a), and grain surface transient in LWR fuel (34MWd/kgU,400℃) (b).

References

[1] J. O. Barner, M. E. Cunningham, M. D. Freshley, and D. D. Lanning, HBEP-61, 1990, Battelle Pacific Northwest Laboratories.

[2] T. Sonoda, M. Kinoshita, I.L.F. Ray, T. Wiss, H. Thiele, D. Pellottiero, V.V. Rondinella and Hj. Matzke, Nucl. Instr. and Meth. B, **191** (2002) 622-628.

[3] G. Szenes, Phys. Rev. B**51** (1995) 8026.

[4] M. Toulemonde, J. M. Costantini, C. Dufour, A. Meftah, E. Paumier, F. Studer, Nucl. Instr. Meth. Phys. Res. B **116** (1996) 37.

JP0650046

7.5 EFFECTS OF Zr ION IRRADIATION AND SUBSEQUENT ANNEALING ON SUPERPLASTIC CERAMIC 3Y-TZP

Y. MOTOHASHI[1], T. SHIBATA, S. HARJO[1], T. SAKUMA[1],
M. ISHIHARA, S. BABA and K.SAWA

Superplastic ceramics have potential ability to be formed into net or near-net shapes by means of plastic working [1]. Although the application of the superplastic ceramics to nuclear energy field is very promising, there have been only a few studies so far relating to the irradiation effects on them [2-5]. Tetragonal ZrO_2 polycrystal containing 3mol% Y_2O_3 (3Y-TZP) is known to be a typical superplastic ceramic [1]. We have investigated some superplastic characteristics of Zr-ion irradiated 3Y-TZP, and have shown in previous works [3,5] that the flow stress and apparent activation energy for the superplastic deformation of the 3Y-TZP are increased by the Zr-ion irradiation. The present study aims to clarify the effects of Zr ion irradiation and subsequent annealing on room temperature mechanical and microstructural properties of the 3Y-TZP.

Chemical composition of the 3Y-TZP is ; Y_2O_3=5.15, HfO_2=1.7, $Al_2O_3 \leq 0.10$, $SiO_2 \leq 0.02$, $Fe_2O_3 \leq 0.01$, $Na_2O \leq 0.04$ and ZrO_2 = bal., in mass%. The 3Y-TZP specimens were irradiated using 130MeV Zr^{+11} ions at the TANDEM accelerator facility. Irradiation was performed with the fluence of 3.5×10^{12} and 2.1×10^{13} ions/cm^2. The former is hereafter referred to as "weakly irradiated" and the latter as "strongly irradiated". The irradiation induced displacements per atom (dpa) were estimated from Monte Carlo simulations using the TRIM code [6] and are shown in Fig.1. The TRIM simulations indicate that the peak damage emerges at a depth of approximately 10μm from the irradiated surface with 6.37×10^{-2} dpa and 1.06×10^{-2} dpa for the strongly and weakly irradiated cases, respectively. The shape of the 3Y-TZP specimens is a rectangular thin plate with the dimension of 1×2×20mm^3. The Zr^{+11} ions were irradiated to one of the widest side surfaces (2×20mm^2) of the specimens. Thermal annealing treatments were performed in air at temperatures ranging from 573 to 1573K for 30 min, followed by furnace cooling. Residual stress was measured by $\sin^2\psi$ method for the tetragonal (313) peak (2θ= 152.5 °) using characteristic X-ray, CrKα, at a condition of 40kV-30mA.

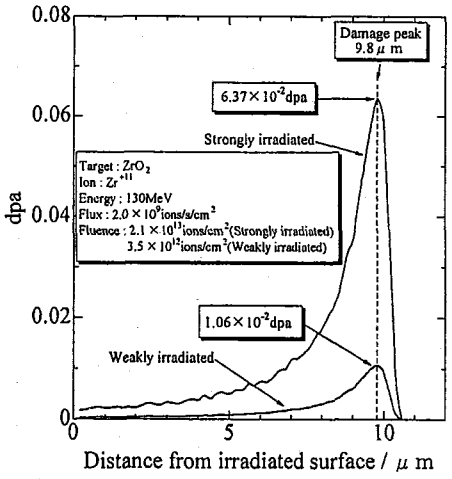

Fig.1 Displacements per atom as a function of depth from irradiated surface.

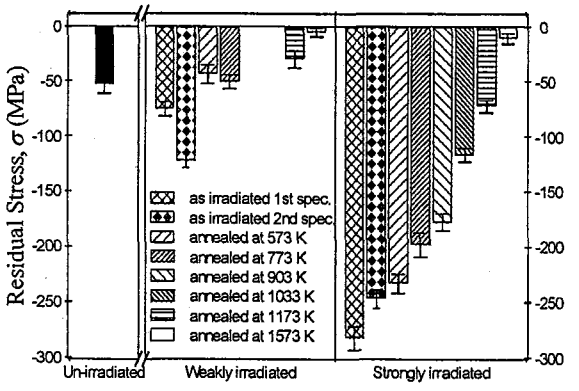

Fig.2 Residual stresses obtained from X-ray $\sin^2\psi$ method. 1st and 2nd spec. indicate specimens produced at different time, i.e., from different batches.

1. The Research Center for Superplasticity, Faculty of Engineering, Ibaraki University.

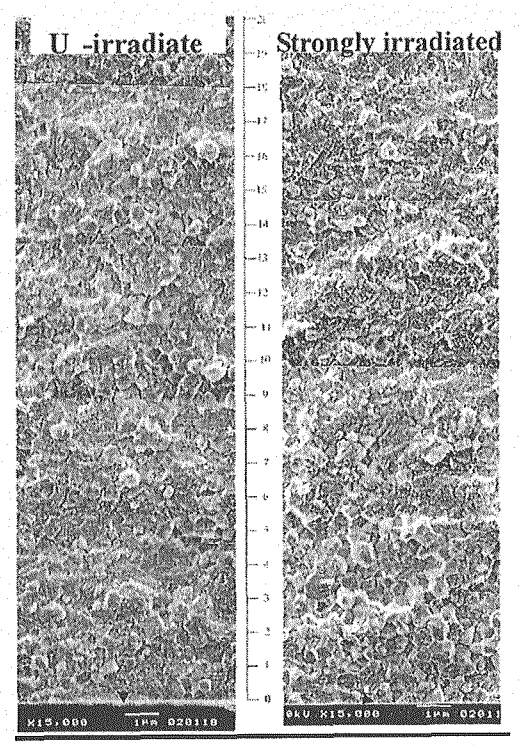

Fig.3 Fracture surfaces of (a) un-irradiated and (b) as-irradiated specimens in which irradiated surface is bottom.

The residual stresses left in the irradiated surface regions as a function of annealing temperature, T_{an}, are shown in Fig.2. It was found that the compressive residual stresses, the magnitude of which depended on the amount of irradiation, existed at the irradiated surfaces, and the residual stresses returned to that of un-irradiated state after annealing at $T_{an} \geqq 1173$K for both strongly and weakly irradiated cases. It appears that these compressive residual stresses were caused by the existence of interstitial atoms knocked-on by the irradiating Zr^{+11} ions as well as implanted ones by the irradiation.

The fracture surfaces of specimens bent to fracture at R.T. with the irradiated surface as the tension side are shown in Fig.3(a) and (b). It is seen that the fracture surface of the un-irradiated specimen consists mostly of brittle intragranular fracture, percentage of which is more than 80%. Meanwhile, the amount of intergranular fracture was increased, the percentage of which is about 60% at the largest, in an area from the irradiated surface up to approximately 10μm in depth direction. This area (region) corresponds to that of the irradiation affected zone as seen in Fig.1, which suggests that the irradiation would have decreased relatively the grain boundary cohesion.

The residual compressive stress was produced in the surface region of 3Y-TZP by the Zr ion irradiation. The annealing treatment for the as-irradiated specimens is able to recover the residual stress. The annealing at 1173K or higher returned the residual stress to former state. The fracture surface of the un-irradiated specimen bent to fracture at room temperature consisted mostly of intraglanular one, whereas the ion irradiation increased the ratio of the intergranular fracture to intragranular one in the irradiation affected zone. We have inferred that the decrease in the grain-boundary cohesion caused by the irradiation was responsible for the increase in the ratio of the intergranular fracture.

References

[1] For example, Y.Motohashi, Shinsozai, **4** (1993)33. (in Japanese).
[2] T.Shibata, Y.Motohashi, M.Ishihara, S.Baba and K.Hayashi, JAERI-Review, 2000-008, (2000) 1 (in Japanese).
[3] T.Shibata, M.Ishihara, Y.Motohashi, S.Baba and T.Hoshiya T.Kobayashi S.Harjo and T.Sakuma, Nucl. Instr. Meth. **B206**(2003)139.
[4] Y.Motohashi, T.Kobayashi, S.Harjo, T.Sakuma, T.Shibata, M.Ishihara, S.Baba and T.Hoshiya, Nucl. Instr. Meth. **B206**(2003)144.
[5] T.Shibata, M.Ishihara, Y.Motohashi, S.Baba, T.Sakuma and a T.Hoshiya, Mater. Sci. Forum **426-432**(2003)2813.
[6] J.F.Ziegler, Instruction manual for TRIM-95, IBM-Research, (1995).

7.6 ELECTRONIC EXCITATION EFFECTS ON POLYCRYSTALLINE SiO_2 BY HIGH ENERGY HEAVY IONS

N. MATSUNAMI[1], N. SHINDE[1], T. SHIMURA[2], M. SATAKA, S. OKAYASU

The energy transfer mechanism from the electronic system to lattice under high-energy heavy ion impact, which has not been established yet except for exciton model [1], is of considerable interest. Based on the experimental sputtering yields and charged fractions in sputtered particles from various oxides measured by the present authors [2, 3], it is concluded that both Coulomb explosion [4] and thermal spike [5] models are unsound, and a multi-exciton model has been suggested [6]. In this study, we report high-energy heavy ion irradiation effects on the electronic sputtering yields of polycrystalline (poly)-SiO_2.We compare the results with those of amorphous (a)- and single crystalline (c)-SiO_2. Use of poly-SiO_2 would give more information of structural modifications by high-energy heavy ion impact.

Poly-SiO_2 films were grown on Si(001) by heating at 1300° C in air for 5 hrs. X-ray diffraction (XRD) measurements were performed and the crystalline structure of the films was identified as tridymite, probably hexagonal structure with c-axis orientation [7, 8], T(002) as shown in Fig.1(a). Rutherford backscattering spectrometry (RBS) with 1.8 MeV He shows that the film thickness is ~1.2 μm and the composition is close to stoichiometric. Atomic force microscopy (AFM) did not give clear image but grain size was estimated to be a few tenth of μm.

We have measured sputtering yields of poly-SiO_2 with 200 MeV Xe and 90 MeV Ni ion irradiation for ion dose well below $10^{14}/cm^2$, applying a carbon (C)-film collector method [2, 3, 6]. As in the previous report that the sputtering yields are the same for a- and c-SiO_2 [6], it is found that the sputtering yields of poly-SiO_2 are the same as those of a- and c-SiO_2, irrespective of the polymorph. Fig. 1(b) illustrates that the XRD-peak-intensity of poly-SiO_2 for 100 MeV Xe ions at $1.7x10^{12}/cm^2$ decreases to a half of that of unirradiated film. The peak intensity of poly-SiO_2 shows monotonous decrease with ion dose, namely amorphisation and dose for amorphisation was found to be ~$10^{13}/cm^2$ and $10^{14}/cm^2$ for 100 MeV Xe and 90 MeV Ni ion irradiation, respectively. These doses are smaller than dose for amorphisation of c-SiO_2 (no amorphisation was observed even for $4x10^{13}/cm^2$). Thus, the electronic sputtering of poly-SiO_2 is taking place not in amorphous but in polycrystalline state. It is noticed that the compositions are remained stoichiometric after ion irradiation.

Interestingly, full-width at half-maximum (FWHM) of the XRD rocking curve around T(002) with 100 MeV Xe ion irradiation at $1.7x10^{12}/cm^2$ decreases to 80 % of the unirradiated value, as shown in Fig. 2. A similar but smaller reduction of FWHM was observed for 90 MeV Ni ion irradiation at somewhat larger dose than 100 MeV Xe ion irradiation. AFM shows no clear image after ion irradiation, i.e., no clear indication of grain-growth in contrast with the result for ZnO film on MgO [9]. From the XRD and AFM results, the decrease in FWHM can be ascribed to alignment of grain-orientation.

[1] Division of Energy Science, EcoTopia Science Institute, Nagoya University
[2] Nano-Materials Division, EcoTopia Science Institute, Nagoya University

It appears that the dose at which FWHM takes its minimum is roughly comparable with the dose at which the XRD intensity drops to a half of the unirradiated intensity. This result indicates that the decrease in FWHM is due to the electronic excitation effects, since it has been known that amorphisation of c-SiO_2 are caused by the electronic excitations.

Alignment of grain orientation as well as track formation and electronic sputtering originate from the electronic excitations. Relations between them are to be investigated for better understanding of the energy transfer mechanism from the electronic system to atomic motion.

The authors thank T. Kato (JAERI) for helpful discussion and T. Masuda (Nagoya University) for technical assistance of ion beam analysis.

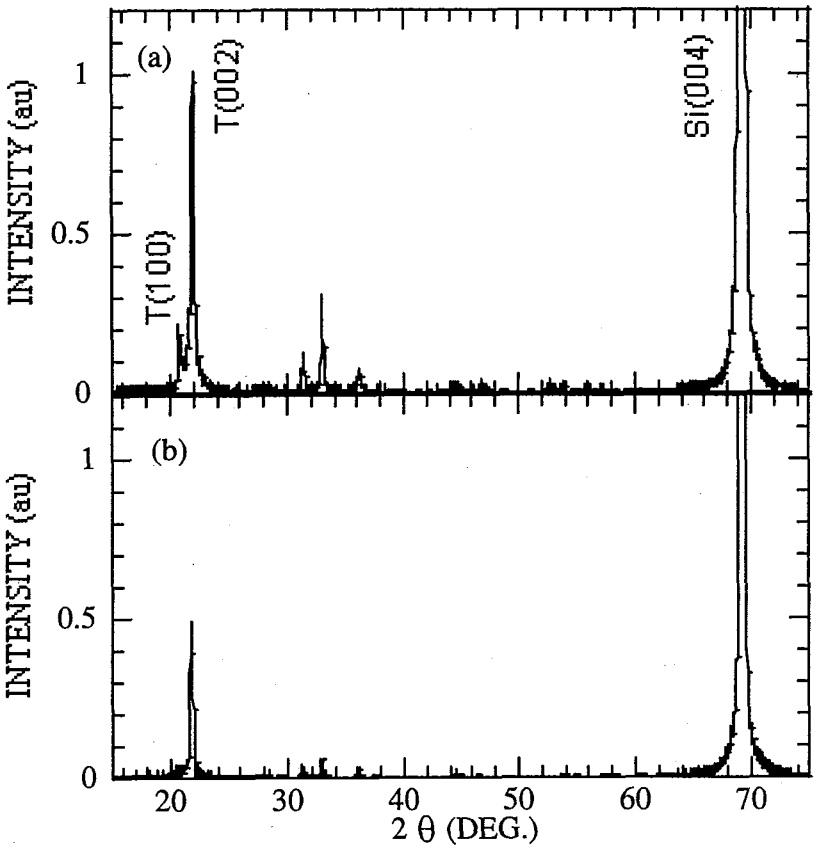

Fig. 1 XRD patterns of poly-SiO_2 films on Si(001) :(a) unirradiated and (b) irradiated with 100 MeV Xe ions at 1.7×10^{12} cm^{-2}. T(002) and T(100) indicate (002) and (100) diffraction peaks of tridymite-hexagonal structure.

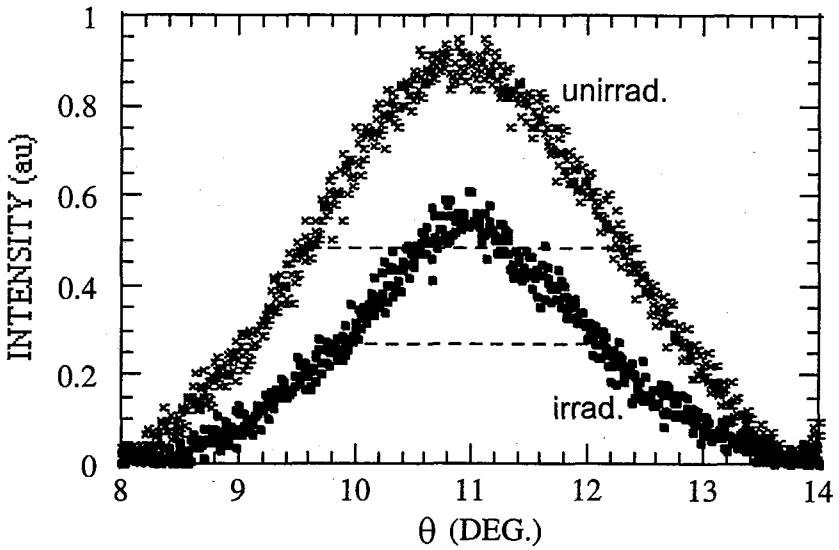

Fig. 2 XRD rocking curves of poly-SiO_2 films on Si(001) around T(002) shown in Fig. 1:(a) unirradiated and (b) irradiated with 100 MeV Xe ions at $1.7x10^{12}$ cm^{-2}. Dashed lines indicate FWHM of the rocking curves.

References

[1] N. Itoh, A. M. Stoneham, "Materials Modification by Electronic Excitation", Cambridge, 2001.
[2] N. Matsunami, M. Sataka, A. Iwase, Nucl. Instrum. Meth. B193(2002)830.
[3] N. Matsunami, M. Sataka, A. Iwase, S. Okayasu, Nucl. Instrum. Meth. B209(2003)282.
[4] R. L. Fleischer, Tracks to Innovation, Springer-Verlag, 1998.
[5] M. Toulemonde, C.H. Dufour, A. Meftah, E. Paumier, Nucl. Instrum. Meth. B166-167 (2000)903.
[6] N. Matsunami, O. Fukuoka, T. Shimura, M. Sataka, S. Okayasu, Nucl. Instrum. Meth. B 230(2005)507.
[7] S. M. Schnurre, J. Grobner, R. S.-Fetzer, J. Non-Cryst. Solids 336(2004)1.
[8] N. R. Keskar, J. R. Chelikowsky, Phys. Rev. B46(1992)1.
[9] N. Matsunami, O. Fukuoka, M. Tazawa, M. Sataka, Surf. Coatings Technol. 196(2005)50.

7.7 HIGH ENERGY HEAVY ION INDUCED DISORDERING IN Li_2TiO_3

T. NAKAZAWA, A. NAITO, T. ARUGA, V. GRISMANOVS[1], Y. CHIMI, N. OOKUBO, A. IWASE[2] and S. JITSUKAWA

The lithium metatitanate (Li_2TiO_3) is regarded as one of the most suitable candidates for the solid tritium breeder material of D-T fusion reactors. It is known that in an operating fusion reactor, the radiation damage in Li_2TiO_3 will be produced by fast neutrons, energetic tritons (2.7MeV) and helium ions (2.1MeV) generated by $^6Li(n,\alpha)^3H$ reaction. The lattice damages caused in the breeder materials by ionising radiation may result in the structural disorder and hence may have an influence on the tritium release behavior, and on thermal and mechanical properties. Thus, the study on structural disorder of the breeder material is essential to evaluate its irradiation performance. In this study, the structural disorder in Li_2TiO_3 due to irradiation with high energy xenon (Xe) ions is examined by use of Raman spectroscopy.

The irradiation with 18-160 MeV Xe ions is carried out for the Li_2TiO_3 ceramics at ambient temperature using Tandem Accelerator of JAERI. The fluence is in the range of $2.4x10^{16}$ to $4.9x10^{17}$ ions/m^2. SRIM 2000 code [1] is used to estimate the damage parameters such as the electronic (S_e) and nuclear (S_n) stopping powers and accumulated electronic energy depositions (D) (see Table 1). The Raman spectra are measured for samples before and after irradiation at ambient temperature with JASCO NR 1100 Raman spectrometer operated at 100 mW using the 488 nm line Ar laser as the excitation source.

Table 1. Irradiation conditions of Li_2TiO_3

Ion	Xe
E (MeV)	18 - 160
R_p (μm)	4.4 - 17
Fluence (ions/m^2)	$2.4x10^{16}$, $2.4x10^{17}$, $4.9x10^{17}$
D (GGy)	0.01 – 0.24
S_e (keV/nm)	5.7 – 16.7
S_n (keV/nm)	0.02 – 0.12

E: energy of ions, R_p: mean projected range, D: accumulated radiation dose, S_e: electronic stopping power at near surface, S_n: nuclear stopping power at near surface. R_p, S_e and S_n are calculated with the SRIM2000 code [1].

The Raman spectra of samples before and after irradiation are shown in Figure 1. The vibrational spectra of lithium titanate oxides have been studied using the results of group-theoretical analyses [2, 3]. An information on short-range order in Li_2TiO_3 can be seen from a Raman spectrum before irradiation. In lithium titanate, the frequencies in the 700-550cm^{-1} region are known to be assigned to Ti-O stretches in TiO_6 octahedra. In oxides where lithium is octahedrally coordinated by oxygen the frequencies of the Li-O stretches are known to lie within the 250-400 cm^{-1} region. When the lithium coordination is tetrahedral, the Li-O stretches lie in the 400-550 cm^{-1} region. In the Li_2TiO_3 structure the lithium occupies both octahedral and tetrahedral positions.

Figure 1 shows that Raman intensities are changed by the irradiation. The changes are remarkable with the increase in the value of S_e, but not the value of S_n. Raman peaks for the samples irradiated by 18MeV Xe ions with S_e of 6.0 keV/nm at surface are slightly

[1]OECD Halden Reactor Project

[2]Division of Radiation Physics, Research Institute for Advanced Science and Technology of Osaka Prefecture University

reduced as the fluence increase from $2.4x10^{16}$ to $4.9x10^{17}$ /m^2. The peak heights for the 663 cm^{-1} peak of Ti-O bond vibration and the 422 cm^{-1} peak of Li- O bond vibration relative to the 355 cm^{-1} peak of Li-O bond vibration are 3.4 and 2.8 before irradiation, respectively. They are reduced to 2.2 and 1.8 with the increase in fluence, respectively (see Figure 2). The heights of the 663 cm^{-1} and 422 cm^{-1} peaks relative to the 355 cm^{-1} peak are reduced to 1.65 and 1.35, respectively, with the increase in the S_e value to 9.5, but not affected with the increase in the fluence and D value. Almost all Raman peaks are not observed for the samples irradiated with larger S_e value such as 13.0 and 16.7 keV/nm. The formation of new phases and decompositions, such as TiO_2, are not confirmed from results of Raman analyses.

Such a reduction and disappearance of Raman peaks indicates that the structural units in Li_2TiO_3, such as TiO_6, LiO_6 and LiO_4 units, are disordered by irradiation. Such a short-range disorder due to the irradiation is significantly connected with the S_e value, but not with the fluence and D value. The results of Raman spectroscopic analyses indicate that the main factor causing short-range disordering of Li_2TiO_3 due to irradiation with high energy Xe ions is considered to be the electronic stopping power of incident ions.

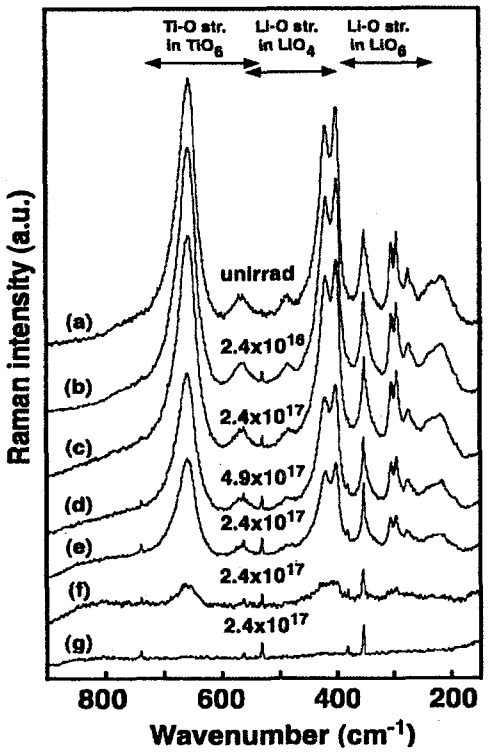

Fig. 1 Changes on Raman spectra of Li_2TiO_3 irradiated with high energy Xe ions. S_e:(a) 0, (b,c,d) 5.7, (e) 9.5, (f) 13.1, (g) 16.7. S_n:(a) 0, (b,c,d) 0.12, (e) 0.07, (f) 0.04, (g) 0.02 (Unit: keV/nm) , D:(a) 0, (b) 0.01, (c) 0.08, (d) 0.17, (e) 0.14, (f) 0.19, (g) 0.24 (Unit: GGy) .

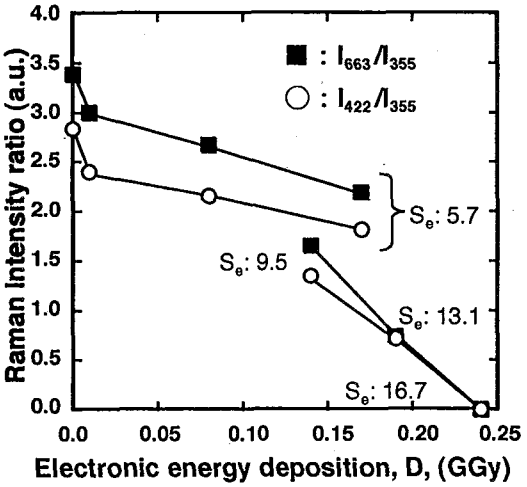

Fig. 2 Changes in Raman intensity ratio of Li_2TiO_3 irradiated with high energy Xe ions.

References

[1] J.F. Ziegler, J.P. Biersack and U. Littmark, The Stopping and Range of Ions in Solids, Pergamon, Oxford, 1985.

[2] E.V. Proskuryakova, O.I. Kondratov, N.V. Porotnikov and K.I. Petrov, Russ. J. Inorg. Chem. 28 (1983) 791.

[3] N.V. Porotnikov, N.G. Chaban and K.I. Petrov, Russ. J. Inorg. Chem. 28 (1983) 1402.

JP0650049

7.8 XRD STUDY ON INITIAL STAGE OF AMORPHIZATION IN SINGLE CRYSTALLINE α-Al_2O_3 IRRADIATED WITH 160 MeV Xe IONS

N. OKUBO, T. NAKAZAWA, Y. CHIMI, N. ISHIKAWA, T. ARUGA and S. JITSUKAWA

Aluminum oxide (α-Al_2O_3) is expected as functional materials in a field of nuclear energy e.g. an insulating material in a fusion reactor and an inert matrix of rock-like oxide fuels including transuranium elements. Recently, amorphization in ceramics such as α-Al_2O_3, which affects the physical properties, is attracted as a phenomenon induced by high energy ion irradiations [1]. In previous studies, we have reported that amorphous phase is caused in polycrystalline aluminum oxide by ion irradiation with high-density electronic energy depositions (S_e), although lattice structure of aluminum oxide is stable against nuclear energy depositions (S_n) [2]. Effects of grain boundaries and crystalline directions on the amorphization induced by ion irradiations, however, have not been studied.

Single crystalline α-Al_2O_3 specimens with (0001) surface were irradiated with 160 MeV Xe ions at ambient temperature, by using the Tandem Accelerator of JAERI. The specimens used were 10 x 10 mm^2 plates with 0.5 mm thickness and with an optical grade surface. The fluences were in the range of 2.0×10^{13} to 2.0×10^{14} ions/cm^2. The projected range (R_p) of the Xe ions for the specimen was calculated to be 10.7 μm with the TRIM code [3]. The electronic energy deposition (S_e) and nuclear energy deposition (S_n) at the surface were also calculated to be 24.5 keV/nm and 0.1 keV/nm, respectively. X-ray diffractometry (XRD) for the specimens before and after irradiations were conducted in the range of 20 to 110 degree for 2 θ. The accumulative time and step angle were 2.0 second and 0.004 degree, respectively, and the specimen was rotated parallel to c axis. The specimen was covered by Au film with 10 μm thickness and 3mmϕ hole to eliminate XRD signals from the unirradiated region.

The XRD patterns of the Al_2O_3 specimens before and after irradiations are shown in the range of 41 to 42.5 degree for 2 θ in Fig. 1. A strong peak is observed at 41.7 degree in the XRD pattern for the specimen before irradiation. The peak is due to Al_2O_3 (0006) plane. The XRD intensities were normalized to that of the pristine Al_2O_3 (0006) peak. After the irradiation to 2.0×10^{13} ions/cm^2, new two peaks appear around 41.4 and 41.6 degree as shown by arrows in the figure, unexpectedly. These peaks grow in the fluence range of 2.0×10^{13} to 5.0×10^{13} ions/cm^2, then, become smaller and broaden remarkably at the fluence of 2.0×10^{14} ions/cm^2. As shown in Fig. 2, the relative areas of the new two peaks to the (0006) peak increase steeply with increasing the fluence to 5.0×10^{13} ions/cm^2 and decrease with increasing the fluence. Interplanar spacings for the new two peaks around 41.4 and 41.6 degree, are calculated to be 0.218 and 0.217 nm, respectively. They are slightly larger than that for the (0006) peak, which is calculated to be 0.216 nm. The both peaks around 41.4 and 41.6 degree shift gradually to smaller angle with increasing fluence. In general, shift of XRD peak to smaller angle means expansion of interplanar spacings.

Such behaviors described above of the new peaks due to the irradiations indicate that in the early stage of irradiation to 5.0 x 10^{13} ions/cm^2 new lattice planes are formed, and that the new lattice planes formed are disordered by the prolonged irradiation above 1.0 x 10^{14} ions/cm^2. That is, amorphization takes place above this fluence. Atomic displacement in insulators is considered to be caused along ion trajectory for ion irradiation with high-density S_e. New lattice planes as observed in present study, thus, are considered to be formed by atoms displaced along the ion trajectory, and result in the expansion of interplanar spacings. In the region of depths measured by the XRD, value of S_e is much larger than that of S_n. Especially, the value of S_e at surface is about 250 times as large as that of S_n.

In summery, the XRD results in this study indicate that in the initial stage of amorphization in single crystalline α-Al_2O_3, high-density S_e causes the formation of new planes and disordering. Detailed elucidation of the amorphization in single crystalline α-Al_2O_3 is in progress by cross sectional TEM measurements.

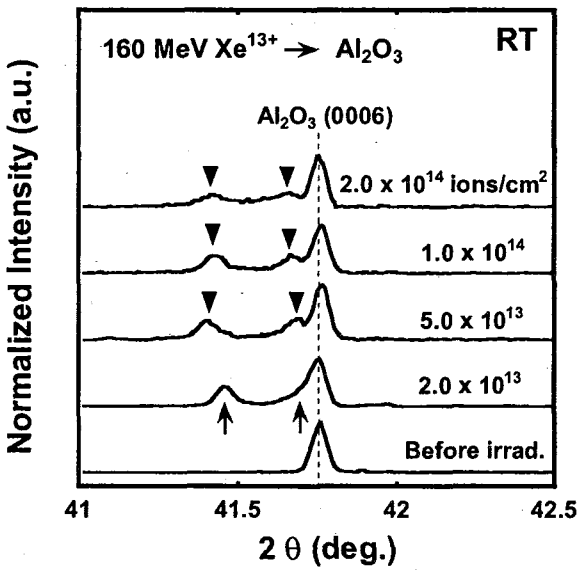

Fig. 1 XRD patterns of Al_2O_3 specimens before and after irradiations. Total fluence was changed up to 2.0 × 10^{14} ions/cm^2.

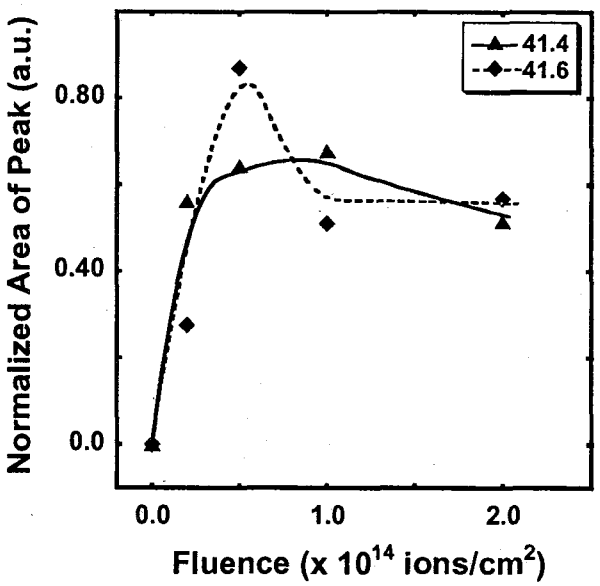

Fig. 2 Change of areas of XRD peaks at 41.4, 41.6 degree normalized by area of peak at 41.7 degree.

References

[1] G. Szenes, J. Nucl. Mater. **336** (2005) 81-89.

[2] T. Aruga, Y. Katano, T. Ohmichi, S. Okayasu, Y. Kazumata, Nucl. Instr. and Meth. B **166-167** (2000) 913-919.

[3] J.F. Ziegler, J.P. Biersack, U. Littmark, The Stopping and Range of Ions in Solids, (Pergamon Press, New York, 1985), Chap 8.

[4] A. AL. Ghamdi, P. D. Townsend, Nucl. Instr. and Meth. **B 46** (1990) 133-136.

7.9 RELEASE BEHAVIOR OF IMPLANTED Xe FROM CeO_2 - IMPLANTATION OF Xe IN CeO_2 -

H.OGAWA, I.IOKA, K.KIUCHI, Y.ISHIJIMA AND Y.NANJO

The gas release behavior of heavy rare gases such as Xe and Kr formed as fission products in nuclear fuel oxides are very important for understanding the pellet – clad interactions on fuel elements at high burn-up. The accumulation of these gases in the gap of fuel elements by gas release acts to decreasing the thermal conductivity and increasing the fuel temperature and internal pressure. Moreover, the swelling due to the void formation of these gases in oxide fuels is one of the most important problems for attaining ultra-high burn-up with respect to economical requirement. However, the release mechanism of these gases is not basically clarified. From the practical experiences in nuclear oxide fuels, the gas release temperature of heavy elements such as Xe and Kr is higher than it of light elements such as He. The fuel temperature for LWRs at the present normal operation is controlled less than 1500°C for inhibiting gas release. However, the modified fuel design applied to the advanced LWRs are required to enhance the fuel temperature for attaining ultra-high burn-up, controlling the low neutron energy spectrum and applying super critical pressurized water for high temperature operation. Therefore, it is very important to evaluate their release mechanism from the pellet. At the first step, we tried to evaluate Xe distribution in a dummy fuel, CeO_2 irradiated by the tandem.

In this study, Xe^{14+} ion with 180MeV was irradiated into CeO_2 test piece (a porous material) for three hours using the TANDEM. Some surface analyzers, EDX, XPS, SIMS and EPMA, evaluated the depth profile of Xe in the test piece. Xe content was also calculated by SRIM code, and it was estimated that the content was a few atomic present in the test piece around the depth of 10μm. Figure 1 shows the cross section of CeO_2 implanted Xe and the depth profile of each element by EDX. However, the signal of Xe was almost the same as that of background. Their analyzers could not detect implanted Xe. This might be caused by the pore or low irradiation rate.

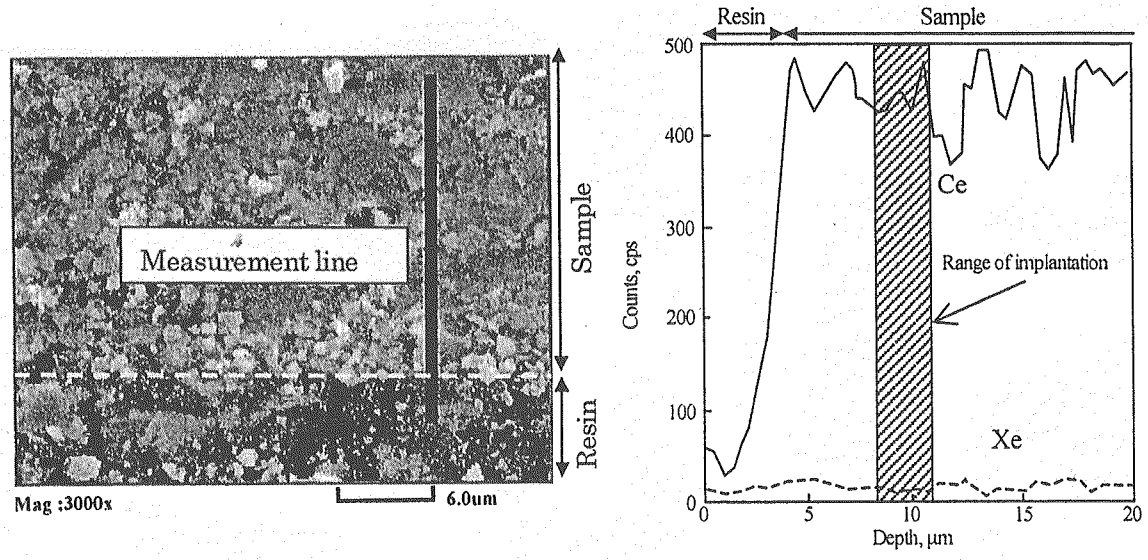

Fig. 1 Cross section of CeO_2 and the depth profile of Ce and Xe by EDX

7.10 STRUCTURE OF DEFECT CASCADES IN HEAVY ION-IRRADIATED NICKEL AT LOW TEMPERATURE BY X-RAY DIFFUSE SCATTERING

H. MAETA, H. SUGAI, T. KATO, H. OHTSUKA, N. MATSUMOTO and M. SATAKA

Displacement cascade is one of the most important problems in the nuclear materials [1]. Energetic heavy ions produce point defects such as vacancy-interstitial pairs and also displacement cascades containing high and local concentrations of these defects. In the study of radiation damage of solids, it is recognized that some radiation-induced defects might be mobile even below liquid hydrogen temperature. In order to retain the defects in the original configuration, it is necessary to irradiate at such as low temperature that the defects can not migrate and to observe the defects at the same low temperature. There are many measurements of the displacement cascade in these materials, but those are measured only by the transmission electron microscopy (TEM). However, few observations have been carried out at the low temperatures [2]. Most of studies were carried out at high temperature where the defects move out and change not only its original structure but also the size. Such a defect should be small size below the visibility limit of TEM. On the other hand, X-ray diffuse scattering [3] is a powerful method to observe nondestructively such a small defect in bulk specimen at low temperature below 10K [3, 4,5]. A cryostat has been developed for both ion irradiation below 10 K and transferring the specimens at low temperature to the x-ray diffraction measurement without any warming. This developed cryostat consists of a liquid helium chamber and a small refrigerator. During irradiation, the specimen is cooled down by means of both the refrigerator and liquid helium flowing. During transporting the specimen was maintained at low temperature by liquid helium flowing from a helium container. On the x-ray measurements the cryostat was settled on the goniometer and the specimen can be maintained at low temperature by the refrigerator for long time measurement.

Single-crystalline Ni specimens (purity:99.999%) were spark-cut from a large single crystal grown by the Czochoralski method. The size of all specimens used is about 10_4_1 mm^3. The specimens were irradiated below 13K with 137 MeV xenon ions (Xe^{10+}) by the Tandem Accelerator at JAERI, Tokai. After the irradiation the cryostat with the specimens were transferred to the x-ray goniometer below 20K. The x-ray diffuse scattering measurements on the irradiated specimens were performed below 20K with four circle diffractometer using CuK_1 from an 18kW rotating X-ray anode. The scattering intensities were measured close to Bragg (111) reflection in the [111] direction. The diffuse scattering intensity was obtained by taking a difference between the intensity from an irradiated and that from a non-irradiated region of the same specimen.

For the fluences of 2.3_10^{13} ions/cm^2 , the results of the diffuse scattering close to the (111) reflection in the [111] direction measured at 20K is shown in Fig.1. We can see a diffuse scattering along a large area in a reciprocal lattice. The diffuse scattering was obtained by subtracting the background intensities from the total intensities and averaging the difference at point +q and –q in the reciprocal space, i.e. $D_{D.S}(q) = 1/2(\Delta I_{+q} + \Delta I_{-q})$.

---

1 Hiroshima Kokusai Gakuinn University

And the q dependence of diffuse scattering intensity is shown in Fig. 2, indicating a deviation from q^{-2} dependence. The diffuse scattering intensities were usually plotted on a double logarithmic scale versus q ($\boldsymbol{q} = \boldsymbol{K} - \boldsymbol{h}$ where $\boldsymbol{K}$ is the scattering vector and $\boldsymbol{h}$ the reciprocal lattice vector). In Fig. 2, the typical $1/q^2$ dependence (Huang diffuse scattering from the point defects and clusters) and the $1/q^4$ dependence (the Stokes-Wilson scattering from a large distorted region, dislocation loops and the cascade [3]) are clearly demonstrated. By the thermal annealing at 40 K the diffuse scattering from a large distance at the Bragg angle disappeared, we can see this behavior in the Fig. 2. At this annealing we did not observe a change of vacuum degree in the cryostat . For Ni after the irradiation by electron, neutron and ions the change of electrical resistivity at recovery stage I_A is very small; this recovery is due to the interstitials rearrangements or rotation at their position by the annealing below 40K [7]. Since the recovery stage I_A of Ni is above 20K, the defects produced by the irradiation can not rearrange or migrate below 20K [7]. The defects, i.e. closed Frenkel pairs, interstitials and vacancies rearranged by the thermal annealing at 40K. The typical q^{-2} and q^{-4} dependence of the diffuse scattering can clearly be seen indicating the presence of the displacement cascades. The change from q^{-2} dependence to q^{-4} dependence is drastically seen at a critical point q_0 where $q_0 \cdot R_0 = 1$ (a distance R_0 at which the lattice distortions change the phase of the scattered wave) [3]. We can roughly estimate the average size of cascade radius R_0 to be about 1.0 nm.

This deviation from the q^{-2} arises from the correlation [3] in the distances between closed Frenkel pairs, vacancies and interstitials inside the cascades. In most metals, the relaxation volume of the interstitial is nearly ten times larger than that of the vacancy, and the correlation does not give rise to cancellation in the long-range strain field of the interstitial [3]. At the inside of the cascades, however, deviation from the q^{-2} dependence suggests that within the cascades region the defects are different from that in crystalline metals. It indicates a deviation from the $1/r^2$ decrease of the elastic displacement of point defects. It suggests the corresponding superposition of the displacements occures at large displacement between the vacancy-interstitial pair and cancellation at lager distances. Similar vacancy-interstitial pairs have been observed for semiconductors of electron irradiated InP and GaAs and Ge [3,6]. In semiconductors, the relaxation volumes of vacancies and interstitial are comparable, giving rise to correlation effects [3,6]. The diffuse scattering along a large area in the reciprocal lattice is associated with a small amorphous zone within the cascades. It is said that the recovery at 40 K is corresponding to the recovery stage I_A at which the closed Frenkel pairs rearrange.

Summary ; Single crystals of Ni were irradiated with 137 MeV xenon ions (Xe^{10+}) of fluences to 2.3_10^{13} ions/cm^2 below 13K. After the irradiation, the X-ray cryostat with the specimens was transferred from an irradiation chamber to the X-ray diffraction equipment below 20K. The results of X-ray diffuse scattering near Bragg reflections at low temperature indicate that the defects are located in cascades and suggest that a small amorphous zone exists within the cascade region. By the thermal annealing at 40K corresponding to the recovery stage I_A, the defects in the cascades rearrange.

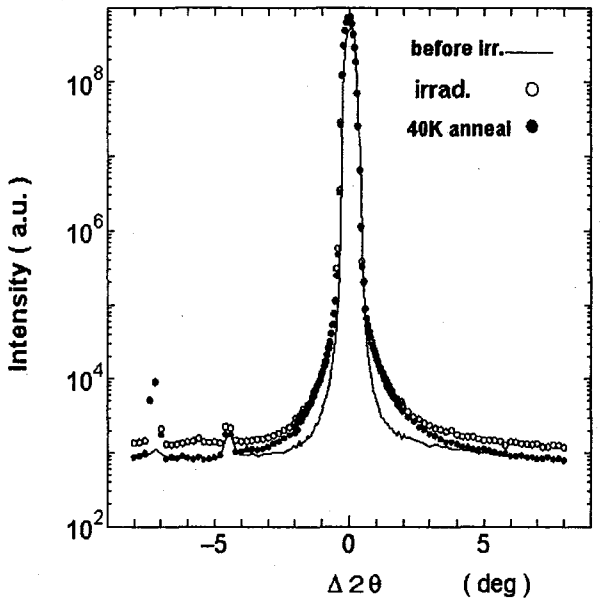

Fig. 1. Intensity of x-ray scattering from the nickel specimen irradiated with Xe ions of 2.3_10^{13} ions/cm^2 close to the (111) reflection in the [111] direction at 13K. The specimens were measured at 20K after the irradiation (○) and the annealing at 40 K (●)).

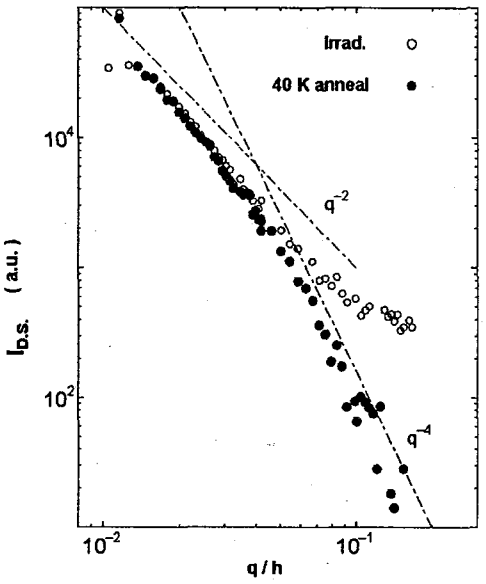

Fig. 2. The q-dependence of diffuse scattering ($I_{D.S}$) in nickel irradiated with Xe ions of 2.3_10^{13} ions/cm^2 at 13K. The specimens were measured at 20K after the irradiation (○) and the annealing at 40K (●).

References

[1] R. S. Averback, J. Nucl. Mater., **216**(1994) 49.
[2] M. A. Kirk, M. L. Jemkins and H. Fukushima, J. Nucl. Mater., **276**, (2000) 50.
[3] P. Ehrhart, J. Nucl. Mater. , **216** (1994) 170.
[4] B. v. Guerard, D. Grasse, and J. Peisl, Phys. Rev. Lett. **44** (1980) 262.
[5] H. Maeta and F. Ono, Mater. Sci. Forum 15, **188** (1987) 1099.
[6] P. Partyka, Y. Zhong, K. Nordlund, R. S. Averback, I. M. Robinson and P. Ehrhart, Phys. Rev. **B64** (2001) 235207-1.
[7] M. F. Bartels, F. Dworschak, M. Weiger, J. Nucl. Mater. **173** (1986) 130.
[8] H. Maeta, N. Matsumoto, T. Kato,H. Sugai, H. Ohtsuka, M. Sataka, Nucl. Instr. And Meth. B(2005) 312.

7.11 EFFECT OF HIGH-ENERGY HEAVY ION IRRADIATION ON MAGNETIC PROPERTIES IN Fe-Pt INVAR ALLOYS

F. ONO[1], H. KANAMITSU[1], Y. MATSUSHIMA[1], A. IWASE[2], Y. CHIMI, N. ISHIKAWA and T. KAMBARA[3]

Fe-Pt alloys around the Fe_3Pt composition are known to show low or even negative thermal expansion in low temperature region [1]. This anomaly in thermal expansion is also seen in Fe-Ni and Fe-Pd alloys with nearly the same concentration of the second element, and has been understood as a result of the instability of the band ferromagnetism in fcc phase. The concentrations of the second element of those alloys are close to the boundary of the martensitic phase transition [2]. The present authors group has made high-energy ion irradiation on Fe-Ni Invar alloys [3-7]. They found that irradiation makes large effects on magnetic properties. Therefore, it seems one of the most effective ways for modification of the physical properties of metals and alloys [4], and also for a search for new functional materials and their practical applications.

Specimens of both ordered and disordered Fe-28.3 at.%Pt Invar alloy were in a form of thin discs of 3×3 mm^2 and the thickness of 30-100 μm. They were irradiated with 200 MeV Xe-ions to the fluence up to 10^{14} ions/cm^2. AC-susceptibility measurements were made using a specially designed apparatus for rapid temperature variation. The range of the Xe-ions was 7 μm, which was smaller than the thickness of the sample.

No significant change has been observed in AC-susceptibility-temperature curves after irradiation up to 10^{13} ions/cm^2. However, after the irradiation with the maximum fluence a weak signal was observed about 10 K below the original Curie temperature. Observed AC-susceptibility versus temperature curves before and after the maximum irradiation are shown in Figs. 1 and 2, respectively. The weak signal observed in the fully irradiated specimen corresponds to the Curie temperature of the area where the ion beams are penetrated. The decrease of the Curie temperature is about 10 K at the irradiation of 10^{14} ions/cm^2. This result is quite in contrast to the case of Fe-Ni Invar alloys, where a large increase of the Curie temperature of about 100 K was observed.

In the case of Fe-Ni Invar alloy at an elevated temperature, ferromagnetic needles were produced along the paths of high energy ions through high-density electronic excitations [4]. This type of modification of introducing thin ferromagnetic needles in paramagnetic media has a possibility of applications for perpendicular high-density memory and giant magneto-resistance materials. On the

[1] Graduate School of Natural Science (Department of Physics), Okayama University
[2] Graduate School of Engineering, Osaka Prefecture University
[3] Atomic Physics Laboratory, The Institute of Physical and Chemical Research

contrary, in the case of Fe-Pt Invar alloy nonmagnetic needles were introduced in the ferromagnetic media through the irradiation.

By comparing the two different experimental results in Fe-Ni and Fe-Pt Invar alloys, it is concluded that there exist at least two factors that contribute to the shift of the Curie temperature. One, which contributes to increase the Curie temperature is acting as a negative pressure introduced through the expansion of the crystal lattice by the irradiation. Another possible factor which contributes to the decrease of the Curie temperature is selective knocking out of atoms that have larger atomic radius.

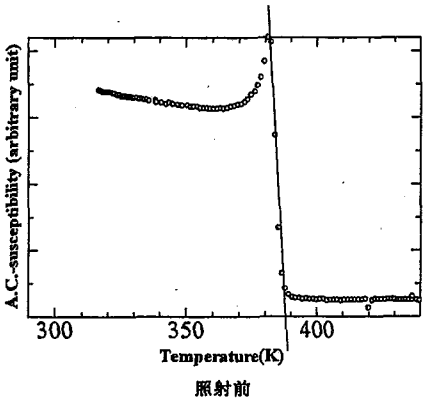

Fig. 1 AC-susceptibility-temperature curve in Fe-28.3at.%Pt Invar alloy before irradiation.

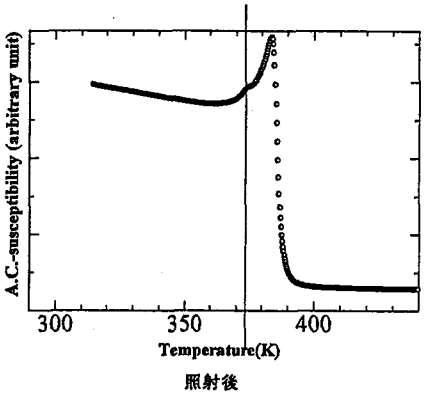

Fig. 2 AC-susceptibility-temperature curve in Fe-28.3at.% Pt Invar alloy after irradiation.

References

[1] For example, see "*The Invar Effect: A Centennial Symposium*" ed. by J. Wittenauer (The Minerals, Metals and Materials Society, 1997)

[2] F. Ono, L. Bang and H. Maeta, in [1], p.197.

[3] F. Ono, Y. Hamatani, Y. Mukumoto, S. Komatsu, N. Ishikawa, Y. Chimi, A. Iwase, T. Kambara, C. Muller, R. Neumann, Nucl. Instrum. Methods Phys. Res. B **206** (2003) 295.

[4] A. Iwase, Y. Hamatani, Y. Mukumoto, N. Ishikawa, Y. Chimi, T. Kambara, C. Muller, R. Neumann and F. Ono, Nucl. Instrum. Methods Phys. Res. B **209** (2003) 323.

[5] F. Ono, S. Komatsu, Y. Chimi, N. Ishikawa, T. Kambara, A. Iwase, Mat. Res. Soc. Symp. Proc. **792** (2004) 441.

[6] Y. Matsushima, F. Ono, H. Kanamitsu, S. Komatsu, A. Iwase, Y. Chimi, N. Ishikawa, T. Kambara, JAERI-Rev. **2004-027** (2004) 86.

[7] F. Ono, S. Komatsu, Y. Chimi, N. Ishikawa, A. Iwase, T. Kambara, Nucl. Instrum. Methods Phys. Res. B **230** (2005) 279.

7.12 ELECTRONIC EXCITATION EFFECTS ON SECONDARY ION EMISSION FROM SOLID MATERIALS BOMBARDED BY HEAVY IONS

T. SEKIOKA[1], M. TERASAWA[1] and M. SATAKA

The interaction between swift heavy ions and solids has been an active research area. We have been studying secondary ion mass spectrometry from thin conductive solid targets irradiated with heavy ion beams from the JAERI tandem accelerator in the energy region where the electronic stopping power is dominant. One of the important problems has been whether electronic excitations can induce the production of lattice defects in simple metals or not. In metals, it had been considered for a long time that on account of the great number of free conduction electrons and of their high mobility, inelastic interactions (electron excitation) could not cause any radiation damage or annealing process. In recent years, there have been extensive studies on the electronic excitation effect in metals irradiated with high-energy heavy ions (1-10MeV/nucleon), where the electronic stopping power $S_e = -(dE/dx)_e$ dominates the nuclear stopping power (S_n) by a factor of about 100-1000 [1, 2].

A thin Cu or Au foil target of 1000 to 2000 Å thickness evaporated on C-foils of 8.5μg/cm^2 was irradiated with high-energy heavy ion beams from the tandem accelerator. The secondary ions ejected from the front surface of the target were collected by a time of flight (TOF) mass spectrometer by applying an acceleration voltage of –500V and detected by an electron multiplier. Secondary electrons from the back side of the target were detected by another electron multiplier and this signal was used as the start signal of the TOF. Immediately before the measurement of the yield of secondary ions from the thin foil target, we maintained the temperature of the target about 500°C by infrared radiation heating for two hours in the vacuum of 1.6×10^{-6} Pa in order to clean the target. Figure 1 shows the yield of the secondary ions of Cu^+ from Cu target as a function of electronic stopping power. The secondary ion yield shows a significant increase with increasing electronic stopping power, which has approximately S_e^2-dependence. This suggests that even in the conductive materials, the electronic excitation effects play an important role in the secondary ion sputtering. We have also measured the secondary ions of Au^+ from Au target normalized by the counts of secondary electron signal. The yield of the Au^+ secondary ions from Au target is very small as compared with the yield of the Cu^+ secondary ions from Cu target, though Cu and Au have the same electronic structure ($^2S_{1/2}$). The tendency of the target mass dependence of the secondary ion yield agrees with the experimental results on the damage creation in metals by high electronic excitation effect by swift heavy ion irradiation [1]: the comparison of two metals with similar electronic and atomic properties shows that the lower target atomic number corresponds to higher sensitivity to damage creation through S_e. To confirm these experimental results, it is important to study the secondary ion mass spectroscopy in a wide range of electronic stopping power with various combinations of projectiles and conductive targets under low background.

We are now developing a new TOF system which is shown in fig. 2. The secondary electrons emitted from a thin C-foil located at the upper stream of the target are detected by an electron multiplier. This signal is used as the start signal for the TOF.

---

[1] Graduate School of Engineering, University of Hyogo

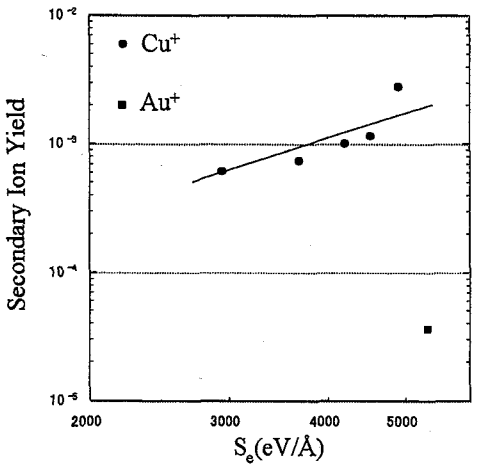

Fig. 1. The yield of the secondary ions of Cu^+ and Au^+ from Cu and Au target respectively normalized by the counts of secondary electrons, as a function of electronic stopping power S_e. The values of the electronic stopping power are obtained by Ziegler's table (TRIM). The solid line shows the S_e^2-dependence.

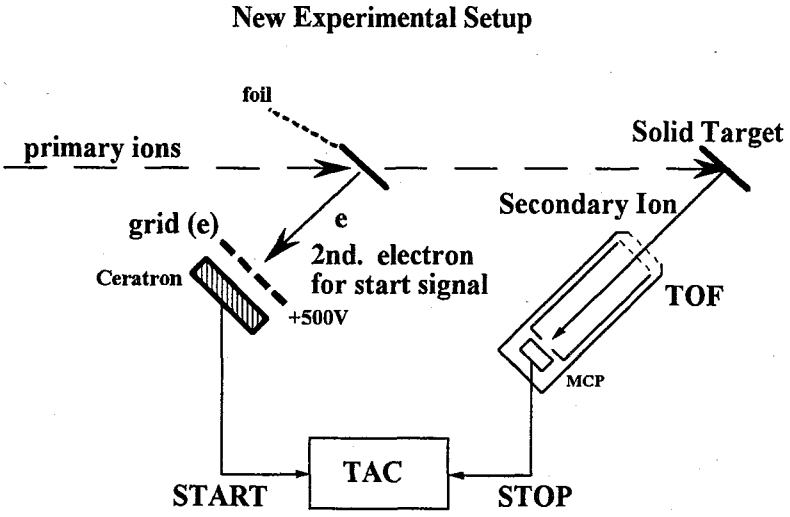

Fig.2. The schematic drawing of the new experimental setup

The secondary ions are detected by a multiple channel plate (MCP) in the TOF with a flight pass of 20 cm, which is much longer than the old TOF system. The target cleaning is carried out by a few keV ion beams which are expected to be more efficient than the infrared radiation heating. So far, the targets we studied have been limited to thin foils. However with this new TOF system, we can study the electronic excitation effect in conductive materials which is difficult to make a thin foil, and also we can widen the scope of our study to the electronic excitation effect in semiconductor and insulator target materials bombarded by swift heavy ions beam.

References

[1] A. Dunlop and D. Lesueur, Radiat. Eff. Def. Solids 126 (1993) 123.
[2] A. Iwase and T. Iwata, Nucl. Instr. and Meth. B 90 (1994) 322.

JP0650054

7.13 RADIATION DEFECTS IN NANOCRYSTALLINE MATERIALS

H.OHTSUKA and H.SUGAI

The aim of this study was to realize a radiation resistant material taking advantage of intrinsic effects of the nanocrystalline. The JAERI tandem accelerator was used to investigate this subject introducing defects into the nanocrystalline specimen. One of the studies was conducted using a transmission electron microscope (TEM). A simulation program was also developed in order to support the TEM observation [1]. The other studies were made using an X-ray diffractometer (XRD). Through a series of those experiments an opinion, 'Nanocrystalline is the radiation resistant material', has been verified [2].

Here, we would like to present an interesting result obtained from subsequent analyses taking FWHM of XRD profile around several Bragg peaks on θ-2θ scan. A typical example of the change in the profile is shown in Fig.1-a, where we consider that broadening of the profile is an index of the damage due to irradiation. Fig.1-b shows a dependence of an increase of the FWHM due to irradiation on the particle size. Clear size effect is demonstrated. In Fig.1-c changes in FWHM are plotted as a function scattering vector. One can see a large difference of FWHM change at (111) point between two cases. The difference was mainly due to ion species, Ni or Ar. So, there is a possibility that defect clusters produced by metallic ion irradiation lie mainly upon (111) surface whereas those by inert-gas ion irradiation do not so. A further study, however, has to be made to confirm that.

Generous supports of the Tandem group are gratefully acknowledged.

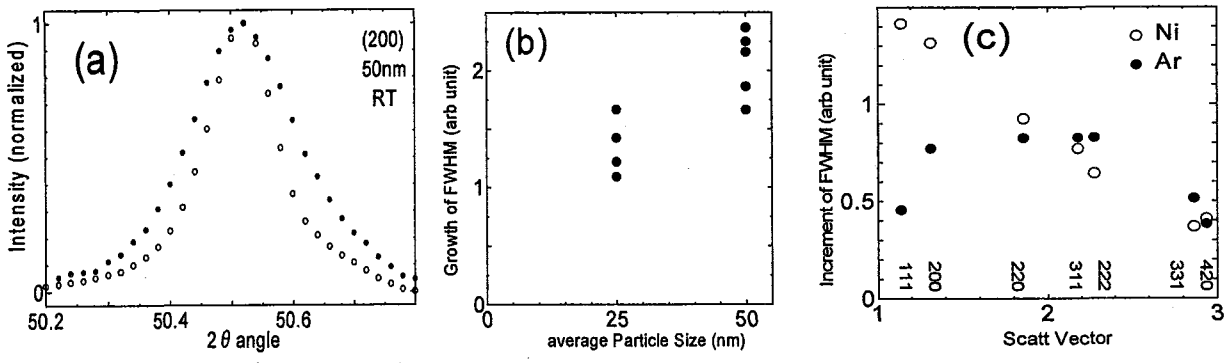

Fig.1-a: An example of XRD profile of θ-2θ scan. Close and open circles refer to before and after irradiation, respectively. 1-b: Growth of FWHM vs average particle size 25nm/50nm. 1-c: Change in FWHM as a function of scattering vector. Ni ion irradiation and Ar ion case are compared. Those data were obtained from Cu nanocrystalline samples under 100 MeV ion irradiation with the dose of ca.10^{15} ions/cm^2.

References

[1] H.Ohtsuka, K.Hojou, H.Maeta, H.Otsu, H.Sugai and H.Yamamoto, Eur. Phys. J.D. **16** (2001) 309.

[2] H.Ohtsuka, H.Sugai and K.Hojou, JAERI-Review 2003-**028**, (2003)113.

JP0650055

7.14 ANNEALING EFFECT ON ELECTRIC RESISTIVITY OF ION IRRADIATED CARBON FIBERS

A. KURUMADA[1], Y. IMAMURA[1], T. OKU[2], M. ISHIHARA,
K. SAWA, T. SHIBATA, S. BABA and J. AIHARA

Carbon/Carbon composite materials have good nuclear characteristics, high thermal conductivity and excellent mechanical properties at high temperatures. They have been taken as one of the candidate materials for the control rod elements of the high temperature gas cooled reactors and for plasma facing components of the next fusion experimental reactors. In order to apply them for nuclear reactors, it needs to study on the changes of the material properties and the microstructures due to irradiation damage and to develop the excellent C/C composite materials having irradiation damage resistance. On the other hand, the material properties of C/C composite materials are well known to depend on those of carbon fibers since carbon fibers in the C/C composite materials are generally less crystalline than the matrix carbon. In this study, high energy ions of nickel are irradiated to carbon fibers with different microstructures and different properties. The effects of ion irradiation and the annealing on the electric resistivity of carbon fibers are evaluated.

Materials tested in this study were three kinds of carbon fiber with different microstructures and different properties, which were a coal tar pitch based carbon fiber (K13C2U), a mesophase pitch based carbon fiber (YS-70-60-S) and a polyacrylonitrile based carbon fiber (M55JB). Nickel ions ($^{59}Ni^{13+}$) of 200 MeV with 0.4 μA were irradiated up to 5.27×10^{-3} dpa by the TANDEM accelerator in Tokai, JAERI. The range of nickel ions calculated by TRIM-98 code was 28.6 μm for the carbon material of 1.9 g/cm^3. Irradiation damages in the carbon fibers were uniform across the cross section because the diameter of the carbon fiber was below about 10 μm and it was smaller than the range. Ions passed through the carbon fibers, perpendicularly.

A single carbon fiber was straightly fixed by an conductive silver adhesive to the center of a frame paper with a square hole (10mm x 25mm) like the tensile specimen.[1-4] The electric resistance was measured by four-terminal method using a DC electric resistance tester (HIOKI Hi-Tester 3220).[5] The cross-sectional area was evaluated from the SEM photograph and the average value was used for calculation of the electric resistivity. The number and the length of the carbon fiber on the frame paper were confirmed by an optical microscope.

Fig.1 and 2 show the changing rate of the electric resistivity of the irradiated carbon fibers by the heat treatment for 10 and 100 minutes, respectively.

---

[1] Faculty of Engineering, Ibaraki University [2] Honorary Professor, Ibaraki University

In the case of figure 1, the recovering behaviors of the electric resistivity of three kinds of carbon fiber were similar and the changing rate was about 1.6 under a condition of a heat treatment for 10 minutes at 1273 K. Recovery of irradiated damage did not occur sufficiently in the case of Fig.1. In the case of figure 2, the recovering behaviors were different. The electric resistivity of the M55JB (PAN based) carbon fiber did not recover in spite of increase of the heat treatment temperature and time. The changing rate was large comparatively and it was over 1.9 under a condition of a heat treatment for 100 minutes at 1073K. On the other hand, the electric resistivity of the YS-70-60-S (mesophase pitch based) carbon fiber recovered easier and the changing rate due to the heat treatment for 100 minutes at 1073 K was 1.39.

Since the electric resistivity is a good index to the thermal conductivity and the irradiation damage, the thermal conductivity of the mesophase pitch based carbon fiber is likely to recover easier by the heat treatment after irradiation. The annealing effect on the material properties is an advantage for an extension of the life time. Therefore, the mesophase pitch based carbon fiber with random structure is effective to develop the excellent C/C composite material having the long life time. The additional experiments, however, will be carried out because the data of the annealing effect are limited now.

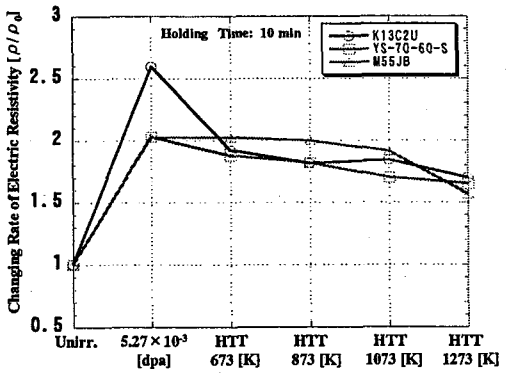

Fig. 1 Changing rate of the electric resistivity of irradiated carbon fibers by the heat treatment for 10 minutes.

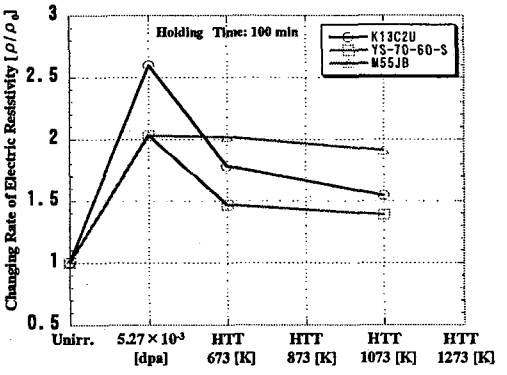

Fig. 2 Changing rate of the electric resistivity of irradiated carbon fibers by the heat treatment for 100 minutes.

References

[1] T. Oku, Y. Imamura, A. Kurumada, M. Inagaki and K. Kawamata, TANSO, No.190 (1999) 262-266.

[2] T. Oku, A. Kurumada, B. McEnaney, T. D. Burchell, M. Ishihara, K. Hayashi, S. Baba and J. Aihara, Eurocarbon 2000, 1st World Conf. on Carbon, Berlin, Germany (2000.7.9-13) Vol.II, 947-948.

[3] T. Oku, A. Kurumada, K. Kawamata and M. Inagaki, J. of Nuclear Materials, 303 (2002) 242-245.

[4] A. Kurumada, Y. Imamura, T. Oku, M. Ishihara, S. Baba and J. Aihara, OECD 2004, NEA No.5309 (2004) 121-128.

[5] T. Oku, A. Kurumada, Y. Imamura, M. Ishihara, S. Baba, J. Aihara and T. D. Burchell, International Nuclear Graphite Specialists Meeting-5, Gwynedd, UK (2004.9.12-15).

JP0650056

7.15 PERMANENT DAMAGE IN SILICON CARBIDE SCHOTTKY BARRIER DIODE CAUSED BY Ni ION IRRADIATION

C. KAMEZAWA[1], H. SHINDOU[1], H. OHIRA[2], T. HIRAO, H. OHYAMA[3], S. KUBOYAMA[1] and S. MATSUDA[1]

Silicon carbide (SiC) is one of the candidates for the next generation semiconductor materials. The most of attractive features of SiC are attributable to its wide-band gap energy of ~3.2eV. Because of the wide-band gap, the SiC devices can be operable under very high temperature and strong electric field as compared with Si devices, and are expected for applications under harsh environments. Previously, a catastrophic failure of SiC Schottky barrier diode (SBD) without any steady increase of leakage current caused by protons was reported and proposed to apply the percolation theory by Scheick et al [1]. Also Single-Event Burnouts (SEBs) were observed with higher LET particles and discussed with their NIEL values.

The SiC SBD used for this work was the commercially available SDP06S60 from Infineon Technologies, AG. According to the specification, the maximum ratings for continuous forward current and reverse voltage are 6A and 600V, respectively. Figure 1 shows the doping profile obtained by C-V measurement on SDP06S60 [2]. It clearly indicates that the SiC SBD has an epitaxial layer of approximately 6μm. The Ni ion of 190MeV used in this experiment has the range of around 20μm that can pass through the epitaxial layer sufficiently. Pre/post-I-V measurements were performed to characterize the permanent damage caused by irradiation. All the irradiations were performed at room temperature.

Figure 2 shows the leakage current at 200V after Ni ions irradiation under several bias voltages (220V~245V) for four different samples (A~D). The leakage current increase is usually caused by defects in active layer of the device, i.e. epitaxial layer in this case, and the introduction rate of the defects is mostly independent of the bias condition. However the observed current increase was proportional to the number of incident ions and strongly depended on the bias voltages which aggregate the epitaxial layer (e.g. sampleA, 220V~235V). The result clearly indicates that each incidence ion creates individual leakage path in the epitaxial layer.

The I-V curve for the leakage path is shown in Fig. 3. The curve apparently indicates that the path has strong field assisted emission effect, which suggests high density trap levels were introduced along the ion track. As mentioned above, it was confirmed that a permanent

[1] Space Component Engineering Center, Institute of Space Technology and Aeronautics, Japan Aerospace Exploration Agency (JAXA)
[2] Components Engineering Section, Engineering Dept., RYOEI TECHNICA Corporation
[3] Dept. of Electronic Engineering, Kumamoto National College of Technology

damage was introduced with irradiation at higher bias voltage. It is supposed that the energy to introduce the damage at higher bias voltage is supplied by excess current pass through the device.

In these experiments, the increase of leakage current was proportional with the number of incident ions and had strong bias voltage dependence by each sample. The fact suggested that the leakage paths were created discretely by individual ions. This is a very unusual phenomenon. There are some subjects for future work; to clarify a mechanism for the creation of leakage defect and to find the mitigation technique for the phenomenon to utilize the SiC devices for space applications with excellent performance.

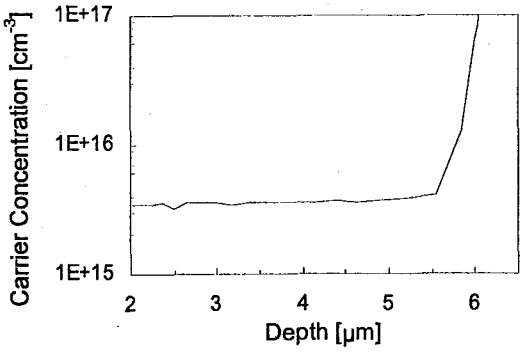

Fig. 1. Carrier concentration profile of the sample device obtained by C-V measurement.

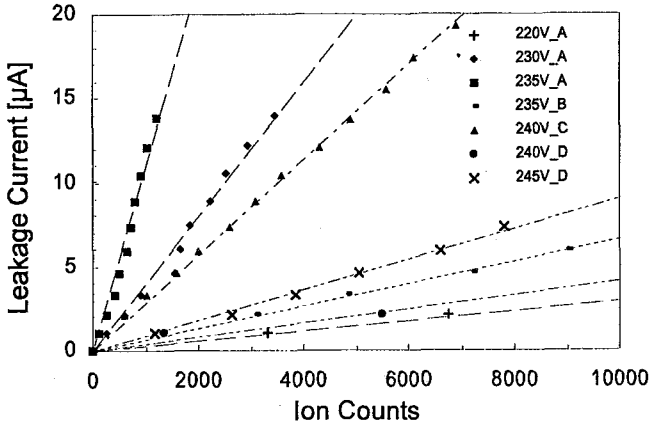

Fig. 2. Increase of leakage current at 200V caused by Ni-ion irradiation of various reverse bias (220V~245V) / samples (A~D).

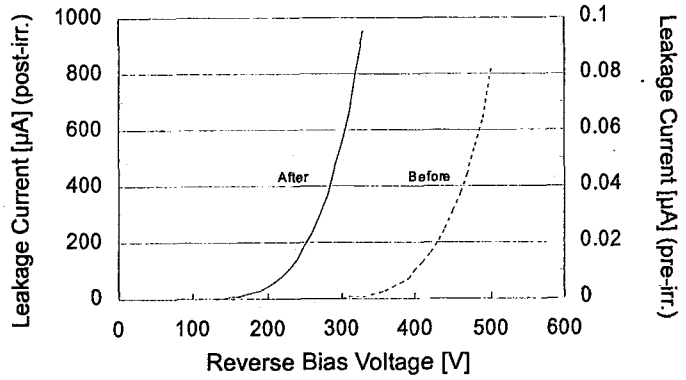

Fig. 3. I-V curves at pre- and post- Ni ion irradiation under reverse bias of 240V. The Ni-ion fluence was 22,500 ions on the device surface.

REFERENCES

[1] L. Scheick, L. Selva and H. Becker, IEEE Trans. Nucl. Sci. NS-51 (2004) 3193.

[2] S. M. Sze, "Physics of Semiconductor Devices," 2nd ed., Wiley, New York. (1981)

7.16 SEMICONDUCTOR-METAL PHASE TRANSITION OF IRON DISILICIDE (β -$FeSi_2$) THIN FILMS BY HIGH ENERGY HEAVY ION IRRADIATION

M. SASASE[1] and S. OKAYASU

β-$FeSi_2$ is a direct transition type semiconductor with band gap of 0.87 eV and high absorption coefficient (>10^{-5} cm^{-1}) [1]. Furthermore, β-$FeSi_2$ consists of resource elements of Fe and Si, which are harmless to the human bodies and the environment [2]. Another attractive feature of β-$FeSi_2$ is that it can be transformed to the metal phase α-$FeSi_2$ when heated above 937 °C [3]. Since the bulk α-$FeSi_2$ has electric resistivity as low as 2.5 x 10^{-4} Ω cm [4], one may consider if a small part of β-$FeSi_2$ can be transformed into α-$FeSi_2$ selectively, it can be used as the electrode of a β-$FeSi_2$ based device.
When the high-energy heavy ions are irradiated into materials, most of their energies are dissipated through an electronic excitation [5]. This leads to strong localization of the dissipated energy along the projectile path. Since the density of energy deposition is quite high, unexpected structural changes take place such as amorphization and phase transformation etc. We therefore attempted to perform the phase transition from β-$FeSi_2$ into α phase by the high-energy heavy-ion irradiation.

The specimens used in this study were iron dicilicides (β-$FeSi_2$) films. The β-$FeSi_2$ film is fabricated with the Ion Beam Sputter Deposition (IBSD) method by deposition of Fe on Si (100) substrates at certain temperatures [6]. The specimens were irradiated by 200 MeV Xe^{14+} ions at room temperature with a fluence of 1.0 x 10^{12} ions cm^{-2} using the Tandem accelerator at Japan Atomic Energy Research Institute (JAERI). The range and deposited ions in β-$FeSi_2$ films were calculated by using the TRIM98 code [7]. Irradiation damage was observed by using X-ray diffraction (XRD: Rigaku RINT) and transmission electron microscopy (TEM: JEOL JEM-3000F) with a field emission gun operated at 300 keV.

If the phase transition from β-$FeSi_2$ to α phase takes place by the high-energy heavy ion irradiation, it is expected that some changes are observed from XRD and TEM results. After the irradiation, X-ray diffraction peaks appeared at the almost same angles and intensity, compared with the spectrum before irradiation. No significant changes were observed in XRD patterns. On the other hand, contrast changes corresponded to defects, induced by ion irradiation were observed from TEM images. The distribution of defect was not uniform and the size was about 10 nm in diameter. The defects were formed by the thermal spike effect due to the energy dissipation through electronic excitation. A recent study revealed [8] that monoclinic zirconia is subjected to transform into the tetragonal or the cubic phase upon irradiation with 340 MeV Xe ions at 120 K. Although the transformation of β-$FeSi_2$ to α phase was not confirmed, our results implied the structural change by swift heavy ion irradiation. We will intend to observe the microstructure of defects and phase transformations in the irradiated films precisely by using both HRTEM image and micro-diffraction.

[1] The Wakasa-wan energy research center (WERC)

References

[1] K. Yamaguchi and K. Mizushima, Phys. Rev. Lett., **25**(2001)6006.

[2] K. Miyake, Y, Makita, Y. Maeda and T. Suemasu(Eds.), Thin Solid Films, **381**(2001)2.

[3] H. Lange, Phys. Stat. Sol., **B 201**(1997)3.

[4] K. Max, M van Rossum, Properties of Metal Silicides, INSPEC-IEE, London, 1995.

[5] M. Toulemonde, S. Bouffard and F. Studer, Nucl. Instrum. Method **B91**(1994)108.

[6] M. Sasase, T. Nakanoya, H. Yamamoto and K. Hojou, Thin Solid Films, **401**(2001)73.

[7] J. F. Ziegler, "Handbook of Stopping Cross Section for Energetic Ions in All Elements"(Pergamon Press, New York) 1980.

[8] A. Benyagoub, F. Couvreur, S. Bouffard, F. Levesque, C. Dufour, E. Paumier, Nucl. Instrum. Method **B175-177**(2001)417.

8. Publication in Journal and Proceedings, and Contribution to Scientific Meetings

This is a blank page.

ACCELERATOR OPERATION AND DEVELOPMENT

Journal/proceedings

M. Matsuda, S. Takeuchi, Y. Tsukihashi, K. Horie, I. Ohuchi, S. Hanashima, S. Abe, N. Ishizaki, H. Tayama, T. Nakanoya, H. Kabumoto, T. Sato, S. Kanda, T. Yoshida
Status Report of the JAERI Tandem Accelerator
Proc. of the 17th Workshop of the Tandem Accelerator and their Associated Technology Chiba, National Institute of Radiological Sciences (Jun. 21-22, 2004) 1-4

H. Kabumoto, S. Takeuchi, M. Matsuda, T. Nakanoya
Research and Development of Superconducting Twin Quarter Wave Resonator for the Acceleration of Low Velocity Heavy Ions
Proc. of the 17th Workshop of the Tandem Accelerator and their Associated Technology Chiba, National Institute of Radiological Sciences (Jun. 21-22, 2004) 135-137

T. Nakanoya, S. Abe, M. Matsuda, K. Nishio, S. Hanashima, S. Ichikawa, Y. Tshukihashi, S. Takeuchi, H.Ishiyama, S. C. Jeong, H. Kawakami, I. Katayama, H. Miyatake
Safety Issues in TRIAC Facility
Proc. of the 17th Workshop of the Tandem Accelerator and their Associated Technology Chiba, National Institute of Radiological Sciences (Jun. 21-22, 2004) 123-126

Meetings

M. Matsuda, S. Takeuchi, Y. Tsukihashi, K. Horie, I. Ohuchi, S. Hanashima, S. Abe, N. Ishizaki, H. Tayama, T. Nakanoya, H. Kabumoto, T. Sato, S. Kanda, T. Yoshida
Status Report of the JAERI Tandem Accelerator
17th Workshop of the Tandem Accelerator and their Associated Technology Chiba, National Institute of Radiological Sciences (Jun. 21-22, 2004)

M. Matsuda
Development of the Tandem Accelerator and the TRIAC Facility
Materials Science Symposium "Materials Science Using Accelerators"
Tokai, JAERI (Jan. 6-7, 2005)

M. Matsuda, T. Nakanoya, H. Kabumoto, S. Takeuchi, S. C. Jeong, M. Oyaizu, E. Tojyo
Acceleration project of Intense Stable Nuclear Beam
First Workshop of TRIAC, Tokai, JAERI(Sep. 21-23, 2004)

H. Kabumoto, S. Takeuchi, M. Matsuda, T. Nakanoya
Research and Development of Superconducting Twin Quarter Wave Resonator for the Acceleration of Low Velocity heavy ions
17th Workshop of the Tandem Accelerator and their Associated Technology Chiba, National Institute of Radiological Sciences (Jun. 21-22, 2004)

T. Nakanoya. S. Abe, M. Matsuda, K. Nishio, S. Hanashima, S. Ichikawa, Y.Tshukihashi, S. Takeuchi, H.Ishiyama, S. C. Jeong, H. Kawakami, I. Katayama, H. Miyatake
Safety Issues in TRIAC Facility
17th Workshop of the Tandem Accelerator and their Associated Technology Chiba, National Institute of Radiological Sciences (Jun. 21-22, 2004)

NUCLEAR STRUCTURE

Journal/Proceedings

H. Miyahara, K. Katoh, N. Marnada, K. Ikeda, K. Fujiki, I. Nishinaka, K. Tsukada, Y. Nagame, M. Asai, S. Ichikawa, H. Haba
Emission Probability Measurement of Principal γ-rays of ^{147}Eu
Nucl. Instrum. Method. Phys. Res. A **523** (2004) 96

M. Asai, M. Sakama, K. Tsukada, S. Ichikawa, H. Haba, I. Nishinaka, Y. Nagame, S. Goto, Y. Kojima, Y. Oura, H. Nakahara, M. Shibata, K. Kawade
EC and α Decays of ^{235}Am
Eur. Phys. J. A **22** (2004) 411

H. Miyahara, K. Katoh, K. Ikeda, K. Fujiki, I. Nishinaka, K. Tsukada, Y. Nagame, M. Asai, S. Ichikawa, H. Haba
Gamma-ray Emission Probability Measurement of ^{149}Eu
Nucl. Instrum. Method. Phys. Res. A **533** (2004) 404

M. Asai, M. Sakama, K. Tsukada, S. Ichikawa, H. Haba, I. Nishinaka, Y. Nagame, S. Goto, Y. Kojima, Y. Oura, H. Nakahara, M. Shibata, K. Kawade
Proton-neutron Configurations in $^{236g,m}Am$ and its EC-decay Daughter ^{236}Pu
Eur. Phys. J. A **23** (2005) 395

T. Shizuma, S. Mitarai, G. Sletten, R.A. Bark, N.L. Gjorup, H.J. Jensen, M. Piiparinen, J. Wrzesinski, Y.R. Shimizu
High-spin Structure in ^{185}Os
Phys. Rev. C **69** (2004) 024305

T. Shizuma, Z.G. Gan, K. Ogawa, H. Nakada, M. Oshima, Y. Toh, T. Hayakawa, Y. Hatsukawa, M. Sugawara, Y. Utsuno, Z. Liu
A New Isomer in ^{136}Ba Populated by Deep Inelastic Collisions
Eur. Phys. J. A **20** (2004) 207

T. Morikawa, M. Nakamura, T. Sugimitsu, H. Kusakari, M. Oshima, Y. Toh, M. Koizumi, A. Kimura, J. Goto, Y. Hatsukawa, M. Sugawara
High-Spin States in ^{43}Sc
Phys. Rev. C **70** (2004) 054323

H. Wang, H. Miyatake, H. Ohba, M. Saeki, M. Miyabe, T. Shibata, H. Iimura
Velocity and Metastable State Population Distributions of Laser-Ablated Neodymium
Rev. Sci. Instrum. **75** (2004) 3775

H. Iimura, M. Asai, S. Ichikawa, J. Katakura, M. Magara, A. Osa, M. Oshima, N. Shinohara, H. Yamamoto
Levels in ^{127}La Fed by the ^{127}Ce Beta-decay
Eur. Phys. J. A **23** (2005) 33

M. Koizumi, A. Seki, Y. Toh, M. Oshima, A. Osa, Y. Utuno, A. Kimura, Y. Hatsukawa, T. Hayakawa, T. Shizuma, J. Katakura, M. Matsuda, M. Sugawara, T. Morikawa, H. Kusakari, T. Czosnyka
Coulomb Excitation of Stable Even-even Zn Isotopes
Proceedings of International Symposium "A New Era of Nuclear Structure Physics (NENS03)", (2004) 92-98

Meetings

M. Koizumi, A. Seki, Y. Toh, M. Oshima, A. Osa, Y. Utuno, A. Kimura, Y. Hatsukawa, T. Hayakawa, T. Shizuma, J. Katakura, M. Matsuda, M. Sugawara, T. Morikawa, H. Kusakari, T. Czosnyka
Coulomb Excitation of Stable Even-even Zn Isotopes
International symposium"A New Era of Nuclear Structure Physics (NENS03)",19-22 Nov. 2003, (Kurokawa Village, Niigata, Japan)

T. Ishii, M. Asai, M. Matsuda, S. Ichikawa, Y. Utsuno, A. Makishima, T. Kohno, M. Ogawa
γ-ray Spectroscopy of $^{47,48}K$ Produced by Deep-Inelastic Collisions
Fall Meeting of the Physical Society of Japan, Kochi (Sep. 27, 2004)

T. Ishii
Overview of the Tokai Radioactive Ion Accelerator Complex
60th Annual Meeting of the Physical Society of Japan, Noda (Mar. 25, 2005)

T. Shizuma, T. Hayakawa, S. Mitarai, T. Morikawa, T. Ishii
High-K Isomers at the A=180 Region Populated in Deep Iinelastic Collisions
Fall Meeting of the Physical Society of Japan,(September 2004)

M. Sugawara, Y. Toh, M. Oshima, M. Koizumi, A. Osa, J. Goto, A. Kimura, Y. Hatsukawa, H. Kusakari, Y. H. Zhang, X. H. Zhou, Y. X. Guo, M. L. Liu
Nuclear Structure of ^{144}Dy
Fall Meeting of the Physical Society of Japan, Kochi(Sep. 27, 2004)

H. Hayashi, I. Miyazaki, M. Shibata, K. Kawade, Y. Kojima, A. Taniguchi
Q_β Measurements using a Total-absorption-type HPGe Detector with Simulated Response Functions by EGS4
3rd International EGS Workshop, KEK Tsukuba (Aug. 4-6 2004)

H. Hayashi, I. Miyazaki, M. Shibata, K. Kawade, Y. Kojima, A. Taniguchi
Q_β Measurements Using a Total-absorption-type HPGe Detector
1st TRIAC Workshop, JAERI Tokai (Sep. 21-23 2004)

T. Morikawa, M. Nakamura, T. Sugimitsu, H. Kusakari, M. Oshima, Y. Toh, M. Koizumi, A. Kimura, J. Goto, Y. Hatsukawa, M. Sugawara
High-Spin Yrast Structure of ^{43}Sc
International Symposium on Correlation Dynamics in Nuclei (CDN05),
Tokyo (Jan.31 - Feb.4, 2005)

NUCLEAR REACTIONS

Journal/Proceedings

I. Nishinaka, Y. Nagame, H. Ikezoe, M. Tanikawa, Y. L. Zhao, K. Sueki, H. Nakahara
Partition of Total Excitation Energy between Fragment Pairs in Asymmetric and Symmetric Fission Modes
Phys. Rev. C **70** (2004) 014609

K. Nishio, H. Ikezoe, Y. Nagame, M. Asai, K. Tsukada, S. Mitsuoka, K. Tsuruta, K. Satou, C.J. Lin, T. Ohsawa
Evidence of Complete Fusion in the Sub-barrier ^{16}O + ^{238}U Reaction
Phys. Rev. Lett. **93** (2004) 162701

T. Hashimoto, T. Ishikawa, T. Kawamura, K. Nakai, H. Ishiyama, M-H. Tanaka, Y.X. Watanabe, H. Miyatake, N. Yoshikawa, S. C. Jeong, Y. Matsuyama, Y. Fuchi, I. Katayama, T. Nomura, S.K. Das, P.K. Saha, T. Fukuda, K. Nishio, S. Mitsuoka, H. Ikezoe, M. Matsuda, S. Ichikawa, T. Furukawa, H. Izumi, T. Shimoda, Y. Mizoi, M. Terasawa
Measurement of the $^{8}Li(\alpha, n)^{11}B$ Reaction Cross Sections of Astrophysical Interest
Nucl. Phys. A **746** (2004) 330c

H. Ikezoe, S. Mitsuoka K. Nishio
Effect of Nuclear Structure on Heavy-Ion Fusion Reaction
BUTSURI, Vol. **60**, No. 2, (2005) 123-128

S. Mitsuoka, H. Ikezoe, K. Nishio, K. Satou, K. Tsuruta, C.J. Lin
Dependence of Heavy-Ion Fusion Reaction on Nuclear Deformation
Prog. Theor. Phys. Suppl. 154, (2004) 53

H. Ikezoe, K. Satou, S. Mitsuoka, K. Nishio, K. Tsuruta, S.C. Jeong, C.J. Lin
Effect of Closed Shell Structure on Heavy-ion Fusion Reactions
Prog. Theor. Phys. Suppl. 154, (2004) 45

H. Miyatake, H. Ishiyama, M.H. Tanaka, Y.X. Watanabe, N. Yoshikawa, S.C. Jeong, Y. Matsuyama, Y. Fuchi, T. Nomura, T. Hashimoto, T. Ishikawa, K. Nakai, S.K. Das, P.K. Saha, T. Fukuda, K. Nishio, S. Mitsuoka, H. Ikezoe, S. Ichikawa, M. Matsuda, Y. Mizoi, T. Furukawa, H. Izumi, T. Shimoda, M. Terasawa

Exclusive Measurement of the Astrophysical $^{8}Li(\alpha, n)$ Reaction Cross Section

Nucl. Phys. A **738**, (2004) 401

P. Heckman, B.B. Back, T. Baumann, M.P. Carpenter, I. Dioszegi, D.J. Hofman, T.L. Khoo, S. Mitsuoka, V. Nanal, T. Pennington, J.P. Seitz, M. Thoennessen, E. Tryggestad, R.L.Varner

Temperature and Spin Dependence of the Giant Dipole Resonance Width

Nucl. Phys. A **750**, (2005) 175

J.P. Seitz, B.B. Back, M.P. Carpenter, I. Dioszegi, K. Eisenman, P. Heckman, D.J. Hofman, M.P. Kelly, T.L. Khoo, S. Mitsuoka, V. Nanal, T. Pennington, R.H. Siemssen, M. Thoennessen, R.L. Varner

Observation of the Hot GDR in Neutron-deficient Thorium Evaporation Residues

Nucl. Phys. A**750**, (2005) 245

Meetings

S. Yoshida, T. Kishimoto, I. Ogawa, S. Umehara, K. Mukaida, K. Ichihara, K. Matsuoka, H. Ikezoe, S. Mitsuoka

Emission Wavelength Spectra of CaF_2 Scintillators

60th Annual Meeting of the Physical Society of Japan, Noda (March 27, 2005)

H. Ishiyama, T. Hashimoto, T. Ishikawa, Y. X. Watanabe, Y. Hirayama, H. Miyatake, M-H. Tanaka, N. Yoshikawa, S. C. Jeong, Y. Matsuyama, Y. Fuchi, I. Katayama, T. Nomura, H. Kawakami, K. Nakai, S.K. Das, P.K. Saha, T. Fukuda, K. Nishio, S. Mitsuoka, H. Ikezoe, M. Matsuda, S. Ichikawa, T. Furukawa, H. Izumi, T. Shimoda, Y. Mizoi, M. Terasawa, T.Sasaqui

Direct Measurement of the Astrophysical $^{8}Li(\alpha, n)\ ^{11}B$ Reaction

5th Italy-Japan Symposium, Recent Achievements and Perspectives in Nuclear Physics, Naples, Italy (Nov.3-7, 2004)

H. Ishiyama
Nuclear Astrophysical Experiments at TRIAC
60th Annual Meeting of the Physical Society of Japan, Noda (Mar. 24-27, 2005)

S.K. Das, T. Fukuda, Y. Mizoi, T. Hashimoto, H. Ishiyama, H. Miyatake, Y.X. Watanabe, Y. Hirayama, M.H. Tanaka, N. Yoshikawa, S.C. Jeong, Y. Fuchi, I. Katayama, T. Nomura, T. Ishikawa, K. Nakai, S. Mitsuoka, K. Nishio, P.K. Saha, M. Matsuda, S. Ichikawa, H. Ikezoe, T. Furukawa, H. Izumi, T. Shimoda, T. Sasaqui
Measurement of the $^{8}Li(\alpha, n)^{11}B$ Reaction in FY 2003 Experiment
60th Annual Meeting of the Physical Society of Japan, Noda (Mar. 24-27, 2005)

T. Hashimoto, H. Ishiyama, H. Miyatake, Y.X. Watanabe, Y. Hirayama, N. Imai, M-H. Tanaka, N. Yoshikawa, S. C. Jeong, Y. Fuchi, I. Katayama, T. Nomura, T. Ishikawa, K. Nakai, S. Mitsuoka, K. Nishio, P.K. Saha, M. Matsuda, S. Ichikawa, H. Ikezoe, Y.Mizoi, S.K. Das, T. Fukuda, T. Furukawa, H. Izumi, T. Shimoda, T. Sasaqui
Study of the $^{8}Li(\alpha, n)^{11}B$ Reaction
60th Anual Meeting of the Physical Society of Japan, Noda (Mar. 24-27, 2005)

T. K. Sato, A. Osa, M. Matsuda, M. Asai, K. Tsukada, S.C. Jeong, H. Kawakami, S. Ichikawa, S. Takeuchi
Development of Ion Source for RNB
TRIAC Workshop, Ibaraki(Sep. 21-23, 2004)

T. K. Sato, M. Matsuda, S. Ichikawa, S. Takeuchi
Ion Source Development for Radio Nuclide Beam
17th Workshop of the Tandem Accelerator and their Associated Technology Chiba, National Institute of Radiological Sciences (Jun. 21-22, 2004)

K. Nishio, H. Ikezoe, Y. Nagame, M. Asai, K. Tsukada, S. Mitsuoka, K. Tsuruta, K. Satou, C.J. Lin, T. Ohsawa
Measurement of Evaporation Residue Cross-sections for the $^{16}O+^{238}U$ Reaction in the Subbarrier-energy Region
Fall Meeting of the Atomic Energy Socierty of Japan, Kyoto (Sep. 2004)

S. Mitsuoka

Heavy-ion Fusion Reaction Mechanism for Superheavy Element Synthesis

Materials Science Symposium "Materials Science using Accelerators" (Jan. 6-7, 2005)

NUCLEAR CHEMISTRY

Journal/proceedings

H. Haba, K. Tsukada, M. Asai, A. Toyoshima, K. Akiyama, I. Nishinaka, M. Hirata, T. Yaita, S. Ichikawa, Y. Nagame, K. Yasuda, Y. Miyamoto, T. Kaneko, S. Goto, S. Ono, T. Hirai, H. Kudo, M. Shigekawa, A. Shinohara, Y. Oura, H. Nakahara, K. Sueki, H. Kikunaga, N. Tsuruga, A. Yokoyama, M. Sakama, S. Enomoto, M. Schädel, W. Brüchle, J. V. Kratz
Fluoride Complexation of Eelement 104, Rutherfordum
J. Am. Chem. Sci. **126** (2004) 5219

A. Toyoshima, H. Haba, K. Tsukada, M. Asai, K. Akiyama, I. Nishinaka, Y. Nagame, D. Saika, K. Matsuo, W. Sato, A. Shinohara, H. Ishizu, M. Ito, J. Saito, S. Goto, H. Kudo, H. Kikunaga, N. Kinoshita, C. Kato, A. Yokoyama, K. Sueki
Elution Curve of Rutherfordium (Rf) in Anion-exchange Chromatography with Hydrofluoric Acid (HF) Solution
J. Nucl. Radiochem. Sci. **5** (2004) 45

Meetings

H. Haba, K. Tsukada, K. Akiyama, M. Asai, A. Toyoshima, Y. Ishii, S. Enomoto, Y. Nagame
Reversed-phase Extraction Chromatography of Zr and Hf in the TBP/HCl System -Model Experiment for Chemical Characterization of Element 104, Rutherfordium-
2004 Annual Meeting of the Japan Society of Nuclear and Radiochemical Science, Tokyo (Oct. 27-29, 2004)

A. Toyoshima, K. Tsukada, M. Asai, H. Haba, K. Akiyama, Y. Ishii, I. Nishinaka, T. Sato, M. Hirata, Y. Nagame, W. Sato, K. Matsuo, Y. Tani, D. Sakai, Y. Kitamoto, H. Hasegawa, A. Shinohara, S. Goto, M. Ito, J. Saito, H. Kudo, M. Sakama, A. Yokoyama, K. Morishita, K. Sueki, H. Nakahara, M. Schädel
Formation of Anionic Fluoride Complex of Rutherfordium (Rf); Anion-exchange Behavior of Hydrofluoric Acid / Nitric Acid Mixed Solution System
2004 Annual Meeting of the Japan Society of Nuclear and Radiochemical Science, Tokyo (Oct. 27-29, 2004)

K. Tsukada, A. Toyoshima, H. Haba, M. Asai, K. Akiyama, I. Nishinaka, Y. Nagame, D. Sakai, K. Matsuo, W. Sato, A. Shinohara, A. Ishizu, M. Ito, J. Saito, S. Goto, H. Kudo, H. Kikunaga, N. Kinoshita, C. Kato, A. Yokoyama, K. Sueki
Anion-exchange Chromatographic Behavior of Rutherforsium (Rf) in Hydrofluoric Acid
2004 Annual Meeting of the Japan Society of Nuclear and Radiochemical Science, Tokyo (Oct. 27-29, 2004)

K. Matsuo, A. Toyoshima, W. Sato, N. Takahashi, T. Yoshimura, A. Shinohara, K. Tsukada, M. Asai, K. Akiyama, I. NishinakaY. Nagame
Development of Electrochemical Method by a Flow-electrolytic-column for Heavy Elements
2004 Annual Meeting of the Japan Society of Nuclear and Radiochemical Science, Tokyo (Oct. 27-29, 2004).

K. Akiyama, H. Haba, K. Tsukada, M. Asai, K. Sueki, A. Toyoshima, T. Yaita, Y. Nagame
EXAFS Study of the ath and 5th Group of Elements in Hydrofloric Acid Solution
2004 Annual Meeting of the Japan Society of Nuclear and Radiochemical Science, Tokyo (Oct. 27-29, 2004)

Nishinaka, Y. Nagame, H. Nakahara
Nuclear Scission Shapes of Pair Fragments in Two Fission Modes
2004 Annual Meeting of the Japan Society of Nuclear and Radiochemical Science, Tokyo (Oct. 27-29, 2004)

M. Hirata, Y. Nagame, J. Anton, B. Fricke
Electronic Structure of hydrated No Ion
2004 Annual Meeting of the Japan Society of Nuclear and Radiochemical Science, Tokyo (Oct. 27-29, 2004)

Y. Nagame
Chemical Studies of the Transactinide Element, Rutherfordium (Rf), at JAERI
2004 Annual Meeting of the Japan Society of Nuclear and Radiochemical Science, Tokyo (Oct. 27-29, 2004).

M. Hirata, Y. Nagame, T. Bastug, J. Anton, B. Fricke
Estimation of Ionic Radius of No^{2+} Ion by the Relativistic Density Functional Theory
85th Spring Meeting of the Chemical Society of Japan, Yokohama (Mar. 26-29, 2004)

A. Toyoshima, K. Tsukada, M. Asai, H. Haba, K. Akiyama, Y. Ishii, I. Nishinaka, T. Sato, M. Hirata, Y. Nagame, W. Sato, K. Matsuo, Y. Tani, D. Saika, Y. Kitamoto, H. Hasegawa, A. Shinohara, S. Goto, M. Ito, J. Saito, H. Kudo, M. Sakama, A. Yokoyama, K. Morishita, K. Sueki, H. Nakahara, M. Schädel
Fluoride Complex Formation of Transactinide Element, Rutherfordium
85th Spring Meeting of the Chemical Society of Japan, Yokohama (Mar. 26-29, 2004)

H. Haba, K. Tsukada, K. Akiyama, M. Asai, A. Toyoshima, Y. Ishii, I. Nishinaka, T. Sato, Y. Nagame, J. Saito, M. Ito, S. Goto, H. Kudo, Y. Oura and K. Sueki
Reversed-phase Extraction Chromatography of Zr and Hf in the TBP/HCl System – Model Experiments for Chemical Characterization of Element 104, Rf -
85th Spring Meeting of the Chemical Society of Japan, Yokohama (Mar. 26-29, 2004)

Y. Nagame
Chemical Studies of Rutherfordium at JAERI
6th International Conference on Nuclear and Radiochemistry, Aachen (Aug. 29 – Sep. 3, 2004)

M. Hirata, K. Tanaka, Y. Nagame, T. Bustug, J. Anton, B. Fricke
Prediction of Ionic Radius and Binding Energy of Hydration for the No^{2+} Ion by Relativistic Density Functional Calculations
6th International Conference on Nuclear and Radiochemistry, Aachen (Aug. 29 – Sep. 3, 2004)

H. Haba, K. Akiyama, K. Tsukada, M. Asai, A. Toyoshima, T. Yaita, M. Hirata, K. Sueki, Y. Nagame
Chloride Complexation of Rutherfordium – X-ray Absorption Fine Structure Spectroscopy of Zr and Hf in HCl
6th International Conference on Nuclear and Radiochemistry, Aachen (Aug. 29 – Sep. 3, 2004)

A. Toyoshima, K. Tsukada, M. Asai, H. Haba, K. Akiyama, I. Nishinaka, D. Saika, K. Matsuo, W. Sato, H. Ishizu, M. Ito, J. Saito, S. Goto, H. Kudo, H. Kikunaga, N. Kinoshita, C. Kato, A. Yokoyama, K. Sueki, Y. Nagame, A. Shinohara
Elution Behavior of Rutherfordium (Rf) in Anion-exchange Chromatography in a Hydrofluoric Acid System
6th International Conference on Nuclear and Radiochemistry, Aachen (Aug. 29 – Sep. 3, 2004)

K. Tsukada, H. Haba, M. Asai, A. Toyoshima, K. Akiyama, I. Nishinaka, M. Hirata, K. Hashimoto, S. Ichikawa, Y. Nagame, K. Yasuda, Y. Miyamoto, Y. Tani, H. Hasegawa, W. Sato, A. Shinohara, S. Goto, M. Ito, J. Saito, H. Ishizu, H. Kudo, Y. Oura, H. Nakahara, K. Sueki, N. Kinoshita, H. Kikunaga, A. Yokoyama
Sorption on Anion-exchange Resin of Dubnium and its Homologues in HF Solution
6th International Conference on Nuclear and Radiochemistry, Aachen (Aug. 29 – Sep. 3, 2004)

Y. Nagame
Atom-at-a-time Chemistry of the Transactinide Element, Rutherfordium (Element 104) – Toward Experimental Verification of Relativistic Effects in Chemical Properties -
5th Italy-Japan Symposium – Recent Achievements and Perspectives in Nuclear Physics, Naples (Nov. 3 – 7, 2004)

NUCLEAR THEORY

Journal/Proceedins

Y. Utsuno
Anomalous Magnetic Moment of ^{9}C and Shell Quenching in Exotic Nuclei
Phys. Rev. C **70** (2004) 011303

Y. Utsuno, T. Otsuka, T. Glasmacher, T. Mizusaki, M. Honma
Onset of Intruder Ground State in Exotic Na Isotopes and Evolution of the N=20 Shell Gap
Phys. Rev. C **70** (2004) 044307

P. Mason, N. Marginean, S. M. Lenzi, M. Ionescu-Bujor, F. Della Vedova, D. R. Napoli, T. Otsuka, Y. Utsuno, F. Nowacki, M. Axiotis, D. Bazzacco, P. G. Bizzeti, Bizzeti-Sona, F. Brandolini, M. Cardona, G. de Angelis, E. Farnea, A. Gadea, D. Hojman, A. Iordachescu, C. Kalfas, Th. Kroell, S. Lunardi, T. Martinez, M. Petrache, B. Quintana, R. V. Ribas, C. Rossi Alvarez, C. A. Ur, R. Vlastou, S. Zilio
High Spin Structure of ^{34}S and the Proton-neutron Coupling of Intruder States
Phys. Rev. C **71** (2005) 014316

G. Neyens, M. Kowalska, D. Yordanov, K. Blaum, P. Himpe, P. Lievens, S. Mallion, R. Neugart, N. Vermeulen, Y. Utsuno, T. Otsuka
Measurement of the Spin and Magnetic Moment of ^{31}Mg: Evidence for a Strongly Deformed Intruder Ground State
Phys. Rev. Lett. **94** (2005) 022501

T. Maruyama, T. Tatsumi, V.N. Voskresensky, T. Tanigawa, S. Chiba, T. Maruyama
Structured Mixed Phase in Kaon Condensation
Prog. Theor. Phys. Suppl. **156** (2004) 145

Y. Maezawa, T. Maruyama, N. Itagaki and T. Hatsuda
Wandering in Color-space --- Why is the Life of Pentaquark so Long?
Acta. Phys. Hung. A **22** (2005) 61

G. Watanabe, T. Maruyama, K. Sato, K. Yasuoka, T. Ebisuzaki
Simulation of Transitions between ``Pasta'' Phases in Dense Matter
Phys. Rev. Lett. **94** (2005) 031101

T. Maruyama, T. Tatsumi, V.N. Voskresensky, T. Tanigawa, S. Chiba
Structured Mixed Phase at Charged Kaon Condensation
Nucl. Phys. A **749** (2005) 186

Y. Akimura, T. Maruyama, N. Yoshinaga, S. Chiba
Stability and Structure of Quark Matter in a Molecular Dynamics Framework
Nucl. Phys. A **749** (2005) 329

T. Endo, T. Tatsumi, T. Maruyama, S. Chiba
Numerical Study of Hadron-quark Mixed Phase
Nucl. Phys. A **749** (2005) 333

T. Asano, T. Wada, M. Ohta, T. Ichikawa, S. Yamaji, H. Nakahara
Dynamical Calculation of Multi-modal Nuclear Fission of Fermium Nuclei
J. Nucl. Radiochem. Sci. **5** (2004) 1

P. Möller, A. J. Sierk, T. Ichikawa, A. Iwamoto
Fission and Fusion at the End of the Periodic System
Prog. Theor. Phys. Suppl. **154** (2004) 21

P. Möller, A. J. Sierk, T. Ichikawa, A. Iwamoto
Cluster Expression in Fission and Fusion in High-dimensional Macroscopic-microscopic Calculations
Nucl. Phys. A **738** (2004) 499

P. Möller, A. J. Sierk, T. Ichikawa, A. Iwamoto
Cluster Expression in Fission and Fusion in High-dimensional Macroscopic-microscopic Calculations
Proceedings of Tours Symposium on Nuclear Physics V, AIP-704 (2004) 49

Y. Akimura, N. Yoshinaga
Stability of Srange Matter with Molecular Dynamics
A New Era of Nuclear Structure Physics
World Scientific, (2004) 319-320

Y. Akimura, T. Maruyama(c), N. Yoshinaga, S. Chiba(d)
Stability and Structure of Quark Matter in a Molecular Dynamics Framework
Nucl. Phys. A **749** (2005) 329-332

Y. Akimura, T. Maruyama, N. Yoshinaga, S. Chiba
Quark/Hadron Phase Transition by a Molecular Dynamics
Soryushiron Kenkyu, **111** (2005) D31-D32

H. Takemoto, M. Fukushima, S. Chiba, H. Horiuchi, Y. Akaishi, A. Tohsaki
Clustering Phenomena in Nuclear Matter Below the Saturation Density
Phys. Rev. C **69** (2004) 035802-1

E.S. Soukhovitsij, S. Chiba, J.Y. Lee, O. Iwamoto, T. Fukahori
Glogal Coupled-channel Optical Potential for Nucleon-actinide Interaction from 1 keV to 200 MeV
J. Phys. G **30** (2004) 905

T. Kajino, T. Sasaqui, M. Orito, K. Otsuki, G J. Mathews, S. Honda, W. Aoki, S. Chiba
Nucleosynthesis in Supernovae and the Early Universe
American Institute of Physics Conf Proc. **704** (2004) 488

T. Maruyama, T. Tatsumi, D.N. Voskresensky, T. Tanigawa, S. Chiba
Kaon Condensation and the Non-Uniform Nuclear Matter
American Institute of Physics Conf Proc. **704** (2004) 519

T. Tanigawa, M. Matsuzaki, S. Chiba
$^1S_0$ Proton Superfluidity in Neutron Star Matter: Impact of Bulk Properties
Phys. Rev. C **70** (2004) 065801-1

T. Matsumoto, E. Hiyama, K. Ogata, Y. Iseri, M. Kamimura, S. Chiba, M. Yahiro
Four-body CDCC Analysis of ^{6}He + ^{12}C Scattering
Phys. Rev. C **70** (2004) 061601(R)

H. Koura, T, Tachibana, M. Uno, M. Yamada
Nuclidic Mass Formula on a Spherical Basis with an Improved Even-odd Term
Prog. Theor. Phys. **113** (2005) 305

Meetings

T. Maruyama, T. Tatsumi, D.N. Voskresensky, T. Tanigawa, S. Chiba
Nuclear-pasta Structure and the Coulomb Screening Effects
International Nuclear Physics Conference 2004, Gothenborg (Jun 28-Jul 2, 2004)

Y. Maezawa, T. Maruyama, N. Itagaki, T. Hatsuda
Dynamics of PentaQuark in Color Molecular Dynamics Simulation
International Workshop on PENTAQUARK04, SPring-8 (July 20-23, 2004)

T. Maruyama, T. Tatsumi, D.N. Voskresensky, T. Tanigawa, S. Chiba
Non-uniform Matter Structure in Kaon Condensation
International Workshop on Strangeness Nuclear Physics, Osaka (Jul 29-31)

T. Tatsumi, T. Maruyama, D.N. Voskresensky, T. Tanigawa, S. Chiba
Nuclear Pasta Structures in Neutron Stars and the Coulomb Screening
Dubna International Advanced School of Theoretical Physics, Dubna, (Aug 2 - 13, 2004)

T. Endo, T. Tatsumi, T. Maruyama, S. Chiba
Hadron Quark Matter Phase Transition in Neutron Star
Dubna International Advanced School of Theoretical Physics, Dubna, (Aug 2 - 13, 2004)

T. Maruyama, T. Tatsumi, D.N. Voskresensky, T. Tanigawa, S. Chiba
Structured Mixed Phase in Kaon Condensation
18th Nuclear Physics Division Conference of European Physics Society, Prague (Aug 23-29, 2004)

T. Endo, T. Tatsumi, T. Maruyama, S. Chiba
Numerical Study of Hadron-quark Mixed Phase
18th Nuclear Physics Division Conference of European Physics Society, Prague (Aug 23-29, 2004)

Y. Akimura, T. Maruyama, N. Yoshinaga, S. Chiba
Stability and Structure of Quark Matter in a Molecular Dynamics Framework
18th Nuclear Physics Division Conference of European Physics Society, Prague (Aug 23-29, 2004)

T. Maruyama, T. Tatsumi, D.N. Voskresensky, T. Tanigawa, S. Chiba
Non-uniform Nuclear Matter Structure and the Coulomb Screening Effects
Fall Meeting of the Physical Society of Japan, Kochi (Sep 27-30, 2004)

Y. Akimura, T. Maruyama, N. Yoshinaga, S. Chiba
Molecular Dynamics Aapproach for Quark Matter and its Stability
Fall Meeting of the Physical Society of Japan, Kochi (Sep 27-30, 2004)

T. Endo, T. Maruyama, T. Tanigawa S. Chiba, D.N. Voskresensky, T. Tatsumi
Mixed Phase in Hadron-quark Phase Transition
Fall Meeting of the Physical Society of Japan, Kochi (Sep 27-30, 2004)

Y. Akimura, T. Maruyama, N. Yoshinaga, S. Chiba
Quark-hadron Phase Transition Studied by Molecular Dynamics
Workshop on Baryonic Interaction and Baryonic Matter, Morioka (Nov 27-29, 2004)

T. Endo, T. Maruyama, T. Tatsumi, S. Chiba
Path of Mixed Phase in Hadron-quark Phase Transition
Workshop on Baryonic Interaction and Baryonic Matter, Morioka (Nov 27-29, 2004)

G. Watanabe, T. Maruyama, H. Sonoda, K. Sato, K. Yasuoka, T. Ebisuzaki
Dynamical Transition of Nuclear Pasta Structure
60th Annual Meeting of the Physical Society of Japan, Noda (Mar 24-27, 2005)

T. Endo, T. Maruyama, T. Tanigawa S. Chiba, D.N. Voskresensky, T. Tatsumi
Various Pictures of Hadron-quark Mixed Phase
60th Annual Meeting of the Physical Society of Japan, Noda (Mar 24-27, 2005)

Y. Akimura, T. Maruyama, N. Yoshinaga, S. Chiba
Structure and Property of Quark/Hadron Phase Transition at Finite Density
60th Annual Meeting of the Physical Society of Japan, Noda (Mar 24-27, 2005)

Y. Utsuno
Evolution and Perspectives in Study of the Nuclear Structure in the N=20 Region by the Shell Model
RIKEN Workshop on "Physics of Unstable Nuclei - past 10 Years and Future -",
Wako, Saitama, (June 16, 2004)

Y. Utsuno
Anomalous Magnetic Moment of ^{9}C and Shell Quenching in Exotic Nuclei
The Fourth International Conference on Exotic Nuclei and Atomic Masses
(ENAM'04), Georgia, USA, (Sep. 12, 2004)

Y. Utsuno, T. Otsuka, M. Honma, T. Mizusaki, N. Shimizu
Shell Structure and Correlation Studied by Large-scale Shell-model Calculations
5th Italy-Japan Symposium on Recent Achievements and Perspectives
in Nuclear Physics, Naples, Italy, (Nov. 3, 2004)

Y. Utsuno, T. Otsuka, M. Honma, T. Mizusaki
Positioning of Intruder State in Stable and Exotic Nuclei
Japanese-German Nuclear Structure and Astrophysics Workshop,
Darmstadt, Germany, (Dec. 17, 2004)

Y. Utsuno, T. Otsuka, M. Honma, T. Mizusaki
Shape Coexistence and Mixing in N~20 Region
International Symposium on Correlation Dynamics in Nuclei
-- On the Occasion of the 50th Anniversary of the Configuration Mixing Theory
of Arima and Horie -- (CDN05)--

Tokyo (Feb. 1, 2005)

Y. Utsuno, T. Otsuka, M. Honma, T. Mizusaki, T. Ishii,
Importance of the Full pf-shell Calculation in Nuclei around N=28
60th Annual Meeting of the Physical Society of Japan, Noda, Chiba (March 24, 2005)

T. Ichikawa, A. Iwamoto, P. Moller, A. Sierk
Effective Fusion Barrier in Entrance Channel for Cold Fusion Reaction Leading to SHE Production
2004 Annual Meeting of the Japan Society of Nuclear and Radiochemical Science, Tokyo (Oct. 27-29, 2004)

ATOMIC PHYSICS AND SOLID STATE PHYSICS

Journal/Proceedings

S.C. Jeong, I. Katayama, H. Kawakami, H. Ishiyama, Y. Watanabe, H. Miyatake, E. Tojyo, M. Oyaizu, K. Enomoto, M. Sataka, S. Okayasu, H. Sugai, S. Ichikawa, K. Nishio, Y. Sugiyama, A. Iwase, M. Yahagi, T. Hashimoto, K. Takada, M. Watanabe, M. Tanigaki, T. Shinozuka

^{8}Li and ^{18}F Diffusion Experiments in Solids – an Application of Accelerated RNB-

Nucl. Phys. A **746** (2004) 293c

S.C. Jeong, I. Katayama, H. Kawakami, Y. Watanabe, H. Ishiyama, H. Miyatake, M. Sataka, S. Okayasu, H. Sugai, S. Ichikawa, K. Nishio, T. Nakanoya, N. Ishikawa, Y. Chimi, T. Hashimoto, M. Yahagi, , K. Takada, B.C. Kim, M. Watanabe, A. Iwase, T. Hashimoto, T. Ishikawa

Measurement of Diffusion Coefficients in Solids by the Short-lived Radioactive Beam of ^{8}Li

Nucl. Instrum. Method. B **230** (2005) 596

Meetings

H. Kitô, T. Wada, S. Okayasu, M. Sataka

Heavy-ion Irradiation Dependence of Superconducting Properties of the $YSr_2Cu_3O_{7\pm\delta}$

60th Annual Meeting of the Physical Society of Japan, Noda (Mar. 25, 2005)

RADIATION EFFECT IN MATERIALS

Journal/proceedings

A. Kurumada, Y. Imamura, T. Oku, M. Ishihara, S. Baba, J. Aihara
Ion Irradiation Effects on Tensile Properties of Carbon Fibers
OECD 2004, NEA No.5309, (2004) 121

R. Nakatani, R. Taniguchi, Y. Chimi, N. Ishikawa, M. Fukuzumi, Y. Kato, H. Tsuchida, N. Matsunami, A. Iwase,
Atomic Mixing at Metal-oxide Interfaces by High Energy Heavy Ions
Nucl. Instrum. Method. B **230** (2005) 234

M. Shimada, K. Yasuda, S. Matsumura, C. Kinoshita, Y. Chimi, N. Ishikawa
Atomic Disordering in Magnesium aluminate spinel around ion tracks induced by high-density electronic excitation
Proc. 8th Asia-Pacific Conference on Electron Microscopy, Kanazawa (2004) p. 43

M. Shimada, K. Yasuda, S. Matsumura, C. Kinoshita, Y. Chimi, N. Ishikawa, A. Iwase
Radiation-induced Disordering in Magnesium Aluminate Spinel Subjected to Ionizing Radiation
J. Nucl. Mater. **329-333** (2004) 1445

N. Ishikawa, Y. Chimi, O. Michikami, T. Hashimoto, T. Kambara, R. Neumann, A. Iwase
Ion-velocity Dependence of High-density Electronic Excitation Effects in Oxide Superconductors
Nucl. Instrum. Method. B **230** (2005) 136

F. Ono, S. Komatsu, Y. Chimi, N. Ishikawa, T. Kambara, A. Iwase
Magnetic Properties in Fe-Ni Invar Alloys Irradiated by High-Energy Ions
Mat. Res. Soc. Symp. Proc. 792 (2004) 441

F. Ono, S. Komatsu, Y. Chimi, N. Ishikawa, A. Iwase, T. Kambara
Effect of GeV-Ion Irradiation on Magnetic Properties of Fe-Ni Invar Alloys
Nucl. Instrum. Method. B **230** (2005) 279

M. Fukuzumi, Y. Chimi, N. Ishikawa, F. Ono, S. Komatsu, A. Iwase
Swift Heavy Ion Induced Magnetic Phase Transition of Fe-Rh Alloy
Nucl. Instrum. Method. B **230** (2005) 269

M. Fukuzumi, A. Iwase, M. Suzuki, M. Takagaki, N. Ishikawa, Y. Chimi, J. Mizuki
X-ray Magnetic Circular Dichroism Study on Fe-Rh Alloy Irradiated with Swift Heavy Ions
SPring-8 User Experiment Report No.13 (2004A) 323

T. Shibata, M. Ishihara, Y. Motohashi, S. Baba, T. Hoshiya, T. Kobayashi, S. Harjo,
T. Sakuma
Superplastic Deformation Characteristics of 3Y-TZP after Zr Ion Irradiation,
Nucl. Instrum. Method. B **206** (2003) 139

Y. Motohashi, T. Kobayashi, S. Harjo, T. Sakuma, T. Shibata, M. Ishihara, S. Baba,
T. Hoshiya
Radiation Damage Effects in Superplastic 3Y-TZP Irradiated with Zr Ions,
Nucl. Instrum. Method. B **206** (2003) 144

T. Shibata, M. Ishihara, Y. Motohashi, S. Baba, T. Sakuma, T. Hoshiya
Ion Irradiation Effect on Superplastic 3Y-TZP Ceramics
Mater. Sci. Forum **426-432** (2003) 2813

T. Nishio et al.
Penetration of Vortices into Micro-Superconductor Observed with a Scanning SQUID Microscope
Physica C **412-414** (2004) 379-384

A. Kurumada, Y. Imamura, T. Oku, H. Watanabe, K. Tokunaga, N. Yoshida
Ion Irradiation Effects on Properties and Microstructures of Plasma Facing Materials
Proceedings of RIAM Forum 2004, (2004.6.3-4) 90-93

A. Kurumada, Y. Imamura, Y. Motohashi
Irradiation damage Effects on Properties and Microstructures of Materials for HTGR
Oarai Research Reports, Institute for Materials Research, Tohoku University, (2004.8.26-27)
208-212

Meetings

H. Maeta, N. Matsumoto, T. Kato, H. Sugai, H. Ohtsuka, M. Sataka
Radiation Defects in Heavy ion-irradiated Nickel at Low Temperature by X-ray Diffuse
15th International Workshop on Inelastic Ion Surface Collisions
October 17(Sun)-22(Fri), 2004 Mie, Japan

H. Maeta, N. Matsumo, T. Kato, H. Sugai, H. Ohtsuka, M. Sataka
Structure of Defect Cascades in Heavy ion-irradiated Nickel by X-ray Diffuse Scattering
14th International Conference on Ion Beam Modification of Materials, Sept 5-10,2004 at Monterey, California, USA

T. Oku, A. Kurumada, Y. Imamura, M. Ishihara, S. Baba, J. Aihara, T. D. Burchell
Ion Irradiation Program and Effects of Ion Irradiations on The Electrical Resistivity of Carbon Fibers
International Nuclear Graphite Specialists Meeting-5, Gwynedd, UK, (2004.9.12-15)

A. Iwase
Interaction Between Swift Heavy Ions and Materials; from the Fundamental Process to the Application for Materials Modification
Institute of Modern Physics Seminar, Lanzhou, China (Sept. 29, 2004)

A. Iwase, R. Nakatani, R. Taniguchi, Y. Chimi, N. Ishikawa, M. Fukuzumi, Y. Kato, H. Tsuchida
Atomic Mixing at Metal-oxide Interfaces by High Energy Heavy Ions
21st International Conference on Atomic Collisions in Solids, Genova, Italy (Jul. 6, 2004)

A. Iwase
GeV-ion Induced Electronic Excitation in Materials and Application
Advanced Technology Seminar, Osaka (March 02, 2005)

A. Iwase, Y. Kato, M. Fukuzumi, Y. Chimi, N. Ishikawa, H. Tsuchida
Electronic Mixing at Bi-Alumina Interface
60th Annual Meeting of the Physical Society of Japan, Noda (Mar. 25, 2005)

A. Iwase
Interaction Between Swift Heavy Ions and Material
2nd Symposium on Atomic Collisions in Solids, Tsukuba (Mar. 18, 2005)

T. Yamamoto, M. Shimada, K. Yasuda, S. Matsumura, Y. Chimi, N. Ishikawa
Change in Atomic Configurations of Spinel Irradiated with Swift Heavy Ions
Spring Meeting of the Japan Institute of Metals (Mar. 31, 2005)

N. Ishikawa, Y. Chimi, O. Michikami, T. Hashimoto, T. Kambara, R. Neumann, A. Iwase
Ion-velocity Dependence of High-density Electronic Excitation Effects in Oxide Superconductors
International Conference on Atomic Collision in Solids (ICACS-21), Genova (Jul. 6, 2004)

Y. Matsushima, F. Ono, H. Kanamitsu, S. Komatsu, A. Iwase, Y. Chimi, N. Ishikawa, T. Kambara
Modification of the Magnetic Properties in Fe-Ni Invar Alloys by High-Energy Heavy Ion Irradiation
Annual Meeting of Joint Physical Society of Japan and Applied Physics Society Chugoku-Shikoku-Branch, Takamatsu (July 31, 2004)

F. Ono, S. Komatsu, Y. Chimi, N. Ishikawa, A. Iwase, T. Kambara
Effect of GeV-ion Irradiation on Magnetic Properties of Fe-Ni Invar Alloys
21st International Conference on Atomic Collisions in Solids, Genova, Italy (Jul. 6, 2004)

M. Fukuzumi, R. Taniguchi, A. Iwase, N. Ishikawa, Y. Chimi, T. Kambara, F. Ono
Quantum Beam Irradiation Effects for Magnetic Properties of Fe-Rh Alloy
Fall Meeting of the Atomic Energy Society of Japan, Kyoto (Sep. 15, 2004)

M. Fukuzumi, R. Taniguchi, N. Ishikawa, Y. Chimi, T. Kambara, S. Komatsu, F. Ono, A. Iwase
Swift Heavy Ion Induced Magnetic Phase Transition of Fe-Rh Alloy
21st International Conference on Atomic Collisions in Solids, Genova, Italy (Jul. 6, 2004)

M. Fukuzumi, N. Ishikawa, Y. Chimi, M. Suzuki, M. Takagaki, J. Mizuki, H. Tsuchida, F. Ono, R. Neumann, T. Kambara, A. Iwase
Study on Swift Quantum Beam Induced Magnetic Phase Transition of Fe-Rh Alloy by using SQUID and XMCD
60th Annual Meeting of the Physical Society of Japan, Noda (Mar. 25, 2005)

T. Sonoda, M. Kinoshita, Y. Chimi, N. Ishikawa, M. Sataka, A. Iwase
Electronic Excitation Effects on Microstructural Evolution in CeO_2 under High Energy Ion Irradiation
Fall Meeting of Japan Institute of Metals, Akita (Sept. 28, 2004)

T. Sonoda, Y. Chimi, N. Ishikawa, M. Sataka, A. Iwase
Study of High Dense Electronic Excitation Effects in CeO_2 under irradiation with High Energy ions of Typical Fission Products
Materials Science Symposium "Materials Science uasing Accelerators", JAERI Tokai (Jan. 06-07, 2005)

K. Yasunaga, K. Funamoto, K. Yasuda, S. Matsumura, T. Sonoda
Microstructural Configuration and the Stability of Defect Clusters in CeO_2 under Electron Irradiation
Spring Meeting of Japan Institute of Metals, Yokohama (Mar. 31, 2005)

H. Abe, H. Hamaguchi, T. Sonoda
Microstructural Exchange in CeO_2 under Irradiations with Electrons and Ions
Spring Meeting of Japan Institute of Metals, Yokohama (Mar. 31, 2005)

M. Sasase, K. Shimura, K. Yamaguchi, H. Yamamoto, S. Syamoto, K. Hojou
Interface structure of b-FeSi2 thin film fabricated on Si and SIMOX substrate
Spring Meeting of the Japan Society of Applied Pysics, Tokyo(April 1, 2005)

Y. Motohashi, T. Shibata, S. Harjo, T. Sakuma, M. Ishihara, S. Baba, K. Sawa
Ion Beam Surface Modification of Y-TZP and Effects of Subsequent Annealing
Transactions of Materials and Heat Treatment Proceedings of the 14th IFHTSE Congress, (Oct. 2004)

N. Matsunami, O. Fukuoka, N. Shinde, M. Sataka, S. Okayasu
Mechanism of Electronic Sputtering of Oxides II
Fall Meeting of the Physical Society of Japan, Aomori(Sept, 2004)

T. Nakazawa, A. Naitou, Y. Chimi, D. Yamaki, T. Aruga, S. Jitsukawa
Structural Changes of Li_2TiO_3 Irradiated with High-energy Heavy Ions
2005 Annual Metting of the Atomic Energy Society of Japan in Hiratsuka (Mar. 29-31, 2005)

T. Nakazawa
Infrared Spectroscopy Analysis and MNDO Calculations for Irradiation-induced Structural Change of Lithium Ortho-silicate
Materials Science Symposium " Materials Science using Accelerators "
JAERI Tokai Jan. 6-7, 2005

9. Personnel and Committees

This is a blank page.

(1) Personnel(FY 2004)

Department of Materials Science

Zenko	Yoshida	Director(Apr.-Sep.)
Hiroshi	Ikezoe	Director(Oct.-Mar.)
Katsuyuki	Tomatsuri	Administrative Manager(Apr.-Dec.)
Yoshiyuki	Ozeki	Administrative Manager(Jan.-Mar.)

Tandem Accelerator Group

Scientific Staff

Suehiro Takeuchi※
Susumu Hanashima
Makoto Matsuda
Takamitsu Nakanoya
Hiroshi Kabumoto
Tetsuya Sato
Masahiko Nakamura

Technical Staff

Yoshihiro Tsukihasi
Susumu Kanda
Tadashi Yoshida
Katsuzo Horie
Isao Ohuchi
Shin-ichi Abe
Nobuhiro Ishizaki
Hidekazu Tayama

Entrusted Operators

Akihiko Iijima
Takahiro Yoshida
Takahiro Usami
Tetsusi Hida
Hisashi Sakurayama
Hikaru Nisugi
Nobuo Seki
Teruo Onodera

Entrusted Assistants

Yoshio Fujii
Teruo Kozawa

Research Group for Innovative Nuclear Science

Masumi Oshima※
Hideki Iimura
Tetsuya Hirade
Yuichi Hatsukawa

Akihiko	Osa	
Yutaka	Utsuno	
Yosuke	Toh	
Mitsuo	Koizumi	
Atsushi	Kimura	(Post Doc.)
Jun	Goto	(Post Doc.)
Haiming	Wang	(Visiting Researcher)

Research Group for Nuclear Physics of Heavy Elements

Hiroshi	Ikezoe※	
Tetsuro	Ishii	
Shin-ichi	Ichikawa	
Katsuhisa	Nishio	
Shin-ichi	Mitsuoka	
Kaoru	Tsuruta	(Post Doc.)
Trang Thi	Kieu Hoang	(MEXT)
Soichiro	Shigematsu	(Student)

Research Group for Radiation Effects and Analysis

Shirou	Jitsukawa※	
Masao	Sataka	
Hideo	Ohtsuka	
Satoru	Okayasu	
Hiroyuki	Sugai	
Nariaki	Okubo	
Teruo	Kato	
Norito	Ishikawa	
Yasuhiro	Chimi	
Takeo	Aruga	
Tetsuya	Nakazawa	
Daijyu	Yamaki	
Akira	Naito	

Advanced Science Research Center

Research Group for Many Body Theory of Hadron Systems

Satoshi	Chiba※	
Toshiki	Maruyama	
Hiroyuki	Koura	
Yuka	Akimura	(Student)

Research Group for Atom-at-a-time chemistry of the Heaviest Elements

Yuichiro	Nagame※	
Kazuaki	Tsukada	
Ichiro	Nishinaka	
Masato	Asai	

Kazuhiko Akiyama (Post Doc.)
Takatoshi Ichikawa (Post Doc.)
Atsushi Toyoshima (Student)
Yasuo Ishii (Student)

Department of Nuclear Energy System

Research Group for Compatible Materials

Kiyoshi Kiuchi※
Ikuo Ioka
Hiroaki Ogawa
Yukio Nakahara
Yasuhiro Ishijima

Department of Health Physics

Radiation Control Division

Nobuhito Shishido
Minako Yokoyama
Kenji Yamane

Advanced Photon Research Center

Applied Photon Research Group

Takehito Hayakawa
Toshiyuki Shizuma

Takasaki Radiation Chemistry Research Establishment

Research Group for Severe Environment Materials

Toshio Hirao

Oarai Research Establishment

High Temperature Irradiation Laboratory

Kazuhiro Sawa※
Shin-ichi Baba
Jun Aihara

※ Head

(2) Tandem Consultative Committee

(Chairman)	Shigeru	Kubono	(Professor, The University of Tokyo)
(Vice Chairman)	Hiroshi	Ikezoe	(Director, Department of Materials Science)
	Akihiko	Iwase	(Professor, Osaka Prefecture University)
	Ken-ichiro	Komaki	(Professor, The University of Tokyo)
	Hisaaki	Kudo	(Associate Professor, Niigata University)
	Noriaki	Matsunami	(Associate Professor, Nagoya University)
	Kenji	Morita	(Professor, Meijo University)
	Tetsuo	Noro	(Professor, Kyushu University)
	Tsutomu	Ohtsuki	(Associate Professor, Tohoku University)

	Hiromi	Shibata	(Associate Professor, Kyoto University)
	Tadashi	Shimoda	(Professor, Osaka University)
	Kazuhiro	Yabana	(Associate Professor, Tsukuba University)
(Secretary)	Yuichiro	Nagame	(Leader, Research Group for Atom-at-a-time chemistry of the Heaviest Elements)
	Masumi	Oshima	(Leader, Research Group for Innovative Nuclear Science)
	Masao	Sataka	(Research Group of Radiation Effects and Analysis)
	Suehiro	Takeuchi	(Head, Tandem Accelerator Group)
	Yoshiyuki	Ozeki	(Administrative Manager, Department of Materials Science)

(3) Research Planning and Assessment Committee

(a) Sub-committee for Nuclear Physics and Nuclear Chemistry

(Chairman)	Tetsuo	Noro	(Professor, Kyushu University)
	Tsutomu	Ohtsuki	(Associate Professor, Tohoku University)
	Kazuhiro	Yabana	(Associate Professor, Tsukuba University)
	Motoharu	Mizumoto	(Nuclear Transmutation Group)
	Tadashi	Shimoda	(Professor, Osaka University)
	Nobuo	Shinohara	(R&D Group for Nonproliferation Technology)
	Suehiro	Takeuchi	(Head, Tandem Accelerator Group)
(Secretary)	Susumu	Hanashima	(Tandem Accelerator Group)
	Makoto	Matsuda	(Tandem Accelerator Group)

(b) Sub-committee for Materials and Radiation Damage

(Chairman)	Kenji	Morita	(Professor, Meijo University)
	Noriaki	Matsunami	(Associate Professor, Nagoya University)
	Ken-ichiro	Komaki	(Professor, The University of Tokyo)
	Hiromi	Shibata	(Associate Professor, Kyoto University)
	Shiro	Jitsukawa	(Head, Research Group for Radiation Effects and Analysis)
	Kazumasa	Narumi	(Head, Research Group for Design of New Materials with Energy Beams)
	Suehiro	Takeuchi	(Head, Tandem Accelerator Group)
(Secretary)	Susumu	Hanashima	(Tandem Accelerator Group)
	Makoto	Matsuda	(Tandem Accelerator Group)

10. Cooperative Researches

This is a blank page.

Title	Contact Person Organization
1. Nuclear Structure of Heavy and Transactinide Nuclei	Yasuji OURA Tokyo Metropolitan University
2. Study of nuclear deformation by Coulomb excitation	Yoshifumi SHIMIZU Kyushu University
3. Study of heavy-ion fusion via reverse fission process	Hiroari MIYATAKE High Energy Accelerator Research Organization
4. In-beam gamma-ray spectroscopy of transuranium nuclei produced by transfer reactions	Masao OGAWA Tokyo Institute of Technology
5. Ion source development for mass-separation of short-lived exotic nuclei	Sun Chan JEONG High Energy Accelerator Research Organization
6. Atom-at-a-time chemistry of heavy actinide and transactinide elements in aqueous solution	Atsusi SHINOHARA Osaka University
7. Studies on nuclear isomers at the A=180 mass region	Hiroaki UTSUNOMIYA Konan University
8. Study on the shape coexistence in ^{70}Ge and the coexisting phenomena of magnetic and anti-magnetic rotors	Masahiko SUGAWARA Chiba Institute of Technology
9. Production of New Isotope Sg-264	Takaaki OSAWA Kinki University
10. Study of the explosive nucleo-synthesis by using RNB	Hiroari MIYATAKE High Energy Accelerator Research Organization
11. Decay study on neuton-rich nuclei produced with the fission of actinide elements	Michihiro SHIBATA Nagoya University
12. Study of nuclear fission from moderately excited fermium isotopes produced by break-up fusion reactions	Akihiko YOKOYAMA Kanazawa University
13. Nuclear chemical study on transactinide elements by use of gas phase chemistry	Hisaaki KUDO Niigata University
14. Study of collective motion of deformed high-spin isomer	Kenji SAGARA Kyushu University

15. Study of scintillation properties for particle identification in CaF_2 crystals	Tadashi KISHIMOTO Osaka university
16. Laser spectroscopy of radioactive isotopes in the A=180 mass region	Takayoshi HORIGUCHI Hiroshima International University
17. Systematic study of signature inversion and deformation at high spin in deformed nuclei	Masahiko SUGAWARA Chiba Institute of Technology
18. Study on recovery of properties of new carbon composite materials and carbon fibers with irradiation damage resistance due to high heat treatment after irradiation	Akira KURUMADA Ibaraki University
19. Atomic mixing under swift heavy ion irradiation fields	Akihiro IWASE Osaka Prefecture University
20. Microstructure of oxide ceramics subject to high density electronic excitation	Akira MURAMATSU Kyushu University
21. Ion-velocity effects observed for structural change in oxides irradiated with high-energy ions	Osamu MICHIKAMI Iwate University
22. Atomic displacements induced by high-density electronic excitation in Fe-based ferromagnetic alloys	Fumihisa ONO Okayama University
23. Secondary ions emission induced by electronic excitation effect in the solids bombarded by swift heavy ions	Tsuguhisa SEKIOKA Himeji Institute of Technology
24. Study on heavy ion structure and electronic process using 0-degree electron spectroscopy	Ken-ichiro KOMAKI University of Tokyo
25. Electronic processes in highly charged ion collisions	Kiyoshi KAWATSURA Kyoto Institute of Technology
26. Study of radiation defects in heavy ion-irradiated materials at low temperature by means of x-ray diffuse scattering	Yuuji MAETA Hiroshima Kokusai Gakuin University
27. Effects of ion irradiation on zirconia-base superplastic ceramics	Yoshinobu MOTOHASHI Ibaraki university
28. Study of microstructure re-structuring process under irradiation with high energy fission products in nuclear fuels of light water reactor	Takeshi SONODA Central Research Institute of Electric Power Industry (CRIEPI)
29. Nanoscale transformation of β phase to α phase in $FeSi_2$ films by high-energy heavy ion irradiation	Masato SASASE The Wakasa Wan Energy Research Center

30. Study of single-event effects caused by heavy ions on advanced power devices for space applications	Tomosi KUBOYAMA National Space Development Agency of Japan
31. Heavy-ion irradiation effect for the over-doped cuprate superconductor	Hijiri KITO National Institute of Advanced Industrial Science and Technology (A.I.S.T)
32. Electronic excitation effects in ceramics by high-energy ion beams	Noriaki MATSUNAMI Nagoya University
33. Study of diffusion process in solid using short-lived nuclei	Ichirou KATAYAMA High Energy Accelerator Research Organization